X-ray Emission from Supernovae: A Review of the Observations

Eric Schlegel

Laboratory for High Energy
Astrophysics

High Energy Astrophysics Science
Archive Research Center

NASA Goddard Space Flight Center
Greenbelt, MD 20771

X-ray Emission from Supernovae: A Review of the Observations

Eric M. Schlegel

NASA-Goddard Space Flight Center and Universities Space Research Association, Code 668, Greenbelt, MD 20771

I: eric@heasfs.gsfc.nasa.gov

Submitted: Reports on Progress in Physics Feb 1995

Refereed: May 1995

~~Received~~ _____; accepted _____

ABSTRACT

Supernovae have been expected to be X-ray sources for many years. This paper reviews the observations that have detected or placed upper limits on the emission of X-rays from supernovae. A firm upper limit exists on X-ray emission from Type Ia supernovae based upon an observation of SN 1992A (parent galaxy: NGC 1380) made with *ROSAT*. The Type II supernovae detected include SN 1978K (NGC 1313), SN 1980K (NGC 6946), SN 1986J (NGC 891), SN 1987A (Large Magellanic Cloud), and, most recently, SN 1993J (NGC 3031). These supernovae emit X-rays by at least two different processes. I briefly review the proposed emission mechanisms.

Subject headings: X-Rays: Sources; Stars: Supernovae; Stars: Individual: SN 1978K, SN 1980K, SN 1986J, SN 1987A, SN 1992A, SN 1993J; Nebulae: Supernova Remnants

Contents

1. Introduction

Supernovae are among the most violent, short-lived phenomena in the universe. They essentially liberate the gravitational binding energy of a star, $\sim 10^{53}$ ergs, over times of seconds to hours. Supernovae are very luminous, so they are visible across large distances, but they emit only $\sim 10^{49}$ ergs of electromagnetic energy. This energy constitutes ~0.01% of the total available energy; the kinetic energy of the ejected matter (~1%) and the energy carried away by neutrinos (~99%) account for the remainder of the binding energy. Supernovae have been observed principally in the optical band, but observations have also been made from radio to the γ-ray energies. About 30 supernovae are discovered and observed each year, although most of these are too far away, and therefore too faint, to be useful for detailed studies. Most supernovae are observed relatively often near discovery, but interest fades as the supernova wanes because, in general, the observations become increasingly difficult to carry out.

Supernovae are named for the year of the discovery, which need not be the year of the detonation, followed by a letter indicating the order in which the discovery was made. The lettering scheme starts at 'A' and proceeds through the alphabet. Hence, SN 1987A, the supernova that appeared in the Large Magellanic Cloud in 1987, was also the first supernova of 1987.

The study of supernovae is important for several reasons. Observations of supernovae, and the theory of their formation and evolution, form one part of the study of an endpoint of stellar evolution, especially of massive stars. Stars essentially synthesize the chemical elements (other than hydrogen and helium), so supernovae fundamentally affect the chemical evolution of subsequent generations of stars. This happens because, when a supernova explodes, it

sprays the synthesized elements into the interstellar medium from which new stars form. Hence the observed abundances of elements in the interstellar medium are affected by the input from supernovae. The outgoing shock wave of the blast can also trigger the collapse of nearby molecular clouds, thereby initiating the formation of the next generation of stars. Neutrino astronomy may have started with observations of the Sun, but workers in this field were completely energized by the detection of neutrinos from SN 1987A, which confirmed the basic scenario of massive star evolution, namely, the gravitational collapse of the core. Supernovae also appear to be useful for estimating the cosmic distance scale either as "standard candles" or through the use of the "expanding photospheres" method (Schmidt, Kirshner, & Eastman 1992).

Supernovae are classified on the basis of their optical spectra (Zwicky 1965) and fall into two broad categories. Type II supernovae show emission lines of hydrogen in their spectra. The accepted model for these supernovae is the collapse of the core of a massive star. The ejection of the envelope occurs because matter becomes opaque to neutrinos at the very high temperatures and densities typical of a collapsing core. The model was confirmed by the neutrino burst observed from SN 1987A (Koshiba et al. 1987; Svoboda et al. 1987) the progenitor of which was believed to be a 20 $M_{\odot}$ star based upon a pre-supernova spectrum of the progenitor (Walborn et al. 1987). The collapse of a core of a massive star commences when the pressure of the overlying layers is no longer resisted by the outward energy flow. The core heats as gravitational potential energy is converted to thermal energy. Details of the collapse process are still a subject of vigorous research. The collapse of the core is also expected to leave a remnant, either a neutron star or a black hole. One might expect that, if the core collapses at different times in the evolution of massive stars,

different behaviors will be detected in the resulting supernovae. There is, as yet, few or no recognized connections between specific evolved stars and supernova behavior. One of the important benefits of SN 1987A was that it had a detected progenitor.

Type II supernovae can be subdivided based upon the optical light curve (see, for example, Kirshner 1990). SN II-L show a linear (L)[1] decline from outburst maximum to ~4.5 magnitudes below maximum at which time a different, but still linear, decay rate dominates. Few Type II-L supernovae have been discovered and observed over a sufficiently long time to understand their evolution. The progenitors have as yet not been identified. SN II-P show an approximately constant plateau (P) extending out to about 50-100 days after the explosion, followed by a rapid, ~1 magnitude decline, that is then followed by the decay appropriate to radioactive ^{56}Co. Type II-P supernovae have been modelled reasonably successfully as core collapses of red giant progenitors.

Type I supernovae show no hydrogen in their spectra. This class has been subdivided recently into Type Ia and Type Ib, with the Type Ib subclass showing strong emission lines of oxygen after about 100 days of evolution (see, for example, Porter & Filippenko 1987). The Type Ib objects are also thought to originate from massive stars, so the supernova's evolution also commences with a core collapse (see, for example, Schlegel & Kirshner 1989). The different appearance of a Type Ib supernova and a Type II supernova is very likely related to the apparent lack of hydrogen in the Type Ib objects. This lack suggests the progenitor is an evolved star. The recognition of Type Ib supernovae, therefore,

---

[1]The word 'linear' refers to the light curve behavior when the data are plotted as "magnitude" vs. "time". The magnitude is proportional to the log of the flux.

is the first example of different phases of massive star evolution leading to different supernova behavior

Type Ia supernovae also show no hydrogen in their optical spectra. They are, however, believed to be deflagrating or detonating white dwarfs rather than massive stars (see, for example, Woosley 1990). The difference between "deflagrating" and "detonating" is the speed at which the flame front moves outward through the supernova progenitor: subsonically or supersonically, respectively. On the average, a white dwarf is not sufficiently massive to undergo a thermonuclear detonation or deflagration. If the white dwarf, however, is in a binary system, and if the secondary star fills its Roche lobe, then mass transfer from the secondary to the primary will occur. If the white dwarf can accumulate this matter until the star's mass exceeds the Chandrasekar mass for the star's composition, the pressure of the overlying layers can raise the temperature and density at the base of the hydrogen layer to the thermonuclear ignition point. When this occurs, the white dwarf is completely disrupted and no remnant of the detonation is expected. Progenitors of Type Ia supernovae should then occur in binary systems. Binarity can lead to considerably different objects (cataclysmic variables, Algols, W UMa stars, etc. (Trimble 1983)), yet Type Ia supernovae look incredibly similar in their optical spectra. This remains one of the puzzles of supernova research.

Supernovae may be expected to show significant levels of X-ray emission given the quantity of thermal energy released in a supernova explosion ($\sim 10^{49}$ ergs s^{-1} of electromagnetic radiation (Kirshner 1990)). Extrapolating from observed optical blue and ultraviolet light curves of supernovae which have increasingly rapid decay times, the observer might expect supernovae to be detectable X-ray sources only at the very earliest times in the evolution of the

outburst. For example, the ultraviolet flux of SN 1987A declined by $\sim 10^3$ in three days (Kirshner et al. 1987). A decline of this magnitude occurs more quickly than many satellites can be re-oriented for a pointed observation. X-ray satellites have, however, been pointed at supernovae and several supernovae have been detected. I believe it is an appropriate time to collect and to review the X-ray observations of supernovae and the proposed mechanisms now that the number of supernovae detected has climbed to five (and possibly six). Further, the quality of the observations appears very likely to take a quantum leap upward in the next few years, so a review may focus attention on those questions that higher signal-to-noise observations can answer. Finally, as we shall see, X-ray emission from supernovae occurs by at least two different mechanisms, so it is also timely to compare the data and the proposed mechanisms.

The expected X-ray emission of supernovae can be roughly divided into two temporal phases: 'early' and 'late'. First, we might expect X-rays to appear promptly, accompanying the optical maximum, resulting from the high-temperature flash associated with the break out of the shock wave through the stellar surface, or from the prompt thermal detonation or deflagration of a white dwarf, or from the interaction of the initial photoionization and shock with circumstellar material in the immediate vicinity of the progenitor. Second, we might expect X-rays to appear at late times ($\geq$100 days) whenever the expanding debris field becomes optically thin to X-rays, or when the outgoing shock wave runs into the circumstellar shell from earlier phases of mass loss, or when the material has thinned sufficiently that any radiation from a collapsed remnant (e.g., a neutron star) remaining after the explosion can escape the nebula. The observations of the five supernovae detected to date show X-ray emission at both early and late times. We therefore expect more than one

physical process to be at work.

X-ray observations of supernovae are important because the X-ray emission probes shocked matter as the outgoing shock wave runs into circumstellar material. Radio observations apparently also probe this phase, but the radio and X-ray emission must arise from different locations as a result of the considerably higher temperatures and densities required for thermal X-rays. What is not known is whether the two sets of observations vary together (with a possible phase delay). Prior to 1980, X-ray observations of supernovae did not detect any of them, so only upper limits could be assigned. Early observations of supernovae were motivated by the detection of the extragalactic X-ray background radiation; supernovae provided one possible explanation (e.g., Tucker 1970; Silk 1973). In 1980, SN 1980K in NGC 6946 was detected 35 days after its detonation by Canizares et al. (1982) using the *Einstein* X-ray observatory. Following this, SN 1987A in the Large Magellanic Cloud was detected by the Japanese satellite *Ginga* in 1987 August. The X-ray luminosity of SN 1987A was sufficiently low that it would not have been detected had it been at distances more typical of supernovae ($\sim$10 Mpc, instead of 50 kpc). The launch of the X-ray imaging satellite *ROSAT* in 1990 provided an opportunity to search for additional X-ray emitting supernovae. Current and future satellites can be expected to continue the study of these objects.

The plan of this paper is as follows. The purpose of this review is primarily to assemble all of the X-ray observations of supernovae, but specific mechanisms of X-ray emission, proposed to explain the X-ray behavior of supernovae, will be briefly reviewed in Section 2. Section 3 reviews the X-ray observations of Type Ia supernovae. Section 4 reviews the X-ray observations of Type II supernovae. A discussion of the data and the models is presented in Section 5. A summary

and the future of X-ray astronomy of supernovae are the subjects of Section 6. An appendix (Section 7) briefly describes the X-ray satellites and instruments that have been used over the years to make the observations described in this review. This review was completed in 1995 February and revised in 1995 June.

One final point: I will explicitly list the distances used at the appropriate time in the text, generally using the Nearby Galaxies Catalog (Tully 1988). The value of H_O adopted is 75 km s^{-1} Mpc^{-1}.

2. Mechanisms of X-ray Production

In this section I briefly review proposed production mechanisms. I urge the reader to return to the original references for the details of the calculations or models to understand the mechanisms in greater detail. This brief review of the mechanisms will serve only to provide theoretical context.

2.1. Inverse Compton Scattering

Beall (1979) first noted that a supernova with synchrotron radio emission could be an X-ray source by inverse Compton scattering of the relativistic electrons off the copious optical and ultraviolet photons produced in the detonation. This idea arose after the non-thermal radio detection of SN 1970G in NGC 5457 (=M101) (Gottesman et al. 1972). Chevalier (1982b) has described the problems with the above scenario, showing that the expected flux from inverse Compton scattering could be a factor of ten lower than the originally predicted value. A better match to the original prediction can be made by changing the model parameters; for example, an increase in the effective temperature raises the radiation energy density. Unfortunately, efficient

inverse Compton scattering then decreases the density of synchrotron electrons responsible for any radio emission. If the radio flux is relatively high, then inverse Compton losses must be small. This mechanism may explain a very brief phase of X-ray emission, but it fails for a sustained phase of emission.

2.2. Pulsar-driven Supernova "Remnant"

Pacini & Salvati (1981) appear to have first advanced the idea that a pulsar could inject magnetic energy and relativistic particles into the expanding debris from the supernova explosion, leading to a large flux of non-thermal radiation. Their model was applicable to the non-thermal emission from the Crab. In the Pacini & Salvati picture, radio supernovae were "young Crabs". Since the model requires a pulsar, it only applies to core-collapse supernovae, as detonating white dwarfs are not expected to leave a collapsed remnant (e.g., Woosley 1990). Bandiera et al. (1984) expanded on this suggestion by considering a wider range of parameters.

The model requires a rotating pulsar supplying energy through dipole and quadrupole radiation (the usual braking law for a rotating pulsar is $-\dot{\omega} = A\omega^3 + B\omega^5$, where ω=angular velocity, while A and B are model parameters). Four cases were considered: a rapidly rotating pulsar and a slowly expanding nebula (labeled as 'FS' in Bandiera et al. for Fast pulsar, Slow remnant), a slowly rotating pulsar and a rapidly expanding nebula (SF), a rapidly rotating pulsar and a rapidly expanding remnant (FF), and a slowly rotating pulsar and a slowly expanding remnant (SS). They predicted the radio light curve at 6 cm for each case and found that the FF case produced the largest flux at about 1 year post-outburst with an expected value of $\sim 1 \times 10^{37}$ ergs s^{-1} Hz^{-1}. They also predicted the flux at 1 keV and found again that the

FF case produces the largest amount, $\sim 8 \times 10^{39}$ ergs s^{-1} Hz^{-1}. The SS and FS curves both produce about 100 times less flux. Chevalier & Fransson (1992) followed up this work by developing a similarity solution for the pulsar-driven remnant. They also explored the spectral development for the most-abundant elements. Their model placed an upper limit on the total power input that a pulsar could provide to a nebular remnant. At an assumed distance of 50 kpc, the maximum luminosity is $\sim 5 \times 10^{38}$ ergs s^{-1} assuming a radiative efficiency of $\sim 1.5\%$. Their work made an unambiguous prediction for the presence of a pulsar-driven remnant: the line widths of optical and ultraviolet emission lines should increase with age from ~ 1500 km s^{-1} due to the acceleration of the pulsar bubble.

2.3. Prompt Thermal Burst

The prompt thermal burst, which could also be considered as the earliest possible form of a circumstellar interaction (next section), originated with the idea of the production of cosmic rays by hydrodynamical acceleration (Colgate & Johnson 1960; Colgate & McKee 1969). Chevalier (1990a) provides a summary. A shock wave, running outward from the star's core, accelerates along the negative density gradient that exists in the the progenitor's outer layers and atmosphere. As the shock approaches the surface, a radiative precursor is produced ahead of the shock (which is an ion viscous shock). The precursor heats and accelerates the surface layers. When the shock is at a depth corresponding to an optical depth $\tau \sim 25$, significant quantities of radiation begin to escape. The effective temperature is $\sim 2 \times 10^5$ K with a luminosity of $\sim 10^{45}$ ergs s^{-1} in a burst lasting ~ 1000 seconds. The actual shock break out is accompanied by a small amount of mass heated to $\sim 10^{8-9}$ K (Klein & Chevalier

1978, Falk 1978). Based upon this model, we expect a brief burst of X-rays of energy ~100 keV and an approximately blackbody continuum of ~0.02 keV. The X-ray burst has as yet not been observed, with upper limits from the *HEAO* A-1 experiment (Klein et al. 1979). The blackbody continuum is much too soft (<0.1 keV) for any X-ray telescope yet orbited, as the bulk of the flux lies in the extreme ultraviolet band. Unfortunately, the extreme ultraviolet is the energy band where the absorption cross-section for hydrogen is very large, so observations of sources at distances greater than ~100 pc are impossible because of the high opacity of the interstellar medium. The burst also lasts for a time too short to re-orient a pointed-mode X-ray satellite. Only a sensitive, all-sky X-ray monitor might catch the X-ray burst accompanying shock breakout. All-sky monitors will exist on the *X-ray Timing Explorer* satellite scheduled for launch in late 1995 and the *Spectrum X-*Γ satellite under construction in Russia, although the sensitivity of the *XTE* monitor is probably insufficient to detect any shock break-out bursts.

2.4. Circumstellar Interaction

When the outgoing supernova shock encounters the wind from the progenitor, a shock is established in the material. A reverse shock is also established, as a result of the pressure of swept-up material on the outgoing shock, and it propagates back into the shocked supernova gas. This behavior can occur at least twice in the supernova's life: shortly after the outburst if the immediate circumstellar density is sufficiently high, and at a relatively late stage in the evolution of the proto-remnant, when the outgoing shock catches up to the mass from the progenitor's wind phase. Thus, each time a shock moves into a dense, existing medium, a reverse shock is also generated which moves back into

the expanding, shocked medium. X-ray studies can therefore probe two media: the outgoing shock behavior depends upon the properties of the circumstellar medium, while the reverse shock behavior depends upon the properties of the progenitor's atmosphere. The development of the circumstellar interaction model has largely been the work of Chevalier (1982a, 1984, 1990b), Fransson (1984), and Chevalier & Fransson (1994). A recent review is presented by Fransson (1994).

The presence of a circumstellar medium is stongly dependent upon the immediate prior evolution of the progenitor (Chevalier 1990b). Whether the progenitor is optically red or blue[2] at the time of core collapse affects the immediate environment by the quantity of mass lost just prior to the explosion. Unfortunately, massive star evolution is not very well understood, in particular, the effects of mass loss on the star's structure and the star's subsequent evolution. It is known that a progenitor mass of $\sim$15 $M_{\odot}$ is critical: below this value, circumstellar effects are essentially negligible, as the number of ionizing photons decreases rapidly. Above the mass limit, clear circumstellar effects exist (Chevalier 1990b).

The first supernova to show a clear signature of circumstellar interaction was the Type II SN 1979C in NGC 4321 (Fransson 1984). Ultraviolet observations revealed the presence of emission lines that were interpreted as arising from circumstellar interactions. The turn-on of wavelength-dependent radio emission

---

[2]The terms "red" and "blue" in this context refer to the progenitor's apparent position in the H-R diagram of stellar evolution: "blue" means the star is near the O-B or high temperature side; "red" means the star is near the K-M or low temperature side of the diagram.

about 1 year after the explosion provided definitive evidence (Sramek & Weiler 1990). Radio emission was first seen at short wavelengths and later at longer wavelengths. Such behavior is most easily understood as decreasing free-free absorption in an ionized gas around the supernova site: the optical depth decreases as the supernova expands. (The failure to detect Type Ia supernovae in the radio band is also explained by the circumstellar interaction models. As the progenitor of a Type Ia supernova is expected to be less than 15 $M_{\odot}$, the circumstellar medium is too tenuous to generate measurable emission.)

The strength and duration of circumstellar interaction depends upon the density profiles of the ejected material and of the circumstellar medium. The usual assumption is to approximate the ejected density as a power law distribution $\rho_{ej} \sim \rho_O(t/t_O)^{-3}(V_O t/r)^n$, with ρ_{ej} = the ejected density, ρ_O the density at velocity v_O and time t_O, t = time of observation, t_O the time of explosion, V_O the ejecta velocity, r = radius at the time of the observation, and n = the power law exponent. Hydrodynamic models suggest n $\sim$ 7-12 (e.g., Arnett 1988; Chevalier & Soker 1989). The maximum velocity of the ejecta is $V = R_S / t \sim t^{-\frac{1}{n-2}}$. The circumstellar shock velocity $\frac{dR_S}{dt} = V_S = V\ (\frac{n-3}{n-2})$ while the reverse shock velocity is $V_{rev} = V - V_S = \frac{V}{n-2}$. The temperature in the circumstellar shock is $T_{cs} = 1.36\text{x}10^9\ (\ \frac{n-3}{n-2}\ )^2\ (\ \frac{V}{10^4 kms^{-1}}\ )^2$ while the reverse shock temperature is $T_{rev} = \frac{T_{cs}}{(n-3)^2}$ (Chevalier & Fransson 1994; Fransson 1994). For values of n in the above-cited range, T_{rev} is from 10 to 50 times lower than T_{cs}. Cooling is therefore very important for the reverse shock, but relatively unimportant for the outgoing shock since the shock temperature is so high. A similar power law is often assumed for the circumstellar gas density, with the index usually assumed equal to 2, even though a power law may not be a good representation of supernova density profile.

2.5. Radioactive Decay

The idea of radioactive decay as a power source for supernovae has existed since at least 1946 (Hoyle 1946). Several workers noted the similarity of the late-time decay rate to radioactive decay, and looked around for an appropriate element with which to power the light curve of a supernova. ^{7}Be (Borst 1950) and ^{254}Cf (Burbidge, Burbidge, Fowler, & Hoyle 1957) were suggested based upon their measured half-lives. Colgate & McKee (1969), building upon the work of Truran et al. (1968) and Bodansky et al. (1968), first suggested ^{56}Ni after working out the details of explosive silicon burning (Sutherland 1990). ^{56}Ni is the most tightly-bound nucleus in which the neutron number equals the proton number. It is also the most tightly bound nucleus composed of α particles. It is abundantly produced in nuclear statistical equilibrium. ^{56}Ni decays with a half-life of about 6.5 days to ^{56}Co, which decays with a half-life of 78.5 days to ^{56}Fe, with each being formed in an excited state that quickly decays, by γ-ray emission, to the ground state. For these reasons, ^{56}Ni became the most likely power source for supernovae. There was a side benefit: supernovae could then be invoked to explain the appearance of various elements, such as iron, present in the galaxy.

The presence of radioactively decaying elements in the debris of a supernova immediately produces a source of γ-rays, and by Compton scattering, a source of X-rays. The question for observers of X-rays is then at what time can X-rays be expected to appear from the site of the explosion. The X-rays emerging are expected to be hard (with energies above 20 keV), as the Compton degradation of the γ-rays will produce a pseudo-continuum down to $\sim$20 keV, at which point photoelectric absorption will dominate (Kumagai et al. 1989). No flux is expected below $\sim$16 keV because of the presence of absorption edges in that

region (for example, edges of Fe, Si, S, and O) and, as the photon energy decreases, absorption becomes more important than scattering. The time at which X-rays emerge is set by the time at which the effective optical depth (scattering plus absorption opacity) becomes approximately unity. This time is set by the rate at which the debris expands, thereby decreasing the effective opacity. Thus, X-ray photons below ~16 keV are not Compton-degraded γ-rays. A crude model, using Thomson scattering (symmetric) rather than the more accurate Klein-Nishina scattering (forward peaked), yields an estimate of ~400 days for the time at which a typical Type II supernova envelope becomes optically thin to X-rays (Sutherland 1990). To get the X-rays to emerge earlier requires the mixing of radioactive material outward into the He- or H-rich layers (depending upon the progenitor's structure). (As an aside, the models are best done with Monte Carlo techniques; Sutherland (1990) warns that failure to keep track of all the quantities properly can result in a functioning model which yields incorrect predictions.)

I turn now to the principal purpose of this review: the observations, starting with the Type Ia supernovae.

3. Observations of Type Ia Supernovae

There have been at least 5 X-ray observations of Type Ia supernovae, starting with Gorenstein et al. (1969) but to date, there have been no detections. No obvious mechanism exists for producing X-ray emission in Type Ia supernovae during the first tens of days after the detonation when the supernova is optically bright. There is no shock breakout, because no shock forms in the stellar layers in the absence of a core collapse. No circumstellar medium is expected to be present, given that the typical white dwarf lifetime prior to the

detonation/deflagration of the hydrogen layer should be of sufficient length to dissipate any circumstellar medium, so late-time emission due to circumstellar interaction will not occur. Only a few ~0.5-few 10^6 years are needed prior to the explosion to remove any circumstellar material.

If Type Ia supernovae occur in binary systems, then additional possibilities exist. Interaction of an outgoing shock from the detonation with the wind from a companion star could produce X-ray emission. The evidence that Type Ia supernovae occur in binary systems is as yet largely circumstantial, based on the consistency of deflagration models and observed spectra (e.g., Nomoto, Thielemann, & Yokoi 1984). For example, hydrogen has not yet been detected in any Type Ia supernovae. Applegate & Terman (1989) predict that the detection of hydrogen in the spectrum of a Type Ia would imply that cataclysmic variables are the progenitors. Only future observations will resolve the exact nature of the progenitors of these supernovae.

X-rays may be produced by the thermal radiation accompanying the detonation or deflagration (depending upon the currently favored model for Type Ia supernova outbursts). This production, however, because of the small radius, is unlikely to be sufficient to be detected at intergalactic distances and is likely to be of such short duration that no satellite has sufficiently rapid response time before the X-ray light curve decays. Therefore, a sensitive all-sky monitor (or at least a monitor covering ~π sr) is the most likely method to detect the prompt thermal flash of a Type Ia supernova.

Early upper limits (prior to ~1990) on the X-ray emission from Type Ia supernovae have not strongly constrained possible models due to the relatively low sensitivity and high internal backgrounds of the instruments used. These attempts have generally yielded upper limits in the range of 10^{41-45} ergs s^{-1}.

The upper limits include the following: probable Type I supernovae SN 1967J, SN 1968C, SN 1968H, SN 1968I, and SN 1968J using *OSO-III* by Ulmer et al. (1972); the Type Ia SN 1972E using *Uhuru* and *OSO-7* by Canizares et al. (1974) and Ulmer et al. (1974). Table 1 lists the supernovae studied, the parent galaxies, the date and magnitude of their optical maxima, and the X-ray upper limits. To my knowledge, the best upper limit, previous to the launch of *ROSAT* in 1990, on the X-ray emission from a Type Ia supernova is that of SN 1972E, with a value of $\sim 10^{41}$ ergs s^{-1} (Palmieri et al. 1974; Canizares et al. 1974). Figure 1 shows the temporal and spectral upper limits. The data points have been collected from the literature just mentioned. The temporal upper limit is compared to an *optical* light curve (labeled 'optical' in the figure) for reference. Note that the optical light curve has been normalized to a luminosity of 10^{38} ergs s^{-1}. Several recent satellites (*Einstein*, *Ginga*) are not represented as apparently no specific pointings were made at SN Ia in outburst.

The launch of the X-ray imaging satellite *ROSAT* (a collaboration of the US, the UK, and Germany) created an opportunity to obtain a much lower upper limit on the X-ray emission from a Type Ia supernova. *ROSAT* has excellent X-ray optics which place over 80% of the photons into the central 10" of the point spread function (Aschenbach 1988). In addition, the *ROSAT* Position Sensitive Proportional Counter (PSPC) is characterized by a very low internal background ($\leq 2.5 \times 10^{-5}$ counts s^{-1} arcmin^2 for $\sim$95% of the observing time (e.g., Snowden & Freyberg 1993)). The overall background of the *ROSAT* PSPC then becomes a strong function of the local particle and scattered solar X-ray environment. Such a low internal background can lead to a sensitive upper limit on X-ray emission from any source.

SN 1992A in NGC 1380 was discovered by W. Liller (Liller 1992) on 1992

January 11.16 at mag 12.8. A spectrogram showed the strong Si II absorption line at 6150Å characteristic of Type Ia supernovae at maximum light (Spyromilio et al. 1992). Roth (1992) obtained a high dispersion spectrum to search for interstellar sodium D lines. The lack of such lines indicated a low extinction to the supernova, making this supernova an excellent target for the soft[3] spectral coverage of the *ROSAT* PSPC. An 18 ksec observation using *ROSAT* was obtained on 1992 January 15-18, 16 days after the outburst. Figure 2 shows the SN 1992A region in the *ROSAT* observation. Only 11 counts were detected at the position of the supernova. A Bayesian upper limit (Kraft, Burrows, & Nousek 1991) was assigned based upon the number of counts detected at the source location relative to the mean number of counts in the background contained in identically-sized extraction cells located on either side of the supernova extraction cell (see Figure 2). For an assumed distance of 16.9Mpc (Tully 1988), the 99% upper limit on the 0.5-2.0 keV luminosity is 2.9×10^{38} ergs s^{-1} (the 5σ upper limit is 4.7×10^{38} ergs s^{-1}) (Schlegel & Petre 1993). This upper limit is at least a factor of 100 lower than all previous values. Chevalier (1984) argues that the detection of thermal X-ray emission from the shocked ejecta provides a measure of the mass loss rate surrounding the progenitor. The upper limit obtained for SN 1992A translates into an upper limit on the mass loss rate of SN 1992A of $\sim 2\text{-}3 \times 10^{-6}$ $M_\odot$ s^{-1}, assuming a typical wind velocity of 10 km s^{-1}. Intriguingly, the derived X-ray upper limit rivals limits determined

[3]The terms "soft" and "hard" are relative ones: a 0.5 keV photon is considered "soft" by X-ray astrophysicists, but "hard" by just about everyone else. Generally, "soft" applies to energies below 2 keV, but it can also mean the lower portion of a wide energy band. "Hard" has the opposite connotation.

from radio observations and suggests that X-ray observations are equally useful for probing the circumstellar environment, albeit more difficult to obtain or to schedule.

4. Observations of Massive Supernovae

X-ray emission, based upon the progenitor models, is more generally expected from massive stars, resulting from the break out of the shock through the stellar surface, or from the higher circumstellar density, or from Compton-scattered γ-rays. Early observations of supernovae were aimed at determining their contribution to the X-ray background. Those observations have yielded crude upper limits, generally using the *OSO-III* or *OSO-7* satellites (Figure 3). Table 2 lists the supernovae and the upper limits obtained. More recently, enhanced instrument capabilities have resulted in detections of supernovae in the X-ray band. Five supernovae resulting from massive stars have now been observed with four different X-ray satellites. The supernovae are SN 1980K in NGC 6946, SN 1986J in NGC 891, SN 1987A in the Large Magellanic Cloud, SN 1978K in NGC 1313, and SN 1993J in NGC 3031. The satellites used to observe these objects were *Einstein*, *Ginga*, *ROSAT*, and *Asuka* (*Astro-D*) and are briefly described in the appendix. Table 3 lists the relevant data for these supernovae. I discuss the X-ray observations of the five supernovae in the order in which they have been observed. I also present a portion of the history of each of the sources for context.

4.1. SN 1980K in NGC 6946

SN 1980K was discovered by Wild (1980) on 1980 October 28. An optical spectrum showed the supernova to be Type II (Kirshner, Kriss, & Berg 1980). The optical peak occurred on 1980 November 5 at visual mag 11.5. Radio emission was detected by Sramek, van der Hulst, & Weiler (1980) on 1980 December 4. A 21.7 ksec *Einstein* observation was obtained on 1980 December 11, 35 days after the optical maximum. An X-ray source was present near the optical position of SN 1980K, with SN 1980K lying within the X-ray error circle (Canizares et al. 1982) (Figure 4). This was the first potential detection of a supernova in any X-ray band. The X-ray flux on that date was approximately 1.5×10^{-13} ergs s^{-1} cm^{-2}, corresponding to a 0.5-4.0 keV luminosity[4] of 4.6×10^{38} ergs s^{-1}. (It should be noted that Canizares et al. adopted a distance to NGC 6946 of 10 Mpc while the value from deVaucouleurs (1979) is 5.1 Mpc. Hence, the value quoted in the Canizares et al. paper is a factor of 3 higher due to the different distances adopted.) An earlier 5.1 ksec observation of NGC 6946 obtained 531 days before the optical maximum yielded an upper limit of $\sim 1 \times 10^{-14}$ ergs s^{-1} cm^{-2} for the 0.5-4.0 keV flux at the position of SN 1980K. A subsequent 7.7 ksec observation 82 days after the optical maximum detected SN 1980K at a flux of 3×10^{-14} ergs s^{-1} cm^{-2}. The observations are summarized

[4]The reader must be aware that any quoted flux or luminosity is a function of the bandpass in which the measurement was made. For optical values, there is little need to cite the bandpass, because the optical band is relatively narrow in energy units, and most instruments presently available cover it relatively uniformly (this statement was not true when photographic spectra were the only ones available). In the X-ray band, however, instruments are often built to be sensitive to very different portions of the spectrum, thereby requiring that the energy band be stated.

in Table 4, with the resulting light curve shown in Figure 5.

Despite the limited number of photons, Canizares et al. constrained the spectral parameters. The color excess E_{B-V} of 0.17 was used together with an E_{B-V}-N_H relation (Bohlin, Savage, & Drake 1978; Ryter, Cesarsky, & Audouze 1975) to fix the line-of-sight column density at 1-2x10^{21} cm^2. Fits to the *Einstein* data then indicated a lower limit to the temperature for a thermal spectrum of 0.5 keV. The data, re-extracted by the author from the *Einstein* data bank and fit with a thermal bremsstrahlung model, are shown in Figure 7. The model was fit to the data with the temperature fixed at the Chevalier & Fransson predicted value, and with the column fixed at the above value, so only the normalization was varied.

The combination of an upper limit for the first observation, a $\geq 5\sigma$ detection, and the subsequent marginal detection at ~half the flux strengthened the identification of the X-ray source with SN 1980K, since the X-ray decline time of ~50 days is comparable to decline times of supernovae observed in the optical bands (Doggett & Branch 1985). Figure 6 shows a recent *ROSAT* PSPC observation of NGC 6946. A circle marks the location of SN 1980K. A knot of emission lies off-centered from the SN 1980K circle by ~7" from the optical position but within the X-ray error circle, which is ~20" in diameter. About 20 counts are detected at this position, corresponding to a flux of ~10^{37} ergs s^{-1} in the 0.2-2.0 keV band (Schlegel 1994). Chevalier & Fransson (1994) predicted a source temperature of ~0.7 keV, a 0.2-4 keV luminosity of ~7x10^{37} ergs s^{-1} at an age of 10 years. After correcting for the difference in energy bands, the prediction matches the observation quite well. Given the positional coincidence of an X-ray source with the optical position and the agreement between the predicted and observed fluxes, SN 1980K appears to have been recovered in the

X-ray band. None of the other historical supernovae in NGC 6946 (SN 1917A, SN 1939C, SN 1948B, SN 1968D, and SN 1969P) are apparent in X-rays, however. SN1968D, however, has been detected as a radio source (Van Dyk et al. 1994). Upper limits on the X-ray emission from these sources are given in Schlegel (1994).

The observations of X-rays from SN 1980K, while insufficient to delineate a particular model for the production of X-rays, did produce at least two fruitful results. First, they essentially eliminated supernovae as contributors to the diffuse X-ray background, as had been suggested earlier by Tucker (1970) and Silk (1973). The time-averaged X-ray output of a supernova clearly fell several orders of magnitude below the time-averaged output of an X-ray binary, for example. In a recent re-analysis, Chugai (1992) shows that the 3-100 keV flux of supernovae contribute at most ~5% to the diffuse X-ray background. Second, the observed radio flux from SN 1980K (Sramek, van der Hulst, & Weiler 1980) implies that inverse Compton losses are *not* large, so the amount of inverse Compton scattering occurring must be small. One of the proposed mechanisms for X-ray emission from supernovae, specifically, inverse Compton scattering, died as a result of these observations.

4.2. SN 1987A in the Large Magellanic Cloud

The spectacular detonation of SN 1987A on 1987 February 23.316 in the Large Magellanic Cloud (LMC) spurred numerous efforts to observe the closest supernova in a century. The X-ray band was no exception. The fortuitous launching of *Ginga* (1987 February 5) just weeks prior to the detonation placed an X-ray detector, with the largest effective area flown to date (~4000 cm^2, Makino 1987), in the right place at the right time. Observations commenced

immediately after the optical discovery, but the data only yielded upper limits on the emission from the supernova (Tanaka 1989; Inoue et al. 1991). The observations were performed in two modes to avoid one of the brighter X-ray sources in the LMC (LMC X-1, a black hole candidate): a slow scan mode across the SN 1987A and LMC X-1 positions, and pointed observations approximately 1 degree offset from LMC X-1.

The first detection in 1987 August required considerable work as a result of the contamination from the neighboring sources. The source centroid, for example, corresponded with the position of LMC X-1 for energies below about 10 keV. The centroid shifted toward the position of SN 1987A for increasing energy, essentially corresponding to the optical position of SN 1987A above 15 keV. Potential contamination from other bright X-ray sources in the LMC also decreased with increasing energy. The X-rays from SN 1987A were not present in April 1987, but were present in 1987 August, so the emergence had to occur between May and July 1987 (Makino et al. 1987a; 1987b). Careful pointings were made at the positions of known sources (from Long, Helfand, & Grabelsky 1981) to obtain the X-ray spectra of these sources. None contributed significantly above 15 keV, and the contamination was limited to about 40% above 6 keV. Table 5 lists the soft (relative to the *Ginga* energy coverage) band observations while Table 6 lists the hard band observations. Figure 8a shows the soft band *Ginga* light curve, covering the 5.8-16.1 keV band, while Figure 8b shows the hard band light curve (16.1-27.8 keV). (An approximate flux conversion is that 1 count s^{-1} equals, for the soft band, $\sim 4.6 \times 10^{-12}$ ergs s^{-1} cm^{-2}, and for the hard band, $\sim 32 \times 10^{-12}$ ergs s^{-1} cm^{-2} (Inoue et al. 1991).) The peak count rate in the "flare" corresponds to a hard band luminosity of $\sim 2.4 \times 10^{37}$ ergs s^{-1}. The turn-on is evident, and the remaining light curve is

approximately steady with the exception of the flare-like behavior that occured on 1988 January 7. The hard light curve is essentially identical in behavior (Tanaka 1989; Inoue et al. 1991).

Spectra of SN 1987A were accumulated in three states based upon the X-ray light curve: the faint state, the flaring state, and the phases of approximately constant flux. The faint and constant state spectra are essentially indistinguishable (Tanaka 1989; Inoue et al. 1991) and clearly require at least 2 components to describe them. The hard component of the spectra appears to be constant and requires a cutoff for photons with energy less than about 20 keV. The soft component appears best described by a thermal bremsstrahlung model of kT $\sim$10 keV. The flaring spectrum also appeared to contain the hard component of the other spectra, but, in addition, required a hotter bremsstrahlung component, with kT $\sim$50 keV. An iron line was seen, particularly in the flare, at $\sim$6.8$\pm$0.2 keV with an equivalent width of $\sim$200 eV. The hard component intensity was essentially constant within the errors throughout the time covered by the light curve. This constancy suggests an essentially constant or slowly decreasing energy source as would be provided by, for example, radioactive decay. Figure 9 shows the average overall spectrum at an age of $\sim$0.7 years.

Theoretical predictions for the date when the expanding envelope would become transparent to X- and γ-rays generally landed near the first birthday of the outburst (e.g., Pinto & Woosley 1988). Monte Carlo simulations showed that no flux was expected below $\sim$10 keV due to the high photoelectric opacity. The predicted spectrum was expected to peak around 15-20 keV and then to decline everywhere except for the development of lines in the "few" MeV range. The spectrum was to be dominated by lines by the second birthday of SN 1987A.

Theorists were thus somewhat surprised when *Ginga* detected X-ray photons from SN 1987A at day 154 (Dotani et al. 1987); a ready explanation was, however, available. The early detection of X-rays required a mixed envelope, so that some fraction of ^{56}Ni resided in the H-rich envelope. Mixing radioactive ^{56}Ni into the H-rich envelope lowers the X- and γ-ray optical depths. Mixed models predicted a rapid decline in the hard *Ginga* band (16-28 keV) after about 300 days due to the increasing transparency of the envelope to γ-ray line emission. The increasing transparency decreases the Compton scattering, thereby decreasing the production of X-rays detectable to *Ginga*. SN 1987A, again contrary to theoretical expectations, slowly declined in the 16-28 keV band after 300 days (Tanaka 1989; Inoue et al. 1991). Detailed models (Kumagai et al. 1989) resolved the problem by proposing that in addition to the mixing of ^{56}Ni into the H-rich envelope, the ^{56}Ni was also clumped. The clumping reduced the effective opacity, thereby allowing X-rays to escape, yet locally, the opacity was large to prevent the easy escape of the γ-rays in the lines.

While the observations in the hard band could be understood, the same was not true of the soft band. The photoelectric opacity is too large below $\sim$20 keV for photons with energies less than 20 keV to escape easily from the nebula (e.g., Kumagai et al. 1989), yet photons with energies as soft as $\sim$5 keV were detected. One model that does work is the interaction of the outgoing ejecta with a circumstellar medium that existed very close to the progenitor. The spectrum and intensity of the 5-16 keV photons are consistent with such an interaction (Itoh, M. et al. 1987; Masai et al. 1987, 1988). It is also possible that the soft X-rays are a contaminant from sources near SN 1987A (e.g., the black hole candidate LMC X-1 has a strong soft X-ray component (Schlegel et al. 1994)).

Other instruments also observed SN 1987A during that first year. For example, the HEXE experiment (Na I/Cs I phoswich scintillators), covering the 15-250 keV band first detected SN 1987A in 1987 August (Sunyaev et al. 1987). The Pulsar-1 experiment, which covered the 50-1000 keV band, was able to refine the high energy spectrum. The low-energy telescope (2-32 keV) reported upper limits below 20 keV, but the data may not be adequately calibrated. Other experiments failed to detect SN 1987A: the detectors aboard the *Mir* space laboratory were pointed at SN 1987A, but without any detections with the Coded Mask Imaging Spectrometer (2-32 keV) (Sunyaev et al. 1990). In addition to these experiments, several ballon and rocket flights also occurred, with varying degrees of success (Sutherland 1990).

There are two observational issues now for SN 1987A: the detection of the predicted X-ray resurgence that should result when the outgoing shock hits the known circumstellar envelope blown during the red giant mass loss phase, and the detection of the pulsar. The *Broad Band X-ray Telescope (BBXRT)* was flown on the space shuttle *Columbia* in 1990 December. One of the prime targets was SN 1987A. No photons were detected above the local background. The 90% upper limit in the 2-10 keV band is 1.4×10^{35} ergs s^{-1} (Serlemitsos et al. 1991) assuming a distance to the LMC of 50 kpc.

Recently, two groups have claimed to have detected what may be the start of the X-ray resurgence of SN 1987A (Gorenstein et al. 1994; Beuermann et al. 1994) using *ROSAT*. Table 7 lists the observations of Beuermann et al. Both groups assume the positional coincidence of an X-ray source with the position of SN 1987A to mark the re-emergence. Gorenstein et al. examine the possibility that the source is not SN 1987A but is instead an X-ray binary (specifically, a Be star). They conclude the probability is small (~3%). Both groups obtain a

temperature of ~0.5-0.7 keV by fitting the extracted spectrum of the source. This temperature is approximately the value expected if the emission results from circumstellar interaction. The 0.5-2.0 keV luminosity is $\sim 10^{34}$ ergs s^{-1}.

Whether these observations do indicate the re-emergence of SN 1987A because of circumstellar interaction effects, or because of the presence of a pulsar, will only be known with certainty after additional observations. Once the presence or absence of a trend in the X-ray light curve is established, the identification of the source will be known. If the source is SN 1987A, the X-ray flux should increase as the shock overtakes the dense wind from the red giant mass loss phase (Chevalier 1988; Chevalier & Liang 1989). If the source is an X-ray binary, the flux may be variable, but broadly constant in time. An observation, obtained soon after the launch in 1990, apparently did not detect SN 1987A, suggesting input from a pulsar is less than $\sim 10^{37}$ ergs s^{-1}, according to the Kumagai et al. models. The models suggest the pulsar signal will become stronger over the next few years as the nebula thins, but then start to fade as the pulsar loses energy.

4.3. SN 1986J in NGC 891

SN 1986J was first discovered in the radio (Rupen et al. 1987) and rapidly became the brightest radio source in NGC 891. Optically, the supernova was clearly well-evolved, showing only narrow emission lines characteristic of a supernova at least several hundred days beyond the outburst. The strong radio emission suggested an interaction with a dense circumstellar environment, leading to a prediction for a bright X-ray phase (Chevalier 1987).

SN 1986J was observed with the *ROSAT* PSPC on 1991 August 18-20 for 24.9 ksec (Bregman & Pildis 1992). A strong source was visible in the field

near the optical position of SN 1986J. A slight offset in the pointing position of *ROSAT* was corrected by examining other known X-ray sources, with the result that the optical and radio positions of SN 1986J were well within the *ROSAT* error circle. Weak emission from NGC 891 itself was present, contaminating the emission from SN 1986J. A circular region smaller than the point spread function was used to extract the photons (Bregman & Pildis 1992); the extracted counts were then corrected for the missing fraction of the total counts, for a point-like source, that fell outside of the circular region. The extracted spectrum showed essentially no emission below ~0.65 keV. A thermal bremsstrahlung model was fit to the spectrum, yielding essentially two equally good fits (Bregman & Pildis 1992): a low kT-high N_H solution (kT ~0.5 keV, log N_H ~22.3) and a high kT-low N_H solution (kT ~1.8 keV, log N_H ~21.8). The data were extracted from the *ROSAT* archive (by the author) and refit, yielding the spectrum shown in Figure 10a; the contours are shown in Figures 10b and 10c. Figure 10c shows the low kT-high N_H solution in somewhat greater detail. As Bregman & Pildis (1992) point out, the dual solutions exist because of the low spectral resolution of the PSPC, and because, at low temperatures, L-shell lines of Fe are very strong and, when heavily absorbed, can not be distinguished from a higher temperature plasma. The integrated luminosity in the 0.1-2.4 keV band is ~2-3x10^{40} ergs s^{-1}, assuming a distance to NGC 891 of 10 Mpc.

The lower temperature solution is consistent with the blast wave interaction model of Chevalier & Fransson (1994), while the higher temperature solution is not. On that basis, Bregman & Pildis (1992) suggested that the X-rays from SN 1986J were produced by the inward-moving shock from the interaction of the blast wave with the circumstellar medium. The inward-moving shock produces a dense, cool (~10^7 K) shell. The model then accounts for the observed high

column, N_H $\sim$2x10^{22} cm^2, about 2.6 times larger than the neutral hydrogen column observed in the radio and used to correct the optical spectroscopy. The higher column is partly the galactic column in the direction of NGC 891 and largely the cool, dense shell behind the reverse shock.

The detection of radiatively cooled material behind the shock, if verified, will be the first such observation in the X-ray band. X-ray data could, in principle, be used to infer the density distribution of the circumstellar medium prior to the supernova outburst, an important quantity useful in modeling the evolution of the blast wave (e.g., Chevalier & Fransson 1994; Suzuki et al. 1993a). Verification of the detection of the radiatively cooled material can be achieved by observing the temporal development of the spectrum, which should show a decline in the absorption column as the shell moves through the cool material, or by detecting absorption edges in a high resolution spectral observation, such as should be possible with *Asuka*. Either way, the low energy spectrum should gradually be unveiled.

Chugai (1993) has put forward an alternative view, namely that the X-ray emission arises from a shocked, clumpy wind. A large mass loss rate is required ($\dot{M} \sim 10^{-4}\ M_\odot\ \mathrm{yr}^{-1}$) but with a filling factor of $\sim$5x10^{-3}. Chugai's argument is that the upper limit on the wind density parameter in the double shock and spherically symmetric wind model leads to an inconsistency in the maximum luminosity available. Specifically, the observed luminosity is $\sim$5 times higher than the best-possible predicted value. Instead, in Chugai's model, the expanding ejecta overtake clouds in the wind and drive shocks into the clouds. Chugai cites the optical-X-ray flux ratio of $\sim$1% as evidence for his model (the double shock model should generate a higher value of the ratio). In addition, the clumpy wind naturally accounts for the increased absorption as

the covering factor of the clouds is relatively large (Chugai estimates ~0.4.). Thus, the "excess" absorption observed by Bregman & Pildis is reduced by the covering fraction and becomes consistent with the galactic column in the direction of NGC 891. Additional observations will be necessary to establish the correct interpretation. Some support for Chugai's position comes from the radio observations of SN 1986J that can not be fit by a single, external, thermal absorbing model used for all previous radio supernovae, but can be fit by a mix of thermal absorbers and non-thermal emitters (Weiler, Panagia, & Sramek 1990).

4.4. SN 1978K in NGC 1313

The *ROSAT* PSPC observed NGC 1313 between 1991 April 24 and May 11 for 11.2ksec. Three sources were present: the nucleus (or, at least, a source near the nucleus), a source about 7' south of the nucleus, and a source 11' southwest of the nucleus (Figure 11). The *Einstein* IPC data on NGC 1313, obtained on 1980 January 2 with an exposure of 8.3ksec, were examined for any apparent changes. Two sources were seen in the *Einstein* data (Figure 12), corresponding to the nucleus of NGC 1313 and the source south of the nucleus. The third source in the *ROSAT* data has now become known as SN 1978K (Ryder et al. 1993; Ryder et al. 1992).

In a sense, SN 1978K can be considered as the first X-ray discovered supernova. The original report on the optical spectrum of the source claimed it was an old nova (Dopita & Ryder 1990). The implied X-ray luminosity (to be presented below) plus the optical spectrum, which shows narrow lines of hydrogen, oxygen, helium, nitrogen, and iron, suggested a nova interpretation was incorrect. Furthermore, an intense radio source was discovered to be

coincident with the third X-ray source and the optical position of the purported nova. An optical light curve was constructed from archival photographic plates of NGC 1313 which established that an outburst had occurred in 1978 May/June (Ryder et al. 1993). These observations, when assembled, reinforced the supernova interpretation. For additional details, see Ryder et al. (1993).

The *ROSAT* spectrum of SN 1978K was extracted and fit with several models from which no one model was preferred over the others. The power law fit was uncharacteristically steep for an X-ray source, with an exponent of 5.5. A fit using a Raymond-Smith plasma required very low abundances (Z ~0.017 $Z_{\odot}$[5]. The thermal bremsstrahlung model gave a fitted temperature of ~0.5 keV, similar to that of SN 1986J. The fitted spectrum is shown in Figure 13a and the contours are presented in Figure 13b. Again, the column to the X-ray source is quite high, lying about a factor of two above the 21-cm neutral hydrogen column density in the surrounding region (Ryder et al. 1995). The difference is most likely the absorption of X-rays through the shell of cool material behind the reverse shock. We can again potentially observe the change in the shell position with time by observing the changing column in the fitted spectrum with additional observations. Note, however, that the arguments of Chugai (1992), presented above for SN 1986J, could equally apply to SN 1978K. A covering fraction of ~0.5 would bring the observed absorption column into agreement with the galactic column. The unabsorbed luminosity in this spectrum is ~9.5x10^{39} ergs s^{-1} (Ryder et al. 1993) assuming a distance to NGC 1313 of 4.5 Mpc (de Vaucouleurs 1963).

---

[5]'Z' is the abundance of all of the elements ("metals") except hydrogen (X) and helium (Y), normalized so that the sum X + Y + Z equals 1.0.

A second epoch of *ROSAT* PSPC observations was obtained in November 1993. The fitted spectral parameters were, within the errors, consistent with the April 1991 observation. The harder portions of the PSPC band, however, were weaker, suggesting a drop in temperature or an increase in the soft band flux, as would result from a drop in the absorption column. Unfortunately, the spectral resolution and signal-to-noise ratio were sufficiently poor that either conclusion remains valid.

Luckily, because the long-term light curve is of considerable interest, SN 1978K is evolving while X-ray satellites are in orbit. An upper limit can be assigned to the *Einstein* IPC data as was done for the upper limit on X-ray emission from the Type Ia supernova SN 1992A (Section 3 above). The resulting value is 2×10^{39} ergs s^{-1} in the 1.0-2.0 keV band, a factor of $\sim$4 less than the *ROSAT* luminosity.

Serendipitously, SN 1978K lies in three other *ROSAT* pointings in addition to the two PSPC pointings described above, so a light curve can be constructed (Schlegel et al. 1995). The pointings include one HRI observation obtained on 1992 April 18 and two PSPC exposures obtained on 1990 July 23 and 1991 March 18. All of the observations are listed in Table 9. The two PSPC points were centered on HD 20888, so SN 1978K appears about 20' off-axis, very near the main window support ring of the PSPC. The detected counts from SN 1978K in these two PSPC points must be compensated for the occultation induced from the main support ring and ribs of the PSPC window.

To generate a light curve, the spectra of the three NGC 1313 sources (the "nuclear" source, the probable X-ray binary (XRB), SN 1978K) were extracted. The observations that were made off-axis were corrected for the vignetting of the telescope. There were insufficient counts in many of these spectra to

obtain spectral parameters of any significance. These spectra can, however, yield an observed flux at the observation epoch. A spectral model that provides a reasonable fit to the April 1991 and November 1993 observations was used to obtain fluxes from all of the spectra. These fluxes then represent the best light curve possible. Fluxes were calculated in the energy bands 0.5-2.0 keV and 1.0-2.0 keV. The second band overlaps the *Asuka* flux and also provides a measure of the change in absorption when compared with the 0.5-2.0 keV flux, particularly when the comparison is made over time. This procedure was repeated for the nuclear source and the XRB. These two sources can be used to provide a check on the flux stability of the observations.

The light curves are shown in Figures 14, 15, and 16. Figure 14 shows the 1.0-2.0 keV light curve of SN 1978K, solely based upon the recent observations by *ROSAT* and *Asuka*. Clear evidence for evolution is not present. Figure 15 shows the corresponding light curves for the nuclear source and the probable XRB. A comparison of Figures 14 and 15 demonstrates that the variations are not common to all three sources, so systematic errors from epoch to epoch are not present. Statistically, both the nuclear source and the XRB have varied (Petre et al. 1995). Figure 16 again shows the SN 1978K light curve, but now including the *Einstein* upper limit. Any variation that may have been deduced from Figure 14 can be seen to be a sample of a very small interval in Figure 16.

The decay of the light curve can place limits on the exponent of the power law that is used to describe the ejecta. The expected time dependence of the light curve in the adiabatic phase is $L \sim t^{-\alpha}$, with α [(2s-3)n - 5s + 6] / (n-s) (Fransson et al. 1995), with s and n defined as $\rho \sim r^{-s}$ for the circumstellar matter, and $\rho \sim r^{-n}$ for the supernova ejecta. Usually, s=2, but observations of SN1993J suggest s=1.5 is more appropriate. A fit to the SN1978K light curve

gives $\alpha = 1.37 \pm 3.40 \times 10^{-3}$ (90% confidence range) (Schlegel et al. 1995). For s=2, the value of α implies n $\sim$4. As s approaches 1.5, n becomes larger. The Chevalier-Fransson model of circumstellar interaction requires n < 9 in the adiabatic phase, but n > 8 if radiative cooling is important. Radiative cooling is important for $\sim$0.4, $\sim$24, and $\sim$500 years for n=7, 12, and 20, respectively. If we assume SN1978K has been radiating for $\sim$10-15 years, then n $>$10. Because a constant luminosity (as indicated by the value of α) is consistent with either the radiative or adiabatic phases, the current light curve does not permit us to infer the evolutionary phase of SN1978K.

A preliminary analysis of the July 1993 *Asuka* spectrum (Petre et al. 1994) shows no evidence for strong line emission. No narrow lines exist with equivalent widths >70 eV. No iron lines are present at 6.4 keV (cold Fe) nor at 6.7 keV (ionized Fe) with an upper limit of 1 keV. The continuum is consistent with a power law of index 2.5 or a thermal bremsstrahlung spectrum of kT $\sim$2.4 keV with non-solar abundances (about 25% of solar). These values differ sufficiently from the 1991 *ROSAT* PSPC data (Ryder et al. 1993) that the strongest conclusion inferred from the data is that the spectrum must be evolving rapidly. In the 1-2 keV band common to the *Einstein* non-detection and the *ROSAT* and the *Asuka* observations, the flux of the *Asuka* observation is below the *ROSAT* flux. Petre et al. interpret the lack of lines as the result of the extreme non-equilibrium ionization (NEI) conditions present in the ejecta. Between the *ROSAT* and *Asuka* observations, the spectral index has decreased while the column density increased. This behavior will occur as the shock approaches the outer boundary of the circumstellar envelope. We then expect the flux to drop rapidly as the shock exits the immediate circumstellar envelope, perhaps in the next few years. Continuing observations are planned.

4.5. SN 1993J in NGC 3031 (M81)

The newest member of the X-ray detected supernovae happens to be the second closest member and the brightest northern hemisphere supernova since SN 1937C. The supernova was discovered on 1993 March 28 by Ripero (1993). An optical maximum occurred on 1993 March 28. The supernova declined rather quickly and then recovered to a second maximum, reminiscent of the light curve behavior of SN 1987A (Catchpole et al. 1987). The supernova was classified as a Type II once the hydrogen lines became readily apparent, however, nearly a week went by before the spectrum had any substantially strong features (Wheeler 1993). The progenitor of SN 1993J was identified early (Humphreys et al. 1993), making SN 1993J only the fourth supernova for which the progenitor has been identified (1: SN 1961V in NGC 1058; 2: SN 1987A in the LMC; 3: SN 1978K in NGC 1313). The progenitor appears to be a slightly reddened (E_{B-V} <0.1) K supergiant. The apparent fading of the Hα line (Filippenko & Matheson 1993) suggests behavior similar to SN 1987K (Filippenko 1988), prompting additional observations to understand the apparent "Type IIb" supernovae (Wheeler & Harkness 1990). SN 1987K started out showing a spectrum typical of Type II supernovae. Within a few months, however, the hydrogen emission lines had faded and were replaced with the [O I] 6300Å complex. [O I] lines are a signature of a Type Ib supernova (e.g., Schlegel & Kirshner 1989), hence the designation "IIb". Nomoto et al. (1993) show that the likely progenitor of SN 1987K is a hydrogen-stripped, evolved star in a binary system. The progenitor of SN 1993J may be similar.

Weiler et al. (1993) reported the radio detection of SN 1993J on 1993 April 2.3, just ~4 days after the explosion. By age ~95 days, the 6 cm flux density had increased to 50 mJy, with no sign of a turnover (Van Dyk et al.

1993). Such a strong radio emitter suggested a potential for detecting X-rays. SN 1993J coincidentally entered the observing windows of *ROSAT*, *ASCA*, and *GRO* (*G*amma-*R*ay *O*bservatory) at a very propitious time. Hence, SN 1993J must be accorded another highlight: it is the first supernova to be observed and detected with two X-ray satellites and a γ-ray satellite, all orbiting at the same time. The first observation was obtained with *ROSAT* (Zimmermann et al. 1993a) in a 2.8 ksec exposure on 1993 April 3.4 (UT). An X-ray source was visible within 10" of the optical position and ~1' north of a known X-ray binary (X6 of Fabbiano 1988). The extracted spectrum, shown in Figure 17b, is rather flat, consistent with either a power law having a photon index of -0.7 or a thermal spectrum with kT >7 keV (Zimmermann et al. 1993b). Using the *Hubble Space Telescope* Cepheid distance to M81 of 3.63±0.34 Mpc (Freedman et al. 1993), the corresponding luminosity in the 0.1-2.4 keV band is 3×10^{38} ergs s^{-1}. Based upon different assumptions, with an adopted distance to M81 of 3.25 Mpc, Zimmermann et al. quote a value of 1.6×10^{39} ergs s^{-1} for the same energy band. The fitted column is consistent with the galactic column, implying either that no additional absorption near the source is necessary, or that the absorbing matter near the source has been completely ionized. The second case predicts the emergence of emission lines once the matter recombines.

The second observation, occurring on 1993 April 5 and 6, was made with *Asuka* (Tanaka 1993) in a 37 ksec exposure with both the X-ray CCD spectrometer and the gas scintillation spectrometer. An X-ray source was found within 0'.1 of the optical position. The spectrum is described as "hard; if it is a thermal bremstrahlung spectrum, kT >10 keV and N_H is about 10^{21} cm^2" (Tanaka 1993), which matches the results of Zimmermann et al. who found only a lower limit to the *ROSAT* data of kT ~7 keV. A fitted spectrum to the *Asuka*

data yields a kT of ~200±420 keV[6] and an iron line present at 6.3±0.1 keV. No other spectral features appear to be present. The iron line has definitely been shown not to arise from the X-ray binary that lies 1' away. Early iron line emission is suggestive that the γ-ray transparency has decreased sufficiently that the envelope permits iron-line photons to escape or that iron has been mixed outward in the progenitor before detonation.

Additional *ROSAT* observations were made on 1993 April 7, 9, 10, 12, and 13 (Zimmermann et al. 1993c), with each exposure lasting between 1 and 3 ksec. Table 10 lists the pointings. The count rates showed a decrease of about 30% in the days between the first and last observations. implying a decay time of a few weeks to a few months. Another observation (Zimmermann et al. 1993d) was made when the supernova re-entered *ROSAT*'s observing window on 1993 November 1-2. The count rate had decreased to ~0.035 counts s^{-1} from ~0.054 counts s^{-1} in the May observation, but not as much as expected from a linear extrapolation of the earlier decline. The spectrum had softened considerably, from a lower limit of 7 keV to ~0.5 keV. The column absorption increased from the early value of about $5x10^{19}$ cm^{-2} to $3x10^{21}$ cm^2. A 2 ksec observation with the *ROSAT* PSPC detected SN 1993J on 1994 April 4 at ~0.018 counts s^{-1} in the 0.1-2.4 keV band. The data continue the trend: the temperature decreases while the absorption column increases. The linear decay rate continued. Finally, a 20 ksec observation with the *ROSAT* HRI in 1994 October 19-21 (Zimmermann et al. 1994b) detected a mean count rate of $7.2x10^{-3}$ s^{-1}; assuming that the X-ray spectrum has not changed, this count rate corresponds to an essentially

[6]The error value is correct: the spectrum is very hard, but the limited bandpass (~0.5–10 keV) of *Asuka* can not assign a definitive temperature.

constant source from the April observation. The X-ray light curve is shown in Figure 17a. This light curve will clearly be the definitive X-ray light curve of the early phase of X-ray emission from a supernova for some time to come. It supersedes the crude light curve obtained by the *Einstein* IPC for SN 1980K (Figure 5). An explanation of the light curve using the circumstellar interaction model has been made by Fransson, Lundqvist, & Chevalier (1995).

Very hard X-rays were detected from SN 1993J using the OSSE detector on *GRO* (Leising et al. 1994). The OSSE instrument covers the 0.05-10 MeV energy range. The detected spectrum was consistent with a temperature of kT ~82 keV; it is constrained on the low side to be >40 keV, but high temperatures are not constrained. The light curve is consistent with the outburst date and with the flux declining with a ~60-80 day e-folding time. Leising et al. note that the simplest interpretation of the data suggests the existence of high density clumps in the ejecta. This picture is similar to the model Chugai (1993) proposed for the X-ray emission of SN 1986J. Other explanations are also possible, so the need for additional data is clear.

Models of the X-ray emission have been computed by Suzuki et al. (1993a). The models that explain the optical light curve are those that have a thin hydrogen envelope ejected at relatively high velocities (~few x 10^4 km s^{-1}) (Nomoto et al. (1993)). Rayleigh-Taylor instabilities occuring during the propagation of the shock then mix some ^{56}Ni and ^{56}Fe into the envelope. The presence of radioactive nuclei in the hydrogen envelope then accounts for the optical light curve and allow some γ-rays and Compton-degraded X-rays to escape. This phase occurs somewhat late in the evolution of the supernova (~100 days past maximum). The early X-rays, however, are produced by the outgoing shock running into the dense circumstellar medium, which for

SN 1993J, is apparently extreme. The X-rays arise from thermal bremsstrahlung from the shocked ejecta. Suzuki et al. predict the softening of the X-ray spectrum as the reverse shock decays as it runs into the steep density gradient of the expanding ejecta. Finally, a helium-like Fe line is expected at ~6.7 keV which should increase in contrast as the supernova ages (since the continuum emission declines). Additional emission is expected due to Fe L emission, as well as Si and O lines. Zimmermann et al. (1994c) show that the Suzuki et al. model predicts a faster decline than the observed one. Additional modeling must be be performed to see if the predicted decline is truly discrepant with the observations.

4.6. Other Massive Supernovae

Any supernova detected in the radio band is a good candidate for detection in the X-ray band. Radio emission is potentially a good predictor of X-ray emission because the X-ray luminosity is proportional to the square of the circumstellar matter density. If a source is detected in the radio, X-ray emission ought to follow. Table 11 lists possible additional targets, but the prospects are not particularly good, for various reasons, of obtaining useful data on many of these.

Simple radio detection, for example, while necessary, is apparently not sufficient as a predictor. SN 1968D in NGC 6946, recently detected in the radio (Van Dyk et al. 1994) is not visible in the *ROSAT* PSPC data of nearly the same epoch (Schlegel 1994). There is insufficient data as yet, furthermore, to match X-ray light curves against radio light curves to see if there is a correlation. This will clearly be an important topic for predicting which supernovae to study and when to best observe them. The demonstration of such a correlation may

be crucial, for example, to study the X-ray turn-on phase. X-ray observing time will limit the amount of data acquired. The distance to SN 1988Z is sufficiently large (~90 Mpc) that the expected X-ray flux will be low; the necessary exposure time for a 5σ detection is ~200 ksec with the *ROSAT* HRI. SN 1982AA (Yin 1994) in Markarian 297 may have been detected in a *ROSAT* PSPC exposure, but source confusion is a distinct possibility. An HRI observation will resolve the issue of its detection. If the detection is confirmed, SN1982AA will be the sixth supernova showing X-ray emission. An upper limit of $\sim 10^{38}$ ergs s^{-1} exists for SN 1981K in NGC 4258, based upon a 7.2 ksec exposure using *ROSAT* (Pietsch et al. 1994).

SN 1994I in NGC 5194 (=M51) was not detected in a 10 ksec *ROSAT* HRI observation 53^d after outburst (Lewin et al. 1994). At the assumed distance of 7.7 Mpc, the 95% flux upper limit in the 0.1-2.4 keV band of 2.1×10^{-14} ergs s^{-1} cm^{-2} translates to a luminosity upper limit of 1.5×10^{38} ergs s^{-1}. The values are not sensitive to the assumed model. This upper limit on the X-ray luminosity of a supernova that has been detected in the radio (Rupen et al. 1994a, 1994b) is ~10 times lower than the observation of SN 1993J at the same epoch. The different behaviors implies a that simple radio detection, an indicator that a circumstellar medium exists, is not necessarily a good predictor of X-ray emission, yet both radio and X-ray emission are explained by the circumstellar interaction model.

5. Summary Discussion

The observations detailed in the above section point out the wide variety of behavior seen to date in the X-ray observations of supernovae. Here I summarize the observations by looking at the X-ray emission from the entire class of

supernovae. A connection to supernova remnants (Figure 18) is also examined. Five supernovae have been detected, having produced X-rays by at least two, and possibly three, different emission mechanisms. Gone is the inverse Compton scattering model. The pulsar-nebula interaction model has been developed more widely, but, without observations demonstrating the effects of pulsar input, the model remains untested. So far, only Type II supernovae have been detected as X-ray sources.

The observations and the remaining models can be divided into short-term and long-term behaviors. The criterion is the time elapsed since the outburst, with short-term mechanisms dominant on times of weeks, while the longer-term mechanisms operate after months or years and over times of months or years. This division is not mutually exclusive, as a given supernova can land on either side of the boundary at different phases in its evolution. The short-term mechanisms include prompt thermal emission and the initial shock interacting with a dense, very nearby, circumstellar medium. The long-term mechanisms include Compton-scattered γ-rays from the nuclear decay products produced in the detonation and the interaction of the blast wave with the circumstellar medium.

Of the emission mechanisms considered likely as explanations for the X-ray emission of supernovae, only one is firmly established. The appearance of hard X-rays in SN 1987A could have had several causes, but the gradual disappearance of the X-rays and the infrared ^{56}Ni lines roughly concurrent with the gradual appearance of the γ-ray lines from ^{56}Ni (847 keV, 1238 keV, etc.) confirms the Compton scattering of γ-rays as the production mechanism of the X-rays. The soft X-rays (those below $\sim$15 keV) from SN 1987A, however, are unexplained by this mechanism, and are most likely due to the ejecta impacting

some small quantity of circumstellar matter.

Circumstellar interaction almost certainly accounts for the early X-ray emission observed from SN 1980K and SN 1993J; the lack of early (first ~50 days) X-rays from SN 1987A can also be explained by the low quantity of circumstellar matter. The progenitor of SN 1987A was a blue supergiant, a type of star known to have a low density, high velocity wind. For SN 1987A then, there was no nearby circumstellar medium. In contrast, SN 1993J was detected about 6 days after maximum light. The most likely explanation is that the immediate surroundings of the progenitor of SN 1993J were filled with matter, perhaps from a dense slow wind from a red giant progenitor or as a result of Roche lobe spillage in a binary system.

Initial models (Fransson, Lundqvist, & Chevalier 1995) for the expanding atmosphere, based upon radio observations at different frequencies, require steep density profiles (power law index n >15) to explain the spread in turn-on times of SN 1993J. Fransson et al. show that the X-ray observations also require a steep density profile, under the assumption that the X-ray emission is emitted by the reverse shock. Such steep density profiles were not considered reasonable prior to the SN 1993J observations. Furthermore, the X-ray and radio data also suggest that the circumstellar matter is distributed as $\rho \sim r^{-1.5}$, and not as r^{-2} as is usually assumed. The shallower gradient implies episodes of mass loss, or a geometric effect. The expected profile of uniform, spherical mass loss is r^{-2}; if the mass loss occurs in a plane, for example, the profile should vary as r^{-1}.

The late-time behavior of SN 1986J and SN 1978K requires the interaction of the blast wave with the circumstellar medium. The issue to be addressed by future observations is the exact nature of the interaction. Specifically, does the swept-up mass reveal itself in the X-ray spectrum? The *ROSAT* observation of

SN 1986J argues that it does in the form of increased absorption. An *Asuka* observation should reveal absorption edges of relevant species, such as oxygen and silicon. The data have not yet appeared.

One goal of observations of supernovae is the connection of the detonating star with the visible remnant (van den Bergh 1988). Very little is known about the evolution of supernovae from ~2 years to the ages of the youngest known remnants (for example, Tycho, ~300 years; NGC 4449 remnant, ~150 years). This gap is illustrated in Figure 18 which shows the evolution curve of the X-ray emission at 2 keV from several observed supernovae and known galactic supernova remnants. The energy of 2 keV was chosen because, at this energy, the absorption column to the source will not generally affect the spectrum (unless the source is pathological), yet the energy of 2 keV lies within the observing band of essentially every X-ray satellite lofted or planned. This curve is similar in form to the curve of radio evolution at 4.88 GHz (6 cm) presented in Weiler et al. (1986). We can see at a glance the enormous range in behavior of the few supernovae detected in the X-ray band. The first point for SN 1987A essentially represents its maximum flux at 2 keV; the second point represents SN 1987A upon rediscovery. The calculated luminosity is at least 2 orders of magnitude below that of SN 1980K. The evolution of SN 1987A is also considerably slower than that of SN 1980K. In addition, the 2 keV evolution curve shows that, unless there is a dramatic resurgence in X-ray luminosity, it is very unlikely that SN 1987A could evolve into a remnant similar to the well-known Galactic remnants. We should shortly be able to add data from SN 1986J and SN 1993J to this plot.

6. The Future

What is the future of X-ray observations of supernovae? In two words, quite good.

The observations of SN 1993J by *Asuka* will certainly cover the gap in our understanding of the early emission of X-rays from at least one massive star. Unfortunately, SN 1993J has revealed itself to be yet another "peculiar" Type II supernova (a Type IIb supernova, which is a supernova that has a thin hydrogen shell, so that when it detonates, it looks like a Type II supernova. After about 50 days, the hydrogen lines fade and the oxygen lines become prominent, as with a Type Ib supernova), but it will be valuable in producing detailed observations with which to test models of immediate circumstellar interaction. However, the vast majority of Type II supernovae have yet to be studied in any detail in the X-ray band. We must await another bright, normal Type II supernova before testing our models of circumstellar interaction in more typical conditions.

SN 1987A is expected to become an X-ray source again when the blast wave hits the circumstellar ring, as first predicted by H. Itoh et al. (1987), or when the pulsar emerges from the debris. *ROSAT* may have recovered SN 1987A (Gorenstein et al. 1994; Beuermann et al. 1994), but the observations have yet to be confirmed. Relatively detailed predictions have been published by Suzuki, Shigeyama, & Nomoto (1993b) which show the expected X-ray behavior at 10, 20, and 30 years after the detonation. Whether *Asuka*, *XTE*, *Spectrum X-*Γ, *XMM*, or *AXAF* are operational by that time remains to be seen. Any one of these satellites should provide sufficient photons to constrain detailed models of the emission mechanism.

Observations of SN 1978K with *Asuka* will provide basic input to the blast wave interaction model, although the supernova is sufficiently faint that the spectral details may not be adequately resolved. Continuing observations

with *ROSAT*, particularly the HRI, will provide a light curve to compare to theoretical predictions. A start at the light curve has been made (Schlegel et al. 1995). The satellites now in orbit, plus those planned for the next decade, should provide a sufficiently long baseline for the evolution to be apparent.

SN 1980K appears to have been recovered, perhaps just before fading beyond the capabilities of current X-ray instruments. Definite confirmation will require either the detection of X-ray lines from the forming remnant or the slow fade expected from circumstellar interaction. Either observation will be difficult given the instruments available now or in the next few years. SN 1980K was valuable in providing the first detected X-rays from a supernova, after a decade or so of upper limits. At least in part, SN 1980K spurred a fresh look at the physics of X-ray production, and paved the way for more detailed models for brighter, longer-lasting supernovae.

SN 1986J has been observed by the *ROSAT* PSPC at least one more time, so the investigation of the changing absorption column may be available shortly. An *Asuka* observation was scheduled for mid-1994, although the point spread function of the telescope (FWHM $\sim$1'.3) and the larger distance relative to SN 1978K will make this observation somewhat more difficult than a similar one of SN 1978K.

The models remain to be worked out in greater detail by, for example, high resolution hydrodynamic codes. Progress will likely be driven by the observations as the mechanisms producing X-ray emission are worked out. It is still possible that the X-ray emitting supernovae are an inhomogeneous class. Long-term X-ray light curves and spectroscopic studies are needed to test the models. For example, the quality of the X-ray spectra are as yet insufficient to distinguish between different mechanisms.

One point must be emphasized. SN 1980K is perhaps the only "normal" supernova yet detected in the X-ray band. With only five detections to date, no definitive conclusions may yet be drawn from such a small sample. Four of the five detected are, however, among the more peculiar supernovae of the past 20 years. Whether such a statement is still accurate 20 years from now remains to be seen.

In summary, the X-ray study of supernovae is a newly established twig of the X-ray astrophysics tree. The observations to be obtained in the next decade will increase our understanding of the development and evolution of shocks in a dense circumstellar medium, thereby growing the twig into a branch.

7. Appendix: A Brief Description of the Satellites

This section gives a very brief description of each of the satellites and the scientific instrumentation used in supernova observations to date. This section is not intended to be complete, but only to provide a "thumbnail sketch" of the satellites and instruments. Additional details are contained in the review paper on X-ray astronomy missions by Bradt, Ohashi, & Pounds (1992), and references therein.

7.1. Those That Have Been

OSO-III: This satellite, launched in 1967, carried an instrument that was designed to study the diffuse background in a high-energy band (8-200 keV) (the satellite's prime purpose was solar observations). It was a scanning instrument and used a 0.0010 m^2 NaI crystal scintillator with a CsI shield. The field-of-view was 23^o FWHM and mechanically collimated.

OSO-7: *OSO-7* was launched in 1971 to produce a four-color catalog of X-ray sources. The satellite carried several proportional counters with 1-60 keV energy responses and a crystal scintillator instrument sensitive to energies >10 keV. The satellite scanned the sky, the product of which was a multi-color catalog of ~180 sources.

Uhuru: *Uhuru*, launched in 1970, was the first satellite specifically designed for X-ray observations. It carried proportional counters with an effective area of 0.084 m^2 and sensitive to 2-20 keV X-rays that were collimated in a 1^Ox10^O (FWHM) beam. It scanned the sky slowly (spin period ~12 minutes) and observed the entire sky to about 0.1% of the intensity of the Crab nebula.

HEAO-1: The first of the *High Energy Astronomy Observatories*, *HEAO-1* was launched in 1977 and carried out a survey of the X-ray sky. The Large Area Sky Survey instrument was a 1.0 m^2 proportional counter sensitive to 1-20 keV X-rays. The Modulation Counter instrument provided positional resolution to ~1'. The field-of-view of the instruments was ~1°–4°.

Einstein: This X-ray observatory, launched in 1978, was the first to use fully imaging, grazing incidence optics. The effective area of the telescope was ~0.04 m^2. *Einstein*.carried a High-Resolution Imager with positional resolution of ~4-5", an Imaging Proportional Counter with ~1' positional resolution, a Focal Plane Crystal Spectrometer with a high spectral resolution ($\Delta\lambda/\lambda$ ~0.003 at 1 keV), and a Solid-State Spectrometer. The instruments were sensitive over the 0.1-4 keV band. The overall sensitivity was $\sim 10^{-5-6}$ Crab.

Ginga: The third in a series of X-ray satellites launched by Japan in 1987, *Ginga* was a pointed-mode spacecraft carrying a 0.4 m^2 proportional counter sensitive to X-rays in the 1.5-37 keV band. The spatial resolution was provided by a collimator with a 1^Ox2^O FWHM field-of-view.

BBXRT: The *Broad Band X-Ray Telescope* was carried into orbit on the US Space Shuttle *Columbia* in December 1990. The mission lasted 8 days. *BBXRT* consisted of two identical telescopes with five solid-state detectors, with a field of view of 17' and covering the 0.3-12 keV energy band with an effective area of $\sim$0.03 m^2 at 1.5 keV. The spectral resolution was $\sim$160 eV at 6 keV.

7.2. Those That Still Are (June 1995)

ROSAT: This satellite, launched on 1990 June 1, carried a Position-Sensitive Proportional Counter and an improved version of the *Einstein* HRI. The satellite has extremely good optics so the point spread function was small. The effective area is $\sim$0.02 m^2 at 1 keV. The energy range covered was 0.1-2.4 keV with a spectral resolution of $\sim$40% at 1 keV. The angular resolutions were $\sim$25", with a field-of-view of $\sim$2°, for the PSPC and $\sim$5" for the HRI with a 38' field-of-view. During the first six months of the mission, an all-sky survey was carried out.

Asuka: *Asuka* (also called *ASCA*, which stands for Advanced Satellite for Cosmology and Astrophysics); the pronunciation of *Asuka* is identical to *ASCA*) is essentially a free-flying *BBXRT* as it uses the same mirrors. It was launched in February 1993, primarily to perform spectroscopic observations. Four instruments are on board: two Gas Scintillation Proportional Counters and two X-ray sensitive CCDs. The spatial resolution is $\sim$1'-2'. The energy range covered is 0.5-10 keV with energy resolution of $\sim$120 eV at 6 keV, approximately 30% better than that of *BBXRT*.

GRO: The Oriented Scintillation Spectrometer Experiment (OSSE) on *GRO* covers the high end of the X-ray band from $\sim$50 keV into the MeV range. It has a field-of-view of 4°x11°.

7.3. Those Yet to Be (June 1995)

XTE (X-ray Timing Explorer): This mission, scheduled for launch in mid to late 1995, will cover the 2-200 keV band. It features a large area (~0.7 m^2) mechanically-collimated Proportional Counter array (5 counters) with a field-of-view of 1° FWHM and a NaI/CsI phoswich cluster to cover the 50-200 keV band. The mission is designed to study timing properties of variable sources.

Spectrum X-Γ: This satellite is a multi-wavelength and multi-country collaboration. The satellite, built primarily for imaging studies, will be placed in an elliptical orbit of ~3 day duration sometime in the late 1990s. The SODART telescope will cover the 0.1-20 keV band with an spatial resolution of ~2'. The JET-X experiment will have ~20" spatial resolution.

AXAF (Advanced X-ray Astrophysics Facility): *AXAF-I*, the imaging component of the originally proposed *AXAF*, will be similar to *Einstein*, but with better spatial resolution (~0".5), increased sensitivity by ~10^2–10^3 times, and a broader energy range (0.1-9 keV). It is scheduled for launch in 1998 and the orbit lifetime is approximately 10 years.

Astro-E: A joint Japanese-USA collaboration, *Astro-E* is still in the planning stages for a launch in 1999 or 2000. It will use the nested foil mirrors pioneered by *BBXRT*, but with improved spatial resolution (~0'.5). At least one of the instruments will be a X-ray calorimeter, capable of spectral resolution of ~10 eV.

XMM (X-ray Maximum Mission): The European equivalent of *AXAF*, *XMM* will have a very large effective area (~0.6 m^2 at 2 keV) for spectroscopy and timing. The energy band will extend to 10 keV. An optical/UV telescope will be co-aligned so multi-wavelength studies will be possible.

SAX: A joint mission between Italy, the Netherlands, and the European Space Agency, *SAX* is designed for spectral and variability studies in the 0.1-200 keV band.

I thank U. Zimmermann for sending the SN 1993J data files in electronic form, F. Seward for pointing out a reference on a SN Ia upper limit I initially had missed, and especially Roger Chevalier for his comments on the manuscript. I also thank the referee, J. Pye, for very helpful and constructive comments on the original manuscript.

REFERENCES

Allen, R., Goss, W., Ekers, R., & de Bruyn, A. 1976, A&A, 48, 253-261

Applegate, J. H. & Terman, J. L. 1989, ApJ, 340, 380-383

Arnett, W. D. 1988, ApJ, 331, 377-387

Asehenbach, B. 1988, Appl. Opt., 27, 1404-1413

Bandiera, R., Pacini, F., & Salvati, M. 1984, ApJ, 285, 134-140

Beall, J. H. 1979, ApJ, 230, 713-716

Becker, R., Helfand, D., Szymkowiak, A. 1982, ApJ, 255, 557-563

Beuermann, K., Brandt, S., & Pietsch, W. 1994, A&A, 281, L45-L48

Blair, W., Kirshner, R., & Winkler, P. F. 1983, ApJ, 272, 84-91

Bodansky, D., Clayton, D. D., & Fowler, W. A. 1968, ApJS, 16, 299-372

Bohlin, R. C., Savage, B. D., & Drake, J. F. 1978, ApJ, 224, 132-142

Borst, L. B. 1950, Phys. Rev., 78, 807-808

Bradt, H. V., Naranan, S., Rappaport, S., Zwicky, F., Ogelman, H., & Boldt, E. 1968, Nature, 218, 856-857

Bradt, H. V., Ohashi, T., & Pounds, K. 1992, ARAA, 30, 391-423

Bregman, J. N. & Pildis, R. A. 1992, ApJ, 398, L107-L110

Burbidge, E. M., Burbidge, G. R., Fowler, W. A., & Hoyle, F. 1957, Rev. Mod. Phys., 29, 547-650

Canizares, C., Kriss, G. A., & Feigelson, E. D. 1982, ApJ, 253, L17-L21

Canizares, C., Neighbours, J. E., & Matilsky, T. 1974, ApJ, 192, L61-L63

Catchpole, R., et al. 1987, MNRAS, 229, 15P-25P

Chevalier, R. 1990a, in High Energy Astrophysics in the 21st Century, ed. P. Joss, (New York: American Institute of Physics), 38-47

Chevalier, R. 1990b, in Supernovae, ed. A. Petschek, (Berlin: Springer-Verlag Inc.), 91-110

Chevalier, R. 1988, Nature, 332, 514-516

Chevalier, R. 1987, Nature, 329, 611-612

Chevalier, R. 1984, ApJ, 285, L63-L66

Chevalier, R. 1982, ApJ, 259, 302-310

Chevalier, R. 1982, ApJ, 258, 790-797

Chevalier, R. & Fransson, C. 1994, ApJ, 420, 268-285

Chevalier, R. & Fransson, C. 1992, ApJ, 395, 540-552

Chevalier, R. & Liang, E. P. 1989, ApJ, 344, 332-340

Chevalier, R. & Soker, N. 1989, ApJ, 341, 867-882

Chugai, N. 1993, ApJ, 414, L101-L103

Chugai, N. 1992, Sov. Astron., 36, 164-168

Colbert, E., Petre, R., Schlegel, E. & Ryder, S. 1995, ApJ, 446, 177-193

Colgate, S. A. & Johnson, M. H. 1960, PhysRevLett, 5, 235-238

Colgate, S. A. & McKee, C. 1969, ApJ, 157, 623-643

Cowan, J. & Branch, D. 1985, ApJ, 258, 31-34

Cowan, J., Henry, R. B., & Branch, D. 1988, ApJ, 329, 116-121

deVaucouleurs, G. 1979, ApJ, 227, 729-755

deVaucouleurs, G. 1963, ApJ, 137, 720-732

Doggett, L. & Branch, D. 1985, AJ, 90, 2303-2311

Dopita, M. & Ryder, S. 1990, IAU Circ. 4950

Dotani, T., et al. 1987, Nature, 330, 230-232

Fabian, A., Willingale, R., Pye, J., Murray, S., & Fabbiano, G. 1980, MNRAS, 193, 175-188

Fabbiano, G. 1988, ApJ, 325, 544-562

Falk, S., 1978, ApJ, 225, L133-136

Filippenko, A. & Matheson, T. 1993, IAU Circ. 5787

Filippenko, A. 1988, AJ, 96, 1941-1948

Fransson, C. 1994, in Circumstellar Media in the Late Stages of Stellar Evolution, ed. R.E.S. Clegg, W.P.S. Meikle, & I. R. Stevens, (Cambridge: Cambridge Univ. Pr.), 120-138

Fransson, C. 1984, A&A, 133, 264-284

Fransson, C., Lundqvist, P., & Chevalier, R. 1995, Submitted to ApJ, January

Freedman, W., et al. 1993, ApJ, 427, 628-655

Gorenstein, P., Hughes, J. P., & Tucker, W. 1994, ApJ, 420, L25-L28

Gorenstein, P., Kellogg, E., & Gursky, H. 1969, ApJ, 156, 315-324

Gottesman, S. T., Broderick, J. J., Brown, R. L., Balick, B., & Palmer, P. 1972, ApJ, 174, 383-388

Harkness, R. & Wheeler, J. C. 1990, in Supernovae, ed. A. Petschek, (Berlin: Springer-Verlag Inc.), 1-29

Hasinger, G., Snowden, S., & Schlegel, Eric M., 1993, US *ROSAT* Science Data Center Memo 93-026

Hoyle, F. 1946, MNRAS, 106, 343-383

Humphreys, R. M., Aldering, G. S., Bryja, C. O., and Thurmes, P. M. 1993, IAU Circ. 5739

Inoue, H., et al. 1991, PASJ, 43, 213-223

Itoh, H., Hayakawa, S., Masai, K., & Nomoto, K. 1987, PASJ, 39, 529-537

Itoh, H. & Masai, K. 1989, MNRAS, 236, 885-899

Kirshner, R. 1990, in Supernovae, ed. A. Petschek, (Berlin: Springer-Verlag Inc.), 59-75

Kirshner, R., Kriss, G. & Berg, C. 1980, IAU Circ. 3534

Kirshner, R., Sonneborn, G., Crenshaw, D. M., & Nassiopoulos, G. 1987, ApJ, 320, 602-608

Klein, R. & Chevalier, R. 1978, ApJ, 223, L109-L112

Koshiba, M., et al. 1987, IAU Circ. 4338

Kraft, R. P., Burrows, D. N., and Nousek, J. A. 1991, ApJ, 374, 344-355

Kumagai, S., Nomoto, K., Shigeyama, T., Hashimoto, M., & Itoh, M. 1993, A&A, 273, 153-159

Kumagai, S., Shigeyama, T., Nomoto, K., Itoh, M., Nishimura, J., & Tsuruta, S. 1989, ApJ, 345, 412-422

Lasher, G. & Chan, K. L. 1979, ApJ, 230, 742-754

Leising, M., et al. 1994, ApJ, 431, L95-L98

Lewin, W. et al. 1994, IAU Circ. 6019

Liller, W. 1992, IAU Circ. 5428

Long, K. S., Helfand, D. J., & Grabelsky, D. A. 1981, ApJ, 248, 925-944

Makino, F. 1987, Astrophys. Lett. & Comm., 25, 223-233

Makino, F., et al. 1987a, IAU Circ. 4447

Makino, F., et al. 1987b, IAU Circ. 4466

Masai, K., Hayakawa, S., Inoue, H., Itoh, H., & Nomoto, K. 1988, Nature, 335, 804-806

Masai, K., Hayakawa, S., Itoh, H., & Nomoto, K. 1987, Nature, 330, 235-236

Nomoto, K. & Hashimoto, M. 1987, Ap & Sp. Sci., 131, 395-411

Nomoto, K., Suzuki, T., Shigeyama, T., Kumagai, S., Yamaoka, H., & Saio, H. 1993, Nature, 364, 507-508

Nomoto, K., Thielemann, F.-K., & Yokoi, K. 1984, ApJ, 286, 644-658

Pacini, F. & Salvati, M. 1981, ApJ, 245, L107-L108

Palmieri, T. M., Burginyon, G. A., Hill, R. W., Scudder, J. K., Seward, F. D., & Toor, A. 1973, ApJ, 182, 411-416

Petre, R., Schlegel, E. M., & Miller, S. 1995, Submitted to ApJ (Letters)

Petre, R., Colbert, E., Makishima, K., Mihara, T., & Okada, K. 1994, PASJ, 46, L115-L120

Pietsch, W., Vogler, A., Kahabka, P., Jain, A., & Klein, U. 1994, A&A, 284, 386-402

Pinto, P. & Woosley, S. 1988, ApJ, 329, 820-830

Pisarski, R. L., Helfand, D., & Kahn, S. 1984, ApJ, 277, 710-715

Porter, A. & Filippenko, A. 1987, AJ, 93, 1372-1380

Pravdo, S. & Serlemitsos, P. 1981, ApJ, 246, 484-488

Pye, J., Pounds, K., Rolf, D., Seward, F., Smith, A., & Willingale, R. 1981, MNRAS, 194, 569-582

Reid, P., Becker, R., & Long, K. 1982, ApJ, 261, 485-491

Ripero, J. & Garcia, F. 1993, IAU Circ. 5731

Roth, K. 1992, IAU Circ. 5429

Rupen, M. P., Sramek, R., VanDyk, S., Weiler, K., & Panagia, N. 1994a, IAU Circ. 5963

Rupen, M. P., Sramek, R., VanDyk, S., Weiler, K., & Panagia, N. 1994b, IAU Circ. 5966

Rupen, M. P., van Gorkom, J. H., Knapp, G. R., Gunn, J. E., & Schneider, D. P. 1987, AJ, 94, 61-70

Ryder, S. D., Staveley-Smith, L., Dopita, M. A., Petre, R., Colbert, E., Malin, D. F., & Schlegel, Eric M. 1993, ApJ, 416, 167-181

Ryder, S. D., Staveley-Smith, L., Malin, D. F., & Walsh, W. 1995, AJ, 109, 1592-1607

Ryder, S. D., Dopita, M. A., Staveley-Smith, L., Malin, D., Colbert, E., Petre, R., Schlegel, Eric M., & Campbell-Wilson, D. 1992, IAU Circ. 5615

Ryter, C., Cesarsky, C., & Audouze, J. 1975, ApJ, 198, 103-109

Schlegel, Eric M. 1994, AJ, 108, 1893-1897

Schlegel, Eric M. & Kirshner, R. 1989, AJ, 98, 577-589

Schlegel, Eric M., Marshall, F. E., Mushotzky, R. M., Smale, A., Weaver, K., Serlemitsos, P., Petre, R., & Jahoda, K. 1994, ApJ, 422, 243-247

Schlegel, Eric M., Petre, R., & Colbert, E. 1995, Submitted to ApJ, May

Schlegel, Eric M. & Petre, R. 1993, ApJ, 412, L29-L32

Schmidt, B., Kirshner, R. P., & Eastman, R. 1992, ApJ, 395, 366-386

Silk, J. 1973, ARA&A, 11, 269-308

Snowden, S. & Freyberg, M. J. 1993, ApJ, 404, 403-411

Snowden, S., McCammon, D., Burrows, D., & Mendenhall, J. 1994, ApJ, 424, 714-728

Sprott, G. F., Bradt, H. V., Clark, G. W., Lewin, W. H. G., Schnopper, H., Pigatto, L., & Rosino, L. 1974, ApJ, 191, 739-742

Spyromilio, J., Stathakis, R., NcNaught, R., Sadler, E., Freeman, F., & Cannon, R. 1992, IAU Circ. 5428

Sramek, R., van der Hulst, J., & Weiler, K. 1980, IAU Circ. 3557

Sramek, R. & Weiler, K. 1990, in Supernovae, ed. A. Petschek, (Berlin: Springer-Verlag Inc.), 76-90

Stocke, J., Wang, Q., Perlman, E., Donahue, M., & Schachter, J. 1994, in The Soft X-ray Cosmos, eds. E. Schlegel & R. Petre, (New York: American Institute of Physics), 75-79

Sutherland, P. 1990, in Supernovae, ed. A. Petschek, (Berlin: Springer-Verlag Inc.), 111-142

Sunyaev, R. et al. 1990, Sov. Astron. Letters, 16, 55-58

Sunyaev, R. et al. 1987, Nature, 330, 227-229

Suzuki, T., Kumagai, S., Shigeyama, T., Nomoto, K., Yamaoka, H., & Saio, H. 1993a, ApJ, 419, L73-L76

Suzuki, T., Shigeyama, T., & Nomoto, K. 1993b, A&A, 274, 883-894

Svoboda, R., et al. 1987, IAU Circ. 4340

Tanaka, Y. 1993, IAU Circ. 5753

Tanaka, Y. 1989, Physics of Neutron Stars and Black Holes, ed. Y. Tanaka, (Tokyo: Universal Academy Press, Inc.), 431-440

Trimble, V. 1983, Nature, 303, 137-142

Truran, J. W., Arnett, W. D., & Cameron, A. G. W. 1968, Can. J. Phys., 45, 2315-2332

Tucker, W. 1970, ApJ, 161, 1161-1163

Tully, R. 1988, Nearby Galaxies Catalog, (Cambridge: Cambridge University Press)

Turtle, A., et al. 1987, Nature, 327, 38-40

Ulmer, M., Baity, W. A., Wheaton, W. A., and Peterson, L. E. 1974, ApJ, 193, 535-537

Ulmer, M., Grace, V., Hudson, H. S., and Schwartz, D. A. 1972, ApJ, 173, 205-211

van den Bergh, S. 1988, ApJ, 327, 156-166

Van Dyk, S., et al. 1994, IAU Circ. 6045

Van Dyk, S., Nguyen, H.-A., Weiler, K., Sramek, R., Rupen, M., & Panagia, N. 1993a, IAU Circ. 5828

Van Dyk, S., Weiler, K., Sramek, R., & Panagia, N. 1993b, ApJ, 419, L69-L72

Van Dyk, S., Weiler, K., Sramek, R., & Panagia, N. 1992, ApJ, 396, 195-200

Walborn, N., Lasker, B., Laidler, V., & Chu, Y.-H. 1987, ApJ, 321, L41-L44

Weiler, K., Panagia, N., & Sramek, R. 1990, ApJ, 364, 611-625

Weiler, K., Sramek, R., Van Dyk, S., & Panagia, N. 1993, IAU Circ. 5752

Weiler, K., Sramek, R., Panagia, N., van der Hulst, J., & Salvati, M. 1986, ApJ, 301, 790-812

Wheeler, C. 1993, IAU Circ. 5743

White, R. & Long, K. 1983, ApJ, 264, 196-205

Wild, P. 1980, IAU Circ. 3532

Woosley, S. 1990, Supernovae, ed. A. Petschek, (Berlin: Springer-Verlag), 182-212

Yin, Q. F., 1994, ApJ, 420, 152-158

Zimmermann, H. et al. 1994a, IAU Circ. 6014

Zimmermann, H. et al. 1994b, IAU Circ. 6210

Zimmermann, H. et al. 1993a, IAU Circ. 5748

Zimmermann, H. et al. 1993b, IAU Circ. 5750

Zimmermann, H. et al. 1993c, IAU Circ. 5766

Zimmermann, H. et al. 1993d, IAU Circ. 5899

Zimmermann, H., Aschenbach, B., Hasinger, G., Pietsch, W., Predehl, P., Trumper, J., Lewin, W., Magnier, E., van Paradijs, J., Fabbiano, G., Lubin, L., & Petre, R. 1994c, Nature, 367, 621-623

Zwicky, F. 1965, in Stellar Structure, ed. L. Aller & D. McLaughlin, (Chicago: University of Chicago Press), 367-423

This manuscript was prepared with the AAS LaTeX macros v3.0.

Figure Captions

Figure 1 - Upper limits on X-ray emission from SN Ia. a) upper limits on the light curve; b) upper limits on the spectrum.

Figure 2 - The field surrounding the Type Ia supernova SN 1992A in NGC 1380. The extraction cell for the supernova is the center box of the three shown. The background extraction cells are at the same radius and lie to either side of the supernova cell. The scale bar is 1' long. Figure from Schlegel & Petre (1993).

Figure 3 - The upper limits on X-ray emission from SN II. a) upper limits on the light curve; b) upper limits on the spectrum.

Figure 4 - The field surrounding the Type II supernova SN 1980K in NGC 6946, as seen with the *Einstein* IPC. The supernova lies to the southeast of the field center. The bright patch in the center of the field is the X-ray emission from NGC 6946 itself (Canizares et al. 1982). The image is ~20' on a side. A higher resolution image is presented in Figure 6.

Figure 5 - The light curve of SN 1980K in the 0.5-4.0 keV band as observed with *Einstein*.

Figure 6 - The *ROSAT* PSPC image of NGC 6946. The circles and labels indicate the positions of the historical supernovae. Figure is from Schlegel 1994.

Figure 7 - The (a) *Einstein* IPC spectrum and (b) confidence contours of SN 1980K for the exposure of 1980 December 11 = +35 days post-outburst. The spectrum has not been corrected for the instrumental response.

Figure 8 - a) The 5.8-16 keV light curve of SN 1987A, as detected by *Ginga*; b) the 16.1-27.8 keV light curve of SN 1987A. An approximate conversion from

counts s^{-1} to ergs s^{-1} cm^{-2} has been applied (Figure measured from Tanaka 1989).

Figure 9 - The *Ginga* spectrum of SN 1987A (figure measured from Tanaka 1989). The spectrum has not been corrected for the instrumental response.

Figure 10 - a) The *ROSAT* PSPC spectrum (uncorrected for the instrumental response) and b) and c) the χ^2 contours of the fit parameters for SN 1986J. Note that essentially no flux is detected below about 0.65 keV. Figure 10c expands the low kT-high N_H solution in greater detail. Figure from Bregman & Pildis 1992.

Figure 11 - The *ROSAT* PSPC field of SN 1978K in NGC 1313. The western source is SN 1978K; the other two sources are ~6'.9 apart and are identical to the sources in Figure 12.

Figure 12 - The *Einstein* IPC field of NGC 1313. The northern source is the nuclear source; the southern source is most likely an X-ray binary. The two sources are ~6'.9 apart.

Figure 13 - a) The *ROSAT* PSPC spectrum and b) the χ^2 contours of the fit parameters for SN 1978K for the exposure for the exposure of 1991 April = MJD 48370.0. The spectrum has not been corrected for the instrumental response.

Figure 14 - The 1.0-2.0 keV (top) and 0.5-2.0 keV (bottom) light curves of SN 1978K, assuming a thermal bremsstrahlung model. The extra data point in the 1.0-2.0 keV light curve is from an observation using *Asuka* (Petre et al. 1994).

Figure 15 - The 1.0-2.0 keV luminosity light curves of the nucleus and the probable X-ray binary in NGC 1313.

Figure 16 - The full 1.0-2.0 keV light curve of SN 1978K to date. Figure from Schlegel et al. 1995.

Figure 17 - a) The *ROSAT* PSPC 0.2-2.4 keV light curve of SN 1993J in NGC 3031. An approximate conversion from counts s^{-1} to ergs s^{-1} cm^{-2} has been applied. b) The *ROSAT* PSPC spectrum of SN 1993J. The spectrum has not been corrected for the instrumental response (Figures from Zimmermann et al. 1994c).

Figure 18 - The 2 keV evolution light curve of those supernovae detected in the X-ray band and several Galactic supernova remnants. The figure shows light curves of recent supernovae and the present day luminosities of historical remnants.

Table 1: Upper Limits on Type Ia Supernovae

SN Name	Galaxy	Date of Optical Max	B mag at max	Galaxy Distance	Log of Approx. 3σ Upper Limit (ergs s^{-1})	Satellite used
SN1968A	NGC 1275	1968 Feb 2	~15.5	70Mpc	45.3	Aerobee[a]
SN1968I	NGC 4981	1968 April 23	~13.5	31Mpc	44.1	*OSO-III*[b]
SN1972E	NGC 5253	1972 May 4	8.5	2.1Mpc	40.5	*OSO-7*, *Uhuru*[c]
					41.3	Aerobee[d]
SN1992A	NGC 1380	1992 Jan 19.2	12.6	16.9Mpc	38.8	*ROSAT*[e]

[a]Gorenstein, Kellogg, & Gursky 1969

[b]Ulmer et al. 1972

[c]Canizares, Neighbours, & Matilsky 1974; Ulmer et al. 1974

[d]Palmieri et al. 1973

[e]Schlegel & Petre 1993

Table 2: Upper Limits on Type II Supernovae

SN Name	Galaxy	Date of Optical Max	B mag at max	Galaxy Distance	Log of Approx. 3σ Upper Limit (ergs s^{-1})	Satellite used
SN1971S	NGC 493	1971 Nov 2	~15.5	29.9Mpc	42.7	*OSO-7*
SN1967H	NGC 4254	1967 July 2	~14.5	16.8Mpc	43.1	Aerobee

[a]Sprott et al. 1974

[b]Bradt et al. 1968

Table 3: Supernovae Detected in the X-ray Band

SN Name	Galaxy	Date of Optical Max	B mag at max	SN Type	Galaxy Distance[a]	X-rays first observed	Satellite used
SN 1978K	NGC 1313	[b] ~1978 June10	~13	IIL	4.5Mpc	+~12.1yr	*ROSAT, Asuka*
		[b] ~1978 May 25	~14.5	IIP			
SN 1980K	NGC 6946	1980 Nov 5	11.5	IIL	5.1Mpc	+35d	*Einstein*
SN 1986J	NGC 891	[c]1983 Jan?	?	IIpec	9.6Mpc	?	*ROSAT*
SN 1987A	LMC	1987 May 9	3.5	IIP	50±3kpc	+154d	*Ginga*
SN 1993J	NGC 3031	1993 Apr 18	11.4[d]	IIpec	3.63±0.34Mpc	+5d	*ROSAT, Asuka. GRO*

Notes

[a]Distances from: SN1978K: deVaucouleurs 1963; SN1980K: deVaucouleurs 1979; SN1986J: Tully 1988; SN1987A: numerous; SN1993J: Freedman et al. 1993.

[b]Assume each Type II subtype, matching optical light curve to average SN II optical behavior to derive date of maximum (Ryder et al. 1993a)

[c]Chevalier 1987

[d]Richmond 1993

Table 4: X-ray Observations of Supernovae - SN1980K

MJD[a]	Instrument[b]	Flux[c]	L_X^d
44018	*Einstein* IPC	<0.10	<0.24
44584	*Einstein* IPC	11.2	27.0
44631	*Einstein* IPC	1.85	4.5
48791	*ROSAT* PSPC	0.10	0.24

[a]MJD = Modified Julian Date = JD - 2400000.5.

[b]The energy range of the *Einstein* IPC 0.5-4.0keV. The energy range of the *ROSAT* PSPC is 0.2-2.4 keV.

[c]Unabsorbed flux in units of 10^{-13} ergs s^{-1} cm^{-2}. 'Unabsorbed' means that the flux has been calculated from the model with the line-of-sight column density set equal to 0.0. The 'unabsorbed' flux is the intrinsic flux from the source.

[d]Distance from Table 3. Units = 10^{38} ergs s^{-1}.

Table 5: X-ray Observations of Supernovae - SN1987A[a]: Soft Band

MJD	Flux[b]	Error[b]	L_X^c
46996.0	1.15	1.13	3.4
47010.0	1.38	0.46	4.1
47026.0	2.30	0.32	6.9
47057.0	2.99	0.37	8.9
47081.0	1.06	0.37	3.2
47098.0	1.70	0.92	5.1
48118.0	2.21	0.55	6.6
47155.0	1.98	0.37	5.9
47171.0	0.92	0.23	2.7
47183.0	3.40	0.41	10.1
47187.0	4.55	0.32	13.6
47195.0	4.83	0.28	13.6
47196.0	5.29	0.37	15.8
47197.0	5.20	0.32	15.5
47198.0	4.92	0.28	14.7
47199.0	3.91	0.28	11.6
47200.0	4.28	0.23	12.7
47201.0	3.91	0.46	11.6
47206.0	4.09	0.28	12.2

Table 5, continued: X-ray Observations of Supernovae - SN1987A[a]: Soft Band

MJD	Flux[b]	Error[b]	L_X^c
47207.0	3.59	0.37	10.2
47212.0	3.73	0.28	11.2
47220.0	2.21	0.32	6.6
47221.0	2.76	0.28	8.2
47233.0	2.30	0.37	6.9
47250.0	1.29	0.46	3.8
47279.0	1.52	0.37	4.5
47293.0	1.70	0.64	5.1

[a]Instrument used was the *Ginga* LAC with energy range 5.8-16.1keV.

[b]Units are 10^{-11} ergs s^{-1} cm^{-2}. Approximate flux conversion is 1 count s^{-1} is equal to 4.6×10^{-12} ergs s^{-1} cm^{-2}. See Inoue et al. (1991) for additional details.

[c]Distance from Table 3. Units = 10^{36} ergs s^{-1}.

Table 6: X-ray Observations of Supernovae - SN1987A[a]: Hard Band

MJD	Flux[b]	Error[b]	L_X^c
46971.1	0.80	1.70	2.4
46978.8	1.70	1.92	5.1
46980.3	2.62	1.06	7.8
46996.3	1.76	0.86	5.2
47011.1	2.88	0.74	8.6
47022.7	5.44	1.66	16.2
47039.3	4.70	0.74	14.0
47042.4	3.97	0.96	11.8
47064.8	3.42	0.74	10.2
47066.4	3.01	0.80	8.9
47070.8	4.80	0.74	14.3
47084.2	4.96	2.08	14.8
47104.1	3.74	1.60	11.2
47114.9	3.90	2.14	11.6
47140.1	3.52	0.86	10.5
47156.2	2.98	0.64	8.9
47167.7	6.62	1.06	19.7
47172.9	6.24	0.74	16.6
47180.9	6.94	0.89	20.7

Table 6, continued: X-ray Observations of Supernovae - SN1987A[a]: Hard Band

MJD	Flux[b]	Error[b]	L_X^c
47183.1	8.26	0.89	24.6
47185.5	5.06	1.28	17.5
47192.3	6.30	0.74	18.8
47196.9	5.02	0.74	14.9
47206.1	3.78	0.86	11.3
47207.7	5.22	0.89	15.6
47216.9	4.89	0.89	14.6
47234.4	2.56	1.18	7.6
47235.9	4.54	1.18	13.5
47263.9	3.18	1.02	9.5
47276.7	3.78	1.66	11.3

[a]Instrument used was the *Ginga* LAC with an energy range of 16.1-27.8 keV.

[b]Units are 10^{-11} ergs s^{-1} cm^{-2}. An approximate flux conversion is 1 count s^{-1} equals $32x10^{-12}$ ergs s^{-1} cm^{-2}. See Inoue et al. (1991) for additional details.

[c]Distance from Table 3. Units are 10^{36} ergs s^{-1}.

Table 7: X-ray Observations of Supernovae - SN1987A[a]: Recent Observations

MJD	Flux[b]	Error[b]	L_X^c
48060[d]	<4.8	...	<1.4
48180[e]	<18.4	...	<5.5
48375	3.2	2.1	0.9
48656	5.9	3.5	1.8
48700	5.1	1.4	1.5
48720	9.9	2.8	2.9

[a]Instrument used was the *ROSAT* PSPC with an energy range of 0.2-2.4 keV. Count rates from Beuermann et al. (1994).

[b]Units are 10^{-13} ergs s^{-1} cm^{-2}. An approximate conversion is 1 count s^{-1} equals 2.3×10^{-10} ergs s^{-1} cm^{-2}.

[c]Distance from Table 3. Units are 10^{35} ergs s^{-1}.

[d]Instrument verification phase observation.

[e]All-sky survey phase observation.

Table 8: X-ray Observations of Supernovae - SN1986J

MJD	Instrument[a]	Flux[b]	Error[b]	L_X^c
48487	*ROSAT* PSPC	2.9	0.6	3.2

[a]The energy range is 0.2-2.4keV.

[b]Unabsorbed flux in units of 10^{-12} ergs s^{-1} cm^{-2}.

[c]Distance from Table 3. Units equal 10^{40} ergs s^{-1} cm^{-2}.

Table 9: X-ray Observations of Supernovae - SN1978K

MJD	Instrument[a]	Flux[b]	Error[b]	L_X^c
44240	*Einstein* IPC	<0.81	...	<1.9
48095	*ROSAT* PSPC	4.79	3.06	11.6
48333	*ROSAT* PSPC	3.16	2.51	7.6
48370	*ROSAT* PSPC	5.39	1.54	13.0
48730	*ROSAT* HRI	3.73	0.59	9.0
49181	*Asuka*[d]	3.60	...	8.7
49299	*ROSAT* PSPC	5.34	0.87	12.9
49538	*ROSAT* HRI	4.70	0.71	11.4

[a]The energy range of *ROSAT* is 0.2-2.4 keV. The energy range of *Asuka* is 0.5-10 keV. The flux range reported here is 1.0-2.0 keV, assuming a power law model defined by the *Asuka* observation. The IPC energy range is 0.5-4.0 keV and the upper limit has not been corrected for the different energy range.

[b]Unabsorbed flux in units of 10^{-13} ergs s^{-1} cm^{-2}.

[c]Distance from Table 3. Units are 10^{38} ergs s^{-1}.

[d]Flux from Petre et al. 1994

Table 10: X-ray Observations of Supernovae - SN1993J

MJD	Instrument[a]	Flux[b]	Error[b]	L_X^c
49080.9	*ROSAT* PSPC	1.82	0.13	2.8
49086.4	*ROSAT* PSPC	1.69	0.09	2.6
49090.1	*ROSAT* PSPC	1.40	0.08	2.2
49094.3	*ROSAT* PSPC	1.41	0.27	2.2
49096.8	*ROSAT* HRI[d]	1.07	0.07	1.7
49100.6	*ROSAT* PSPC	1.27	0.07	2.0
49112.8	*ROSAT* PSPC	1.23	0.06	1.9
49121.7	*ROSAT* HRI[d]	0.84	0.08	1.3
49293	*ROSAT* PSPC	0.81	0.03	1.3
49446	*ROSAT* PSPC	0.41	0.07	0.6
49645	*ROSAT* HRI[d]	0.81	0.05	1.3

[a]Energy range of *ROSAT* is 0.2-2.4 keV.

[b]Units are 10^{-11} ergs s^{-1} cm^{-2}. An approximate conversion factor is 1 count s^{-1} equals 2.3×10^{-10} ergs s^{-1} cm^{-2}.

[c]Distance from Table 3. Units are 10^{40} ergs s^{-1}.

[d]1 HRI count per second $\sim$ 2.2 PSPC counts per second (Hasinger, Snowden, & Schlegel 1993), assuming no spectral evolution.

Table 11: Radio Supernovae as Possible X-ray Emitters

Supernova	Galaxy	Distance (Mpc)	6 cm Flux density (mJy)[a]	Reference
SN1950B	NGC 5236	~7	0.5	Cowan & Branch 1985
SN1957D	NGC 5236	~7	1.9	Allen et al. 1976
SN1961V	NGC 1058	12	0.11	Cowan et al. 1988
SN1968D	NGC 6946	5.1	0.15	Van Dyk et al. 1994
SN1970G	NGC 5457	7.2	2.5	Weiler et al. 1986
SN1979C	NGC 4321	17	8.3	Weiler et al. 1986
SN1981K	NGC 4258	6.6	2.0	Van Dyk et al. 1992
SN1982AA[b]	Mrk 297	~64	12.2	Yin 1994
SN1983N	NGC 5236	~7	18.5	Weiler et al. 1986
SN1984L	NGC 991	~24	0.7	Weiler et al. 1986
SN1988Z	MCG+03-28-022	~90	1.90	Van Dyk et al. 1993b
SN1980K	NGC 6946	5.1	2.6	Weiler et al. 1986
SN1978K	NGC 1313	4.5	70	Ryder et al. 1993a
SN1986J	NGC 891	12	124	Rupen et al. 1987
SN1987A	LMC	0.05	150	Turtle et al. 1987
SN1993J	NGC 3031	3.3	>50	Van Dyk et al. 1993a

[a]Flux density at maximum, except SN1993J, which was still increasing at 6 cm at the time of writing.

[b]SN1982AA has probably been detected in the 0.2-2.4 keV band with *ROSAT*, but a confirming observation is necessary.

Table 12: 2 keV Light Curve of Supernovae and Remnants

Source	Age (yrs)	Luminosity[a]	Reference
SN1978K	1.6	1.5(38)	Schlegel et al. 1995
	12.1	6.3(38)	Schlegel et al. 1995
	12.8	4.3(38)	Schlegel et al. 1995
	12.9	7.0(38)	Schlegel et al. 1995
	15.1	5.4(38)	Schlegel et al. 1995
	15.4	6.5(38)	Schlegel et al. 1995
	16.0	1.9(38)	Schlegel et al. 1995
SN1980K	0.1	3.4(38)	Canizares et al. 1982
	0.2	5.3(37)	Canizares et al. 1982
	11.6	2.0(37)	Schlegel 1994
SN1987A	0.9	3.4(35)	Inoue et al. 1991
SN1987A	4.1	9.5(32)	Beuermann et al. 1994
SN 185	1809	4.3(34)	Pisarski, Helfand, & Kahn 1984
SN1006	988	1.1(33)	Pye, et al. 1981
SN1054	940	3.3(36)	Pravdo & Serlemitsos 1981
SN1572	422	3.6(35)	Reid, Becker, & Long 1982
SN1604	390	1.9(35)	White & Long 1983
SN1670	324	4.0(35)	Fabian et al. 1980

[a]Units are ergs s^{-1}; number in parentheses is the exponent.

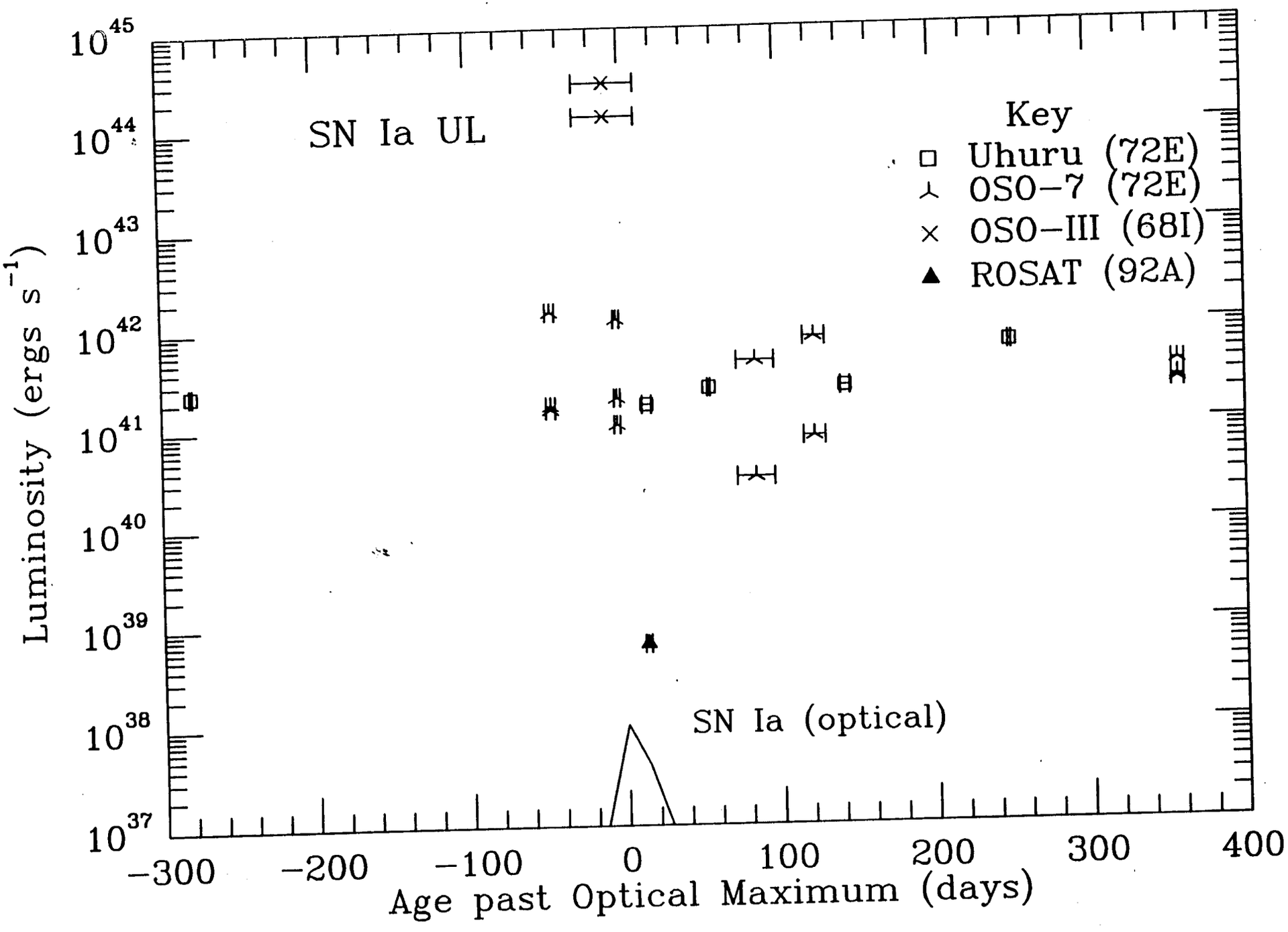
SN Ia UL
Key
Uhuru (72E)
OSO-7 (72E)
OSO-III (68I)
ROSAT (92A)
SN Ia (optical)
Luminosity (ergs s^{-1})
10^{45}
10^{44}
10^{43}
10^{42}
10^{41}
10^{40}
10^{39}
10^{38}
10^{37}
−300
−200
−100
0
100
200
300
400
Age past Optical Maximum (days)

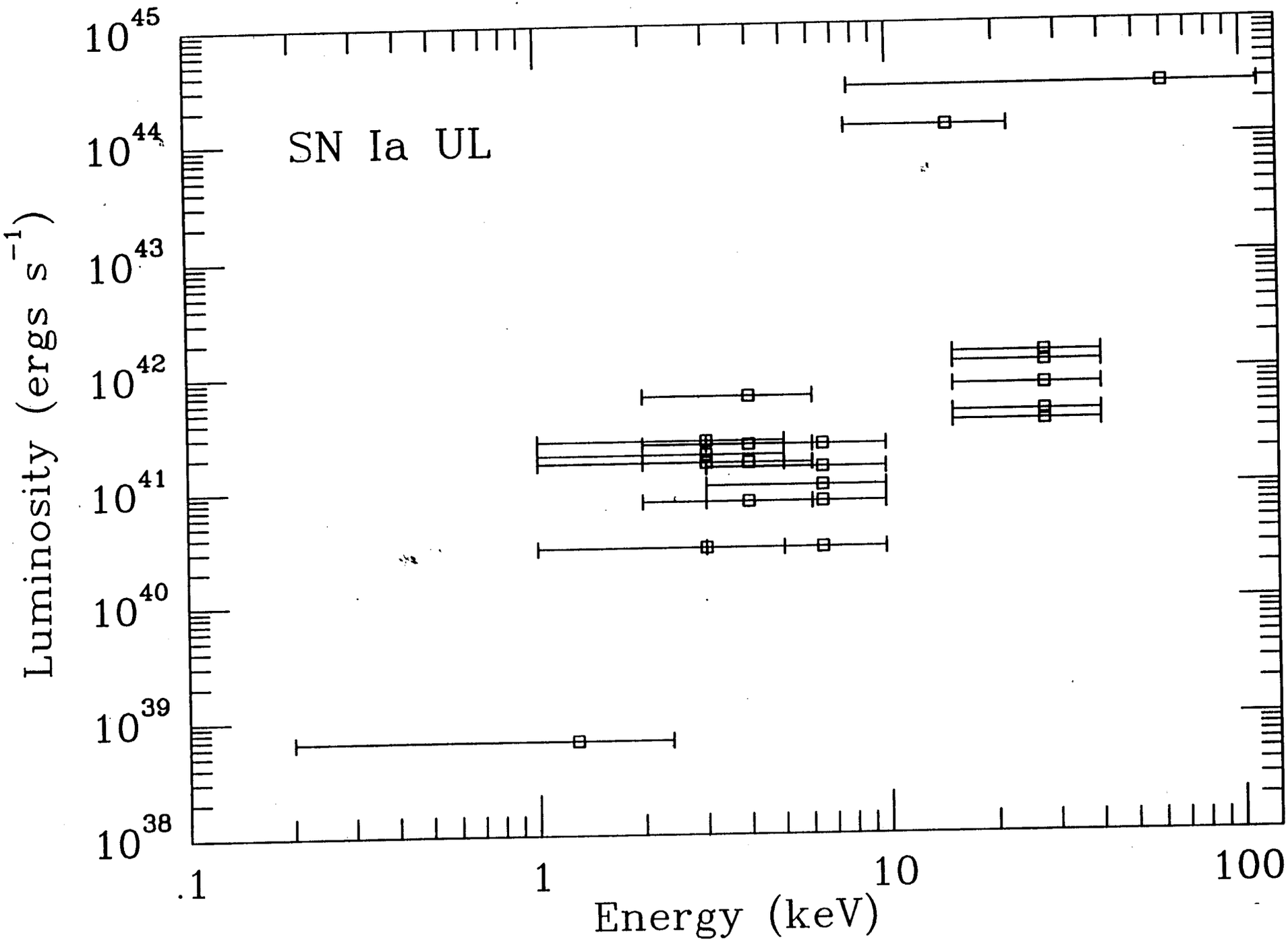
SN Ia UL
Luminosity (ergs s^{-1})
10^{45}
10^{44}
10^{43}
10^{42}
10^{41}
10^{40}
10^{39}
10^{38}
.1
1
10
100
Energy (keV)

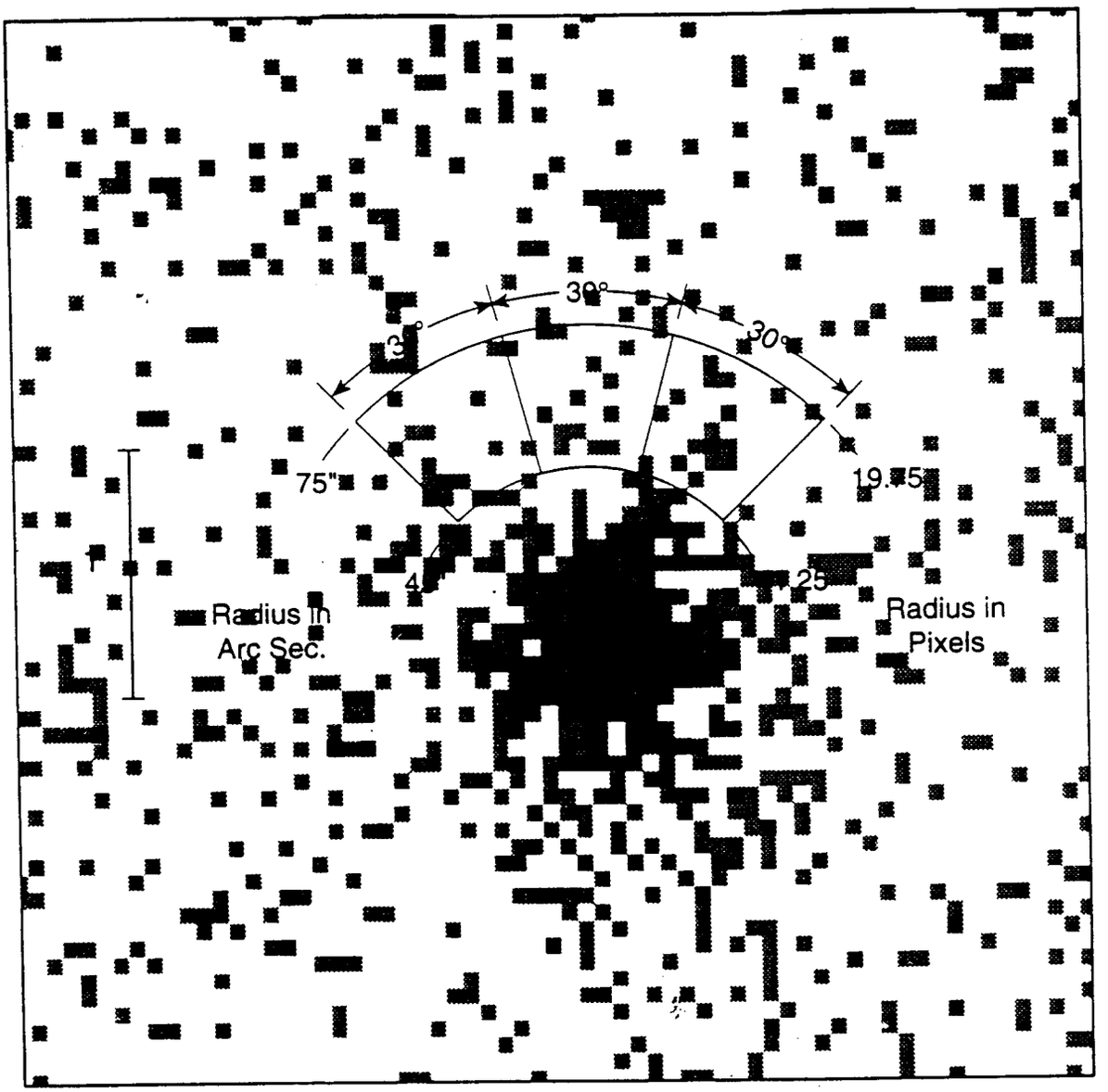
30°
30°
30°
75"
19.5
4
25
Radius in
Arc Sec.
Radius in
Pixels

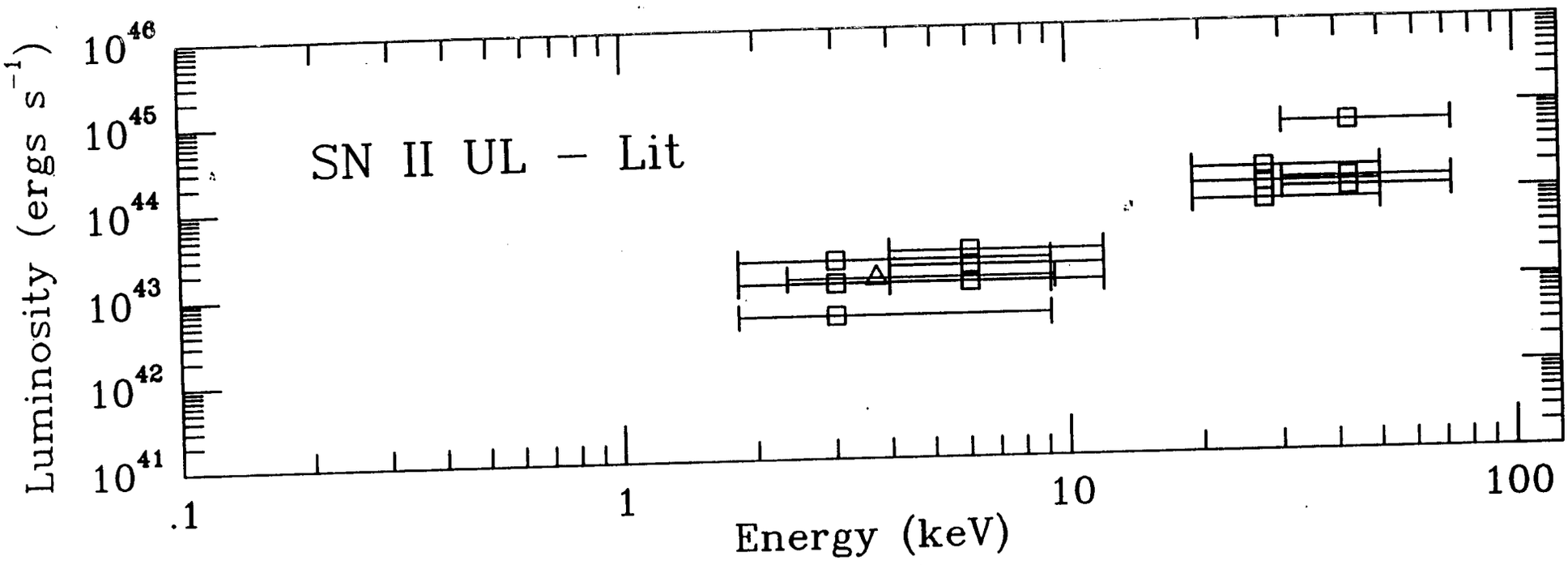
SN II UL – Lit
Luminosity (ergs s^{-1})
10^{46}
10^{45}
10^{44}
10^{43}
10^{42}
10^{41}
.1
1
10
100
Energy (keV)

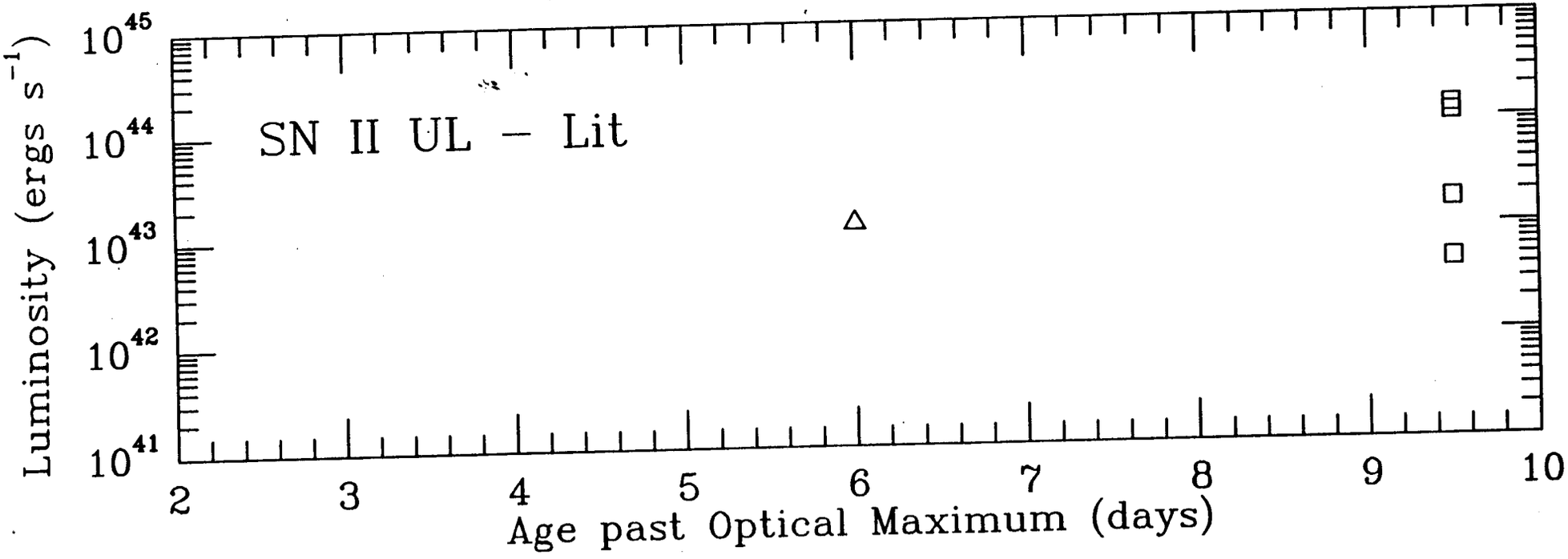
SN II UL – Lit
Luminosity (ergs s^{-1})
10^{45}
10^{44}
10^{43}
10^{42}
10^{41}
2
3
4
5
6
7
8
9
10
Age past Optical Maximum (days)

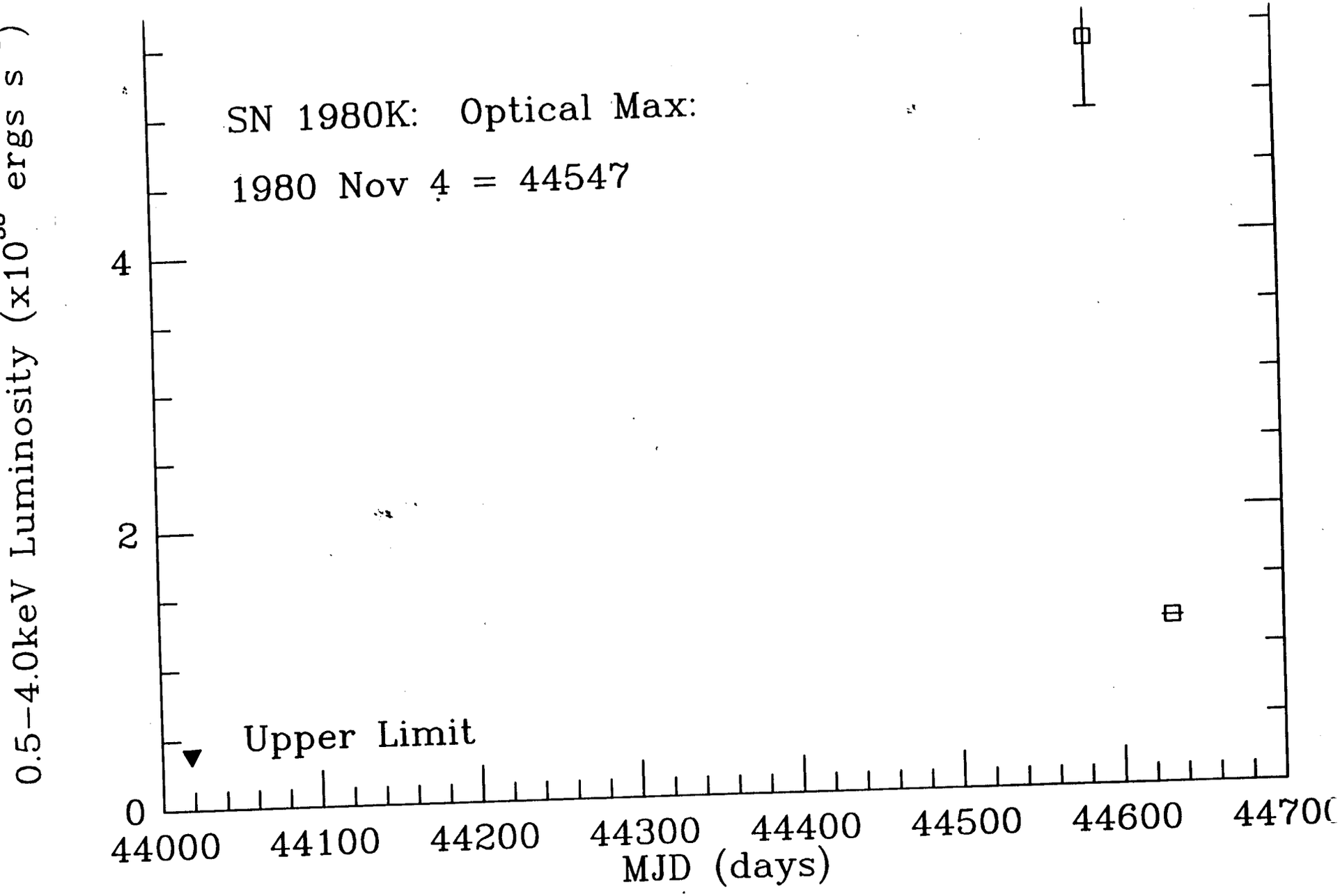
SN 1980K: Optical Max:
1980 Nov 4 = 44547
0.5–4.0keV Luminosity (x10^38 ergs s^-1)
4
2
0
Upper Limit
44000
44100
44200
44300
44400
44500
44600
44700
MJD (days)

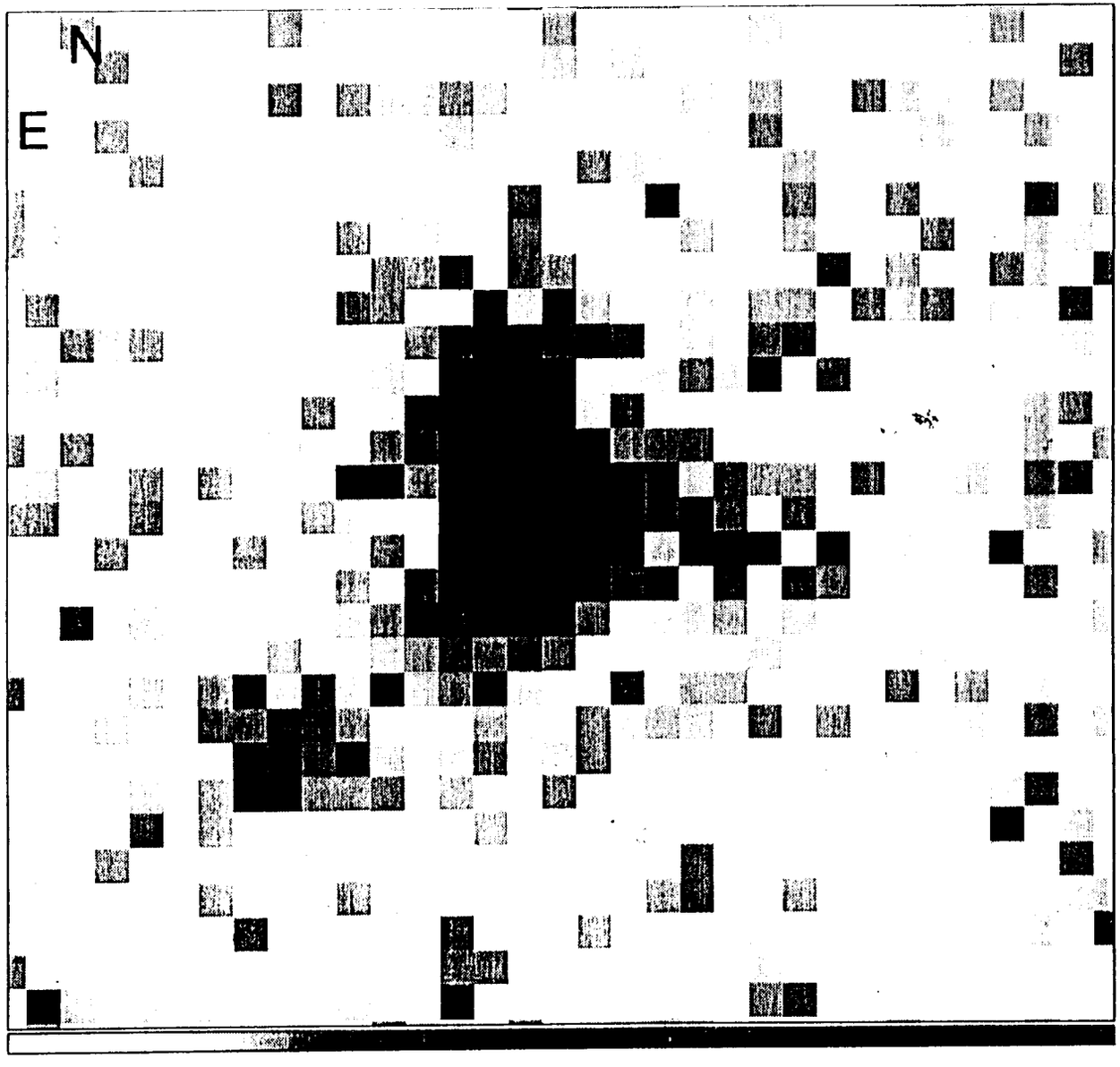
N
E

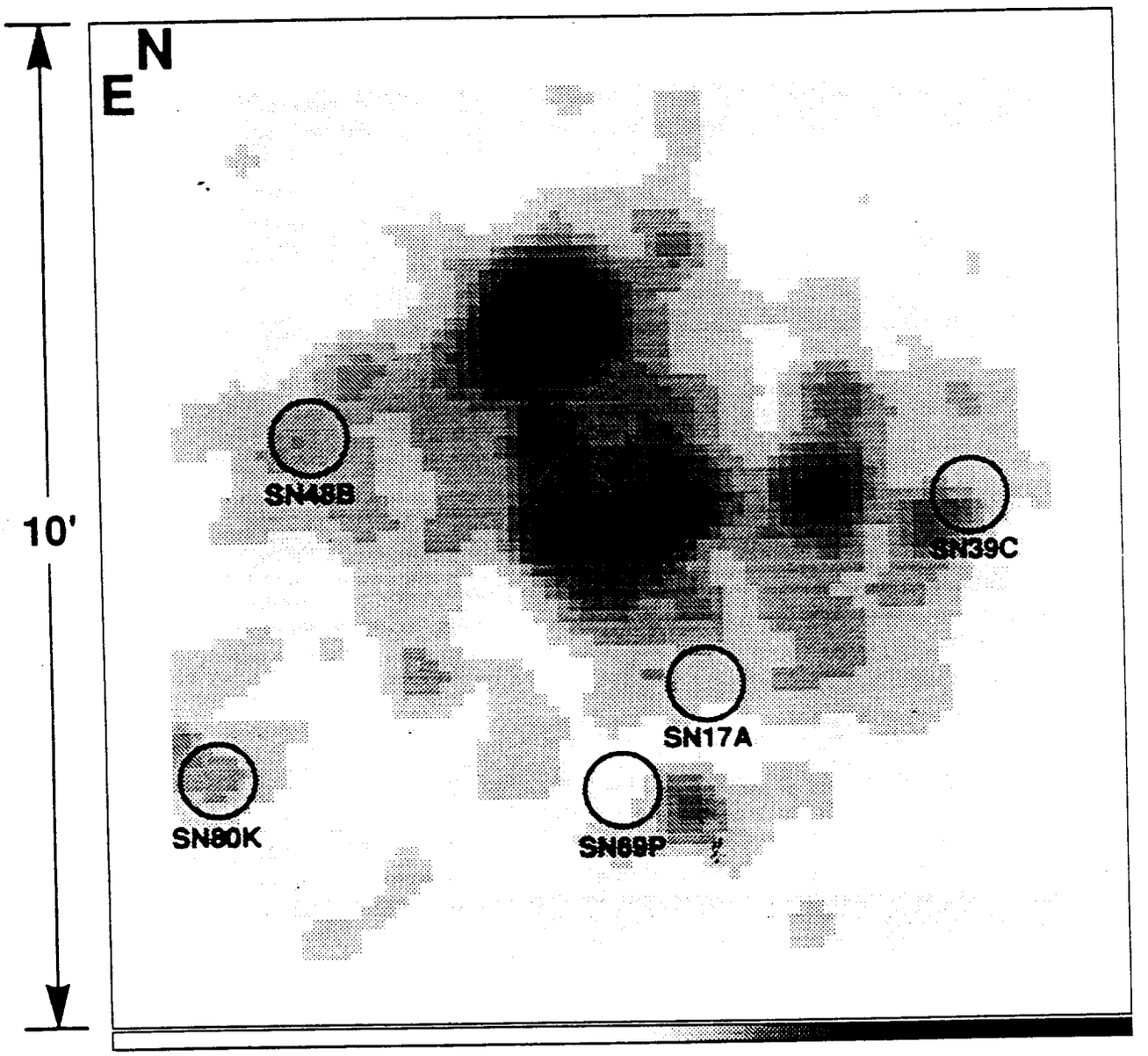
N
E
10'
SN48B
SN39C
SN17A
SN80K
SN69P

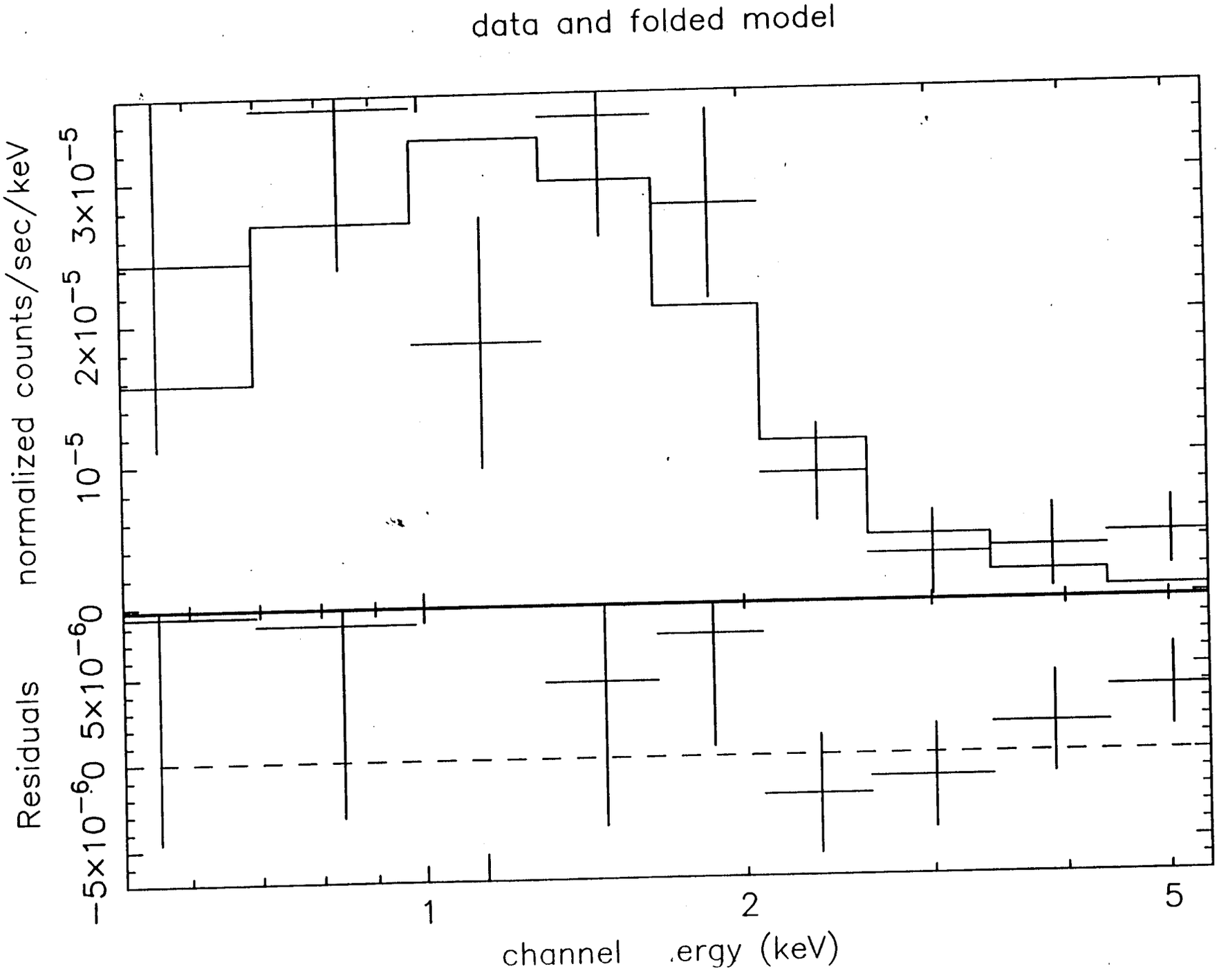
data and folded model
normalized counts/sec/keV
10^{-5}
2×10^{-5}
3×10^{-5}
Residuals
-5×10^{-6}
0
5×10^{-6}
0
1
2
5
channel .ergy (keV)

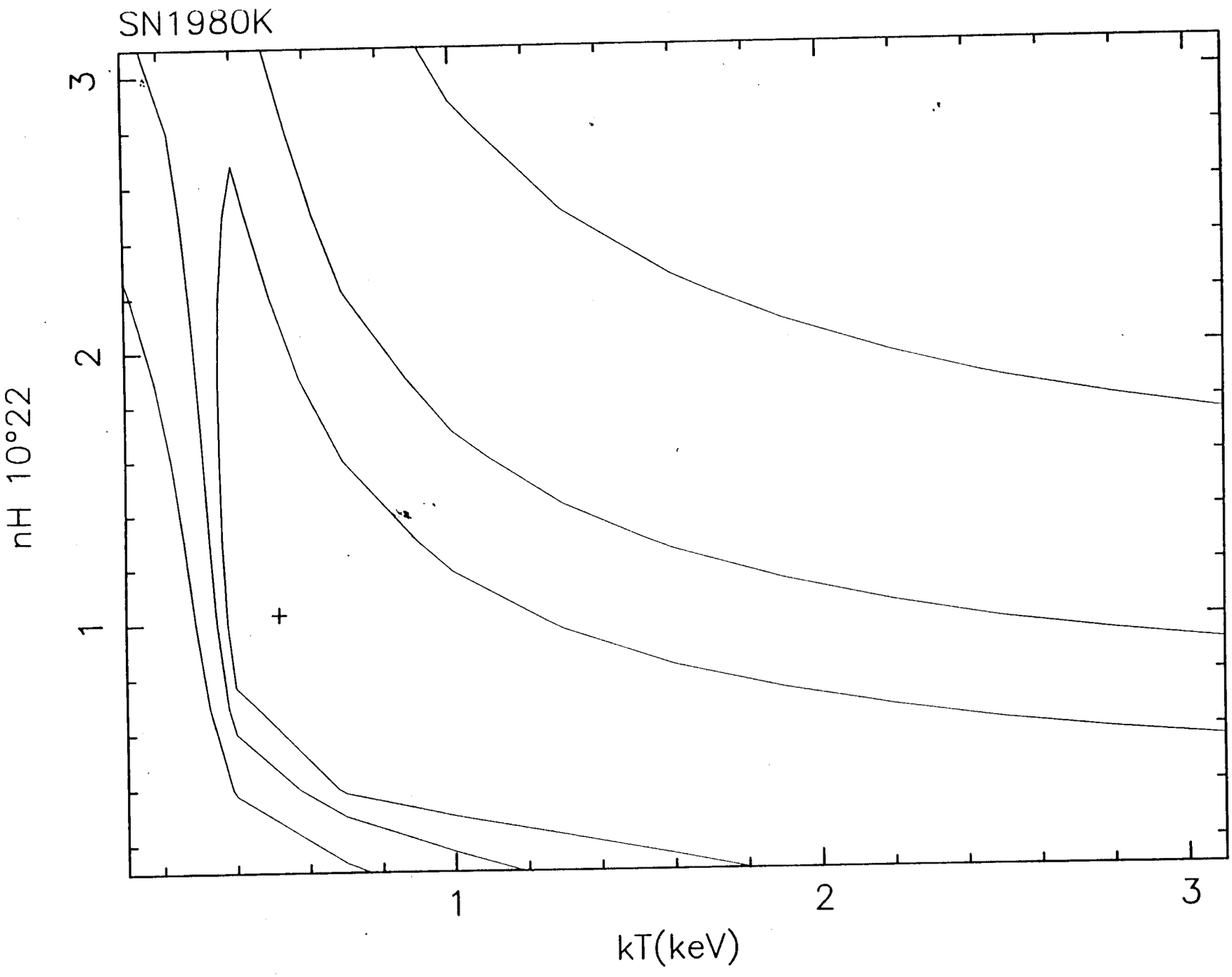
SN1980K
nH 10°22
1
2
3
1
2
3
kT(keV)

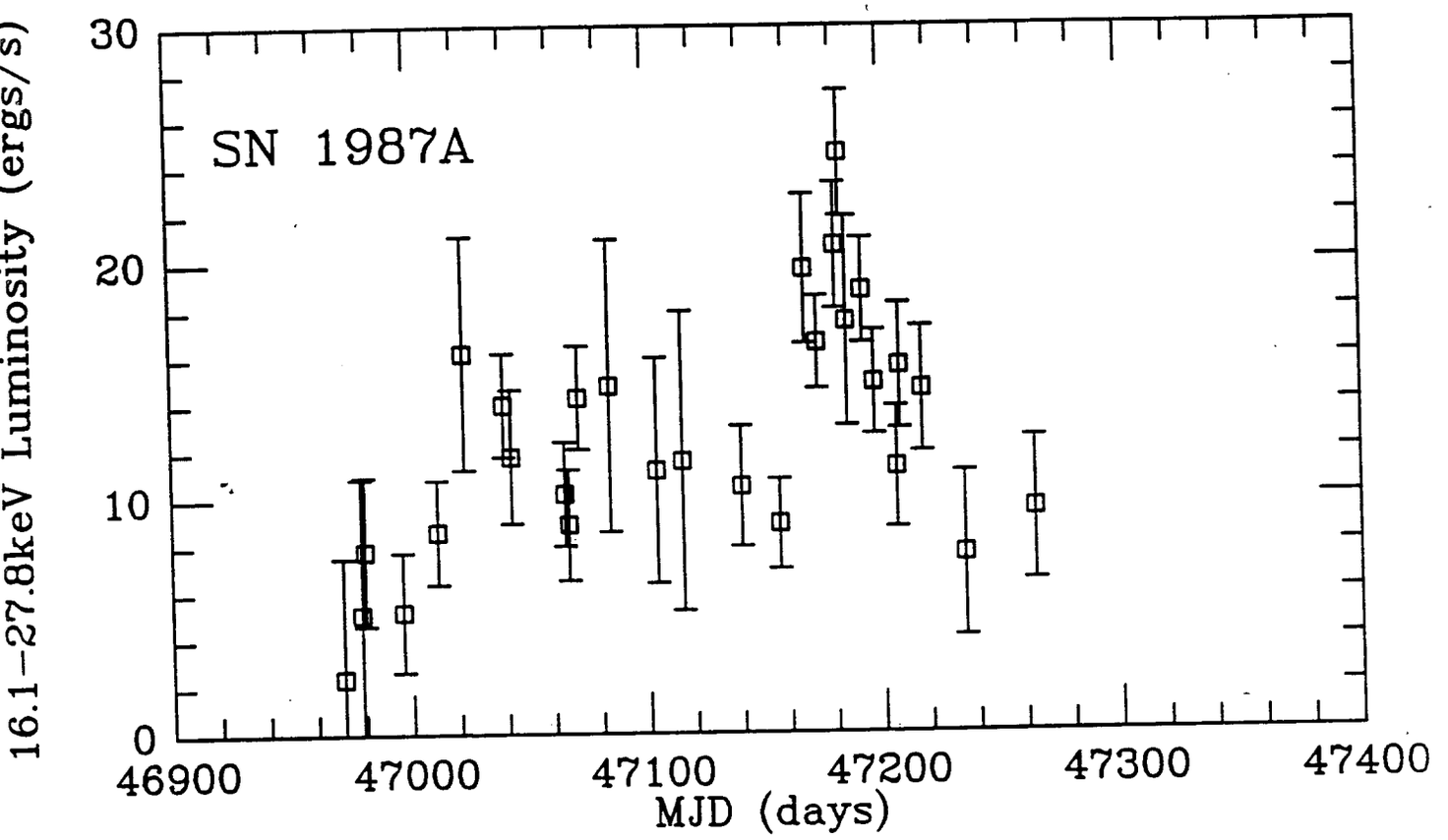
SN 1987A
16.1−27.8keV Luminosity (ergs/s)
30
20
10
0
46900
47000
47100
47200
47300
47400
MJD (days)

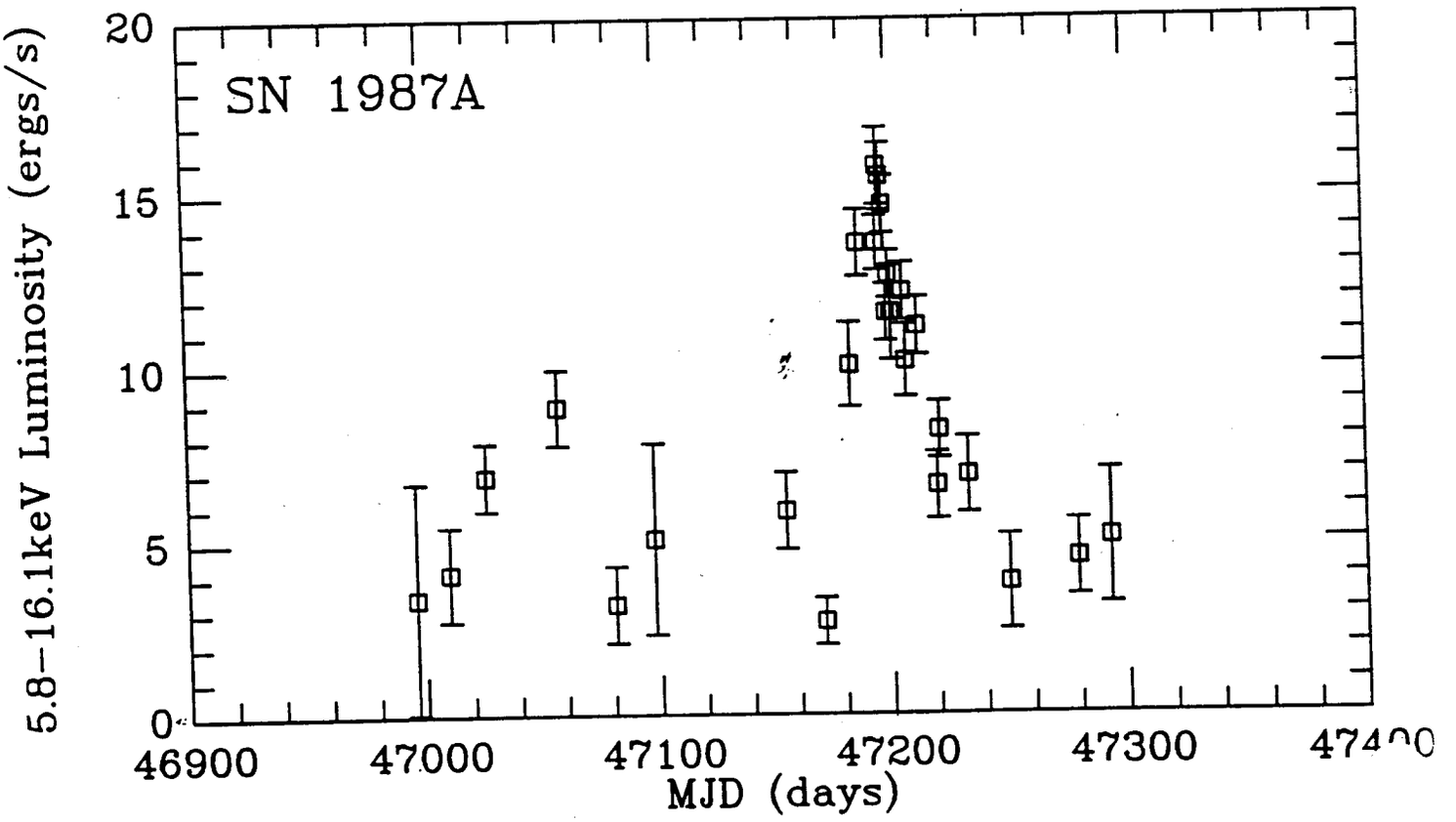
SN 1987A
5.8−16.1keV Luminosity (ergs/s)
20
15
10
5
0
46900
47000
47100
47200
47300
MJD (days)

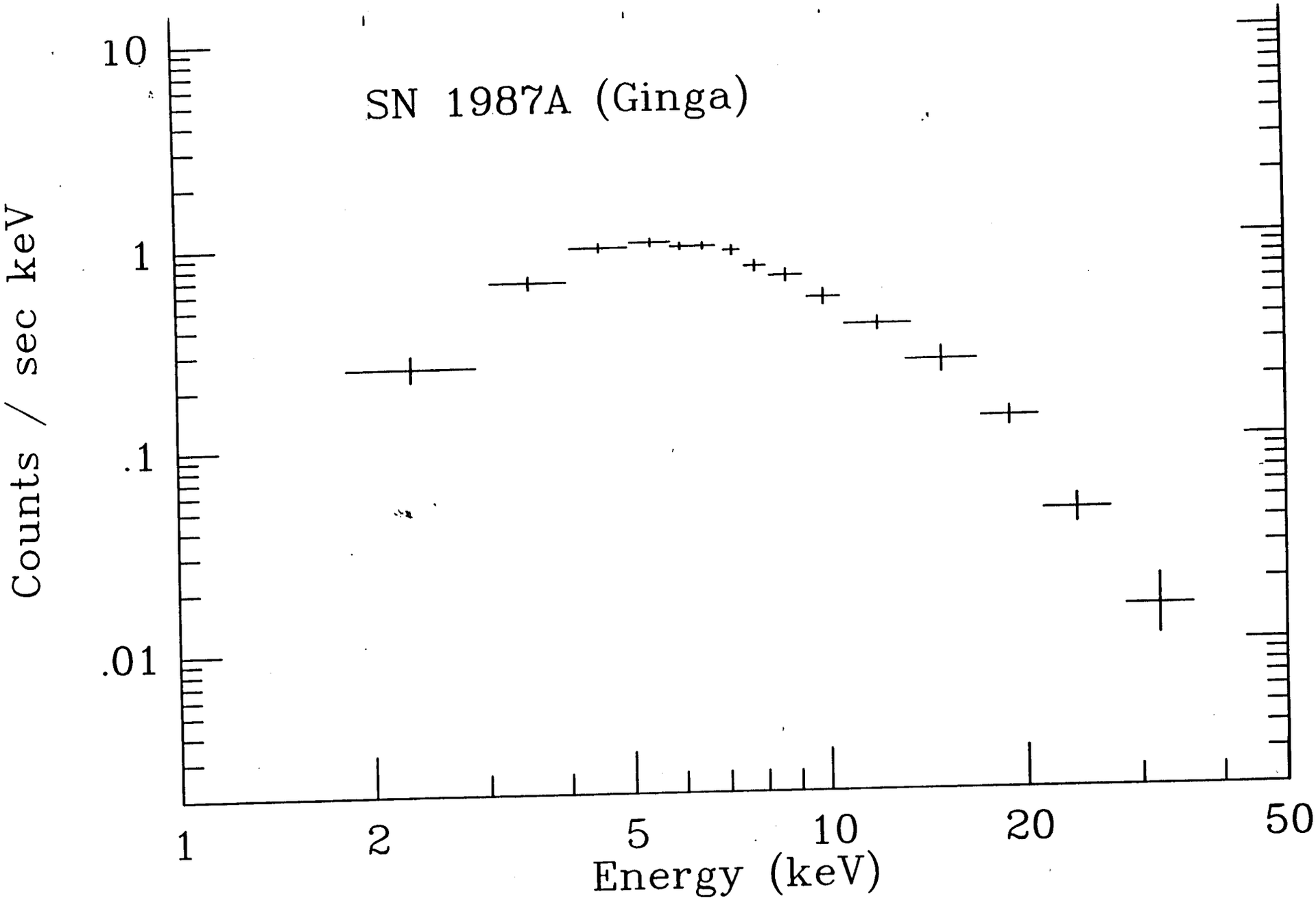
SN 1987A (Ginga)
Counts / sec keV
10
1
.1
.01
1
2
5
10
20
50
Energy (keV)

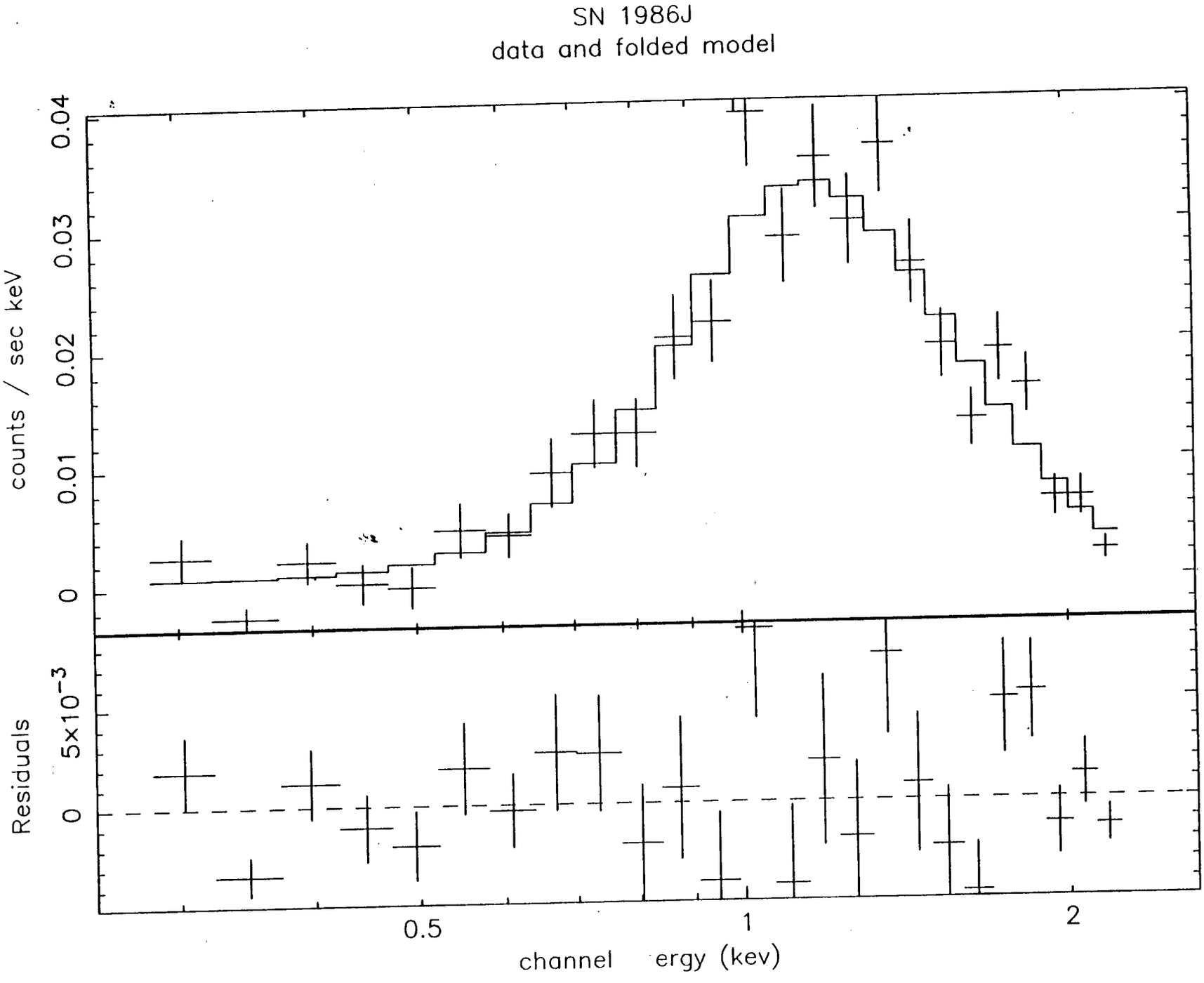
SN 1986J
data and folded model
counts / sec keV
0.04
0.03
0.02
0.01
0
Residuals
5x10^{-3}
0
0.5
1
2
channel ergy (kev)

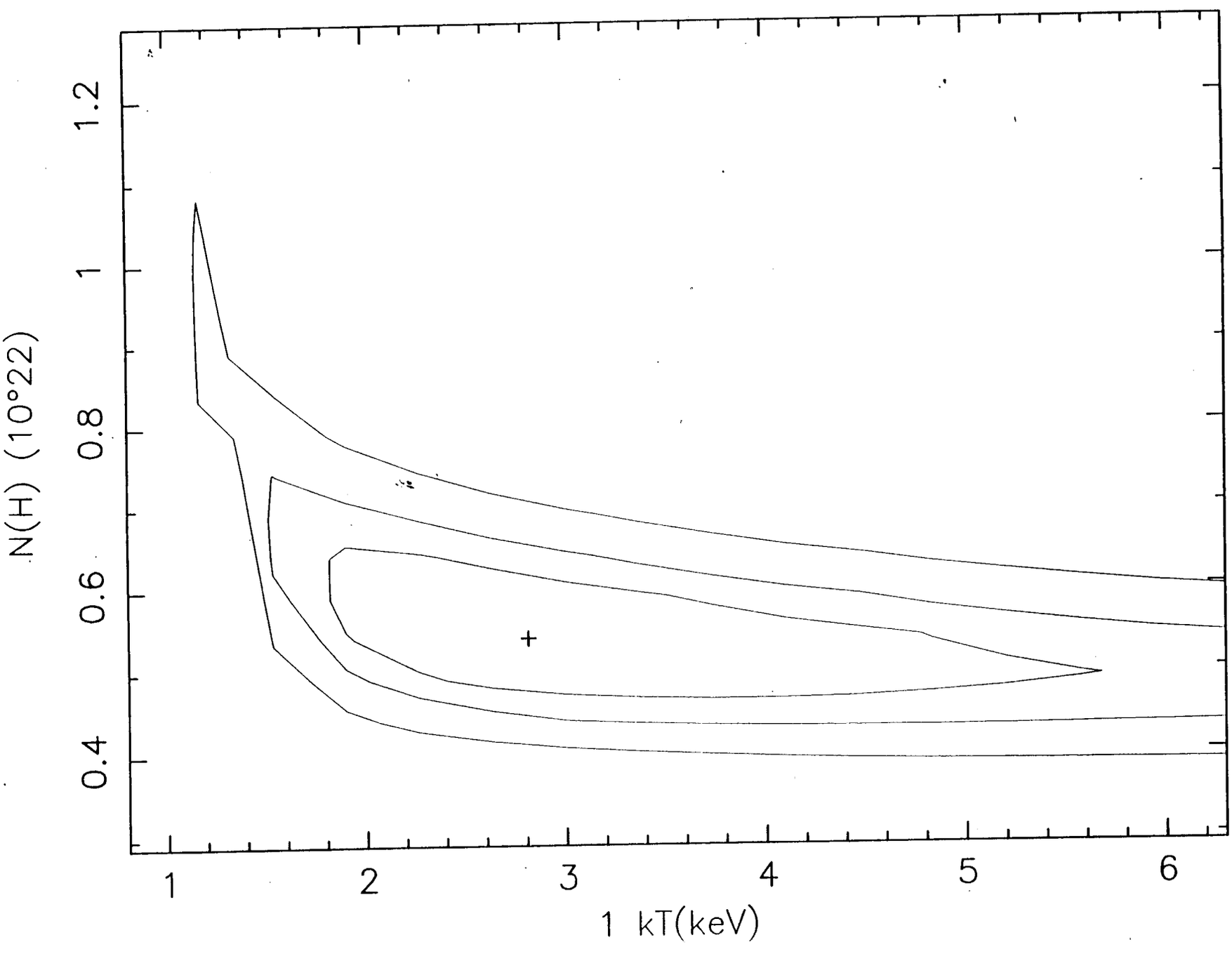
SN 1986J: Confidence contours
N(H) (10^22)
0.4
0.6
0.8
1
1.2
1
2
3
4
5
6
1 kT(keV)

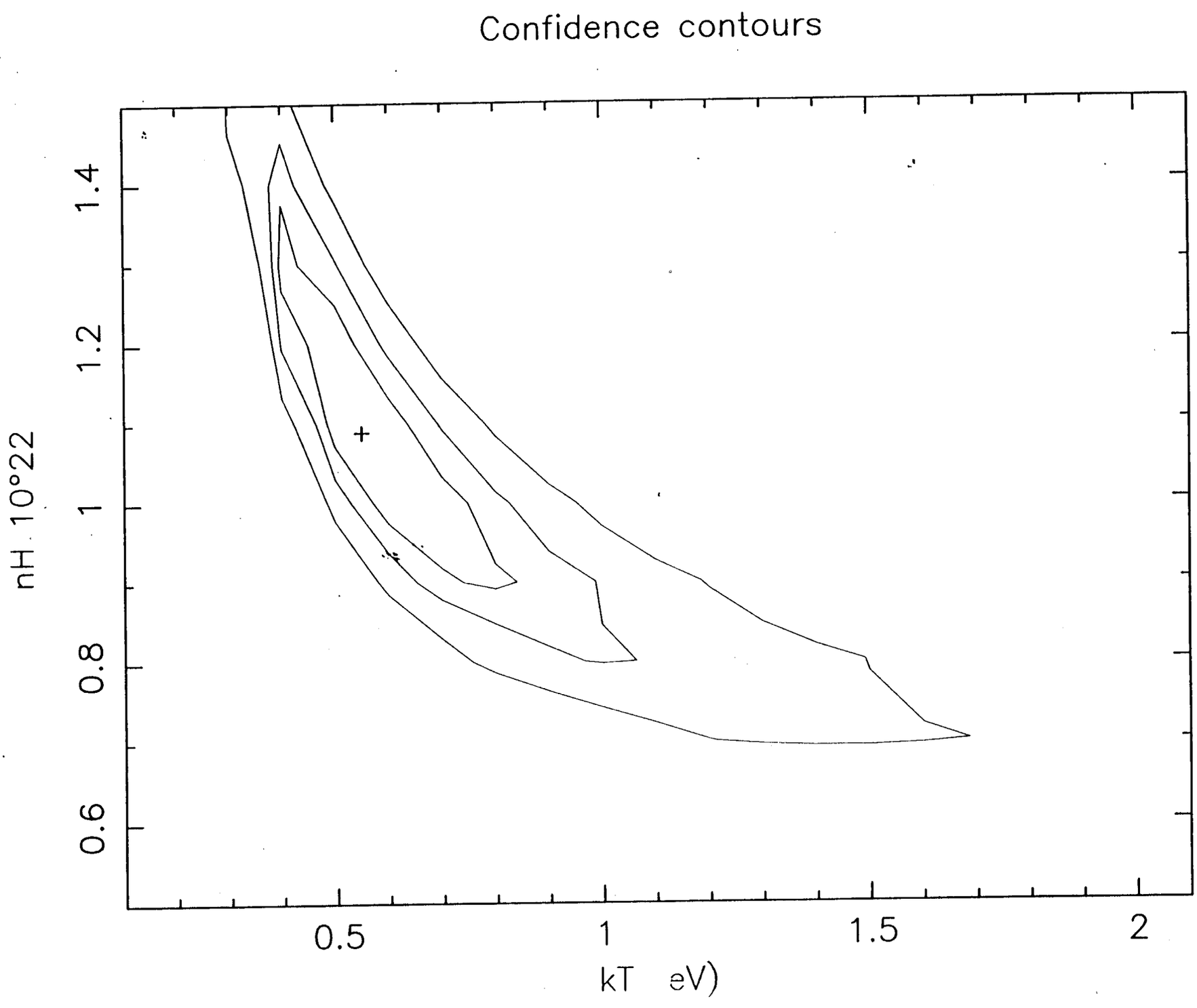
Confidence contours
nH 10°22
0.6
0.8
1
1.2
1.4
0.5
1
1.5
2
kT eV)

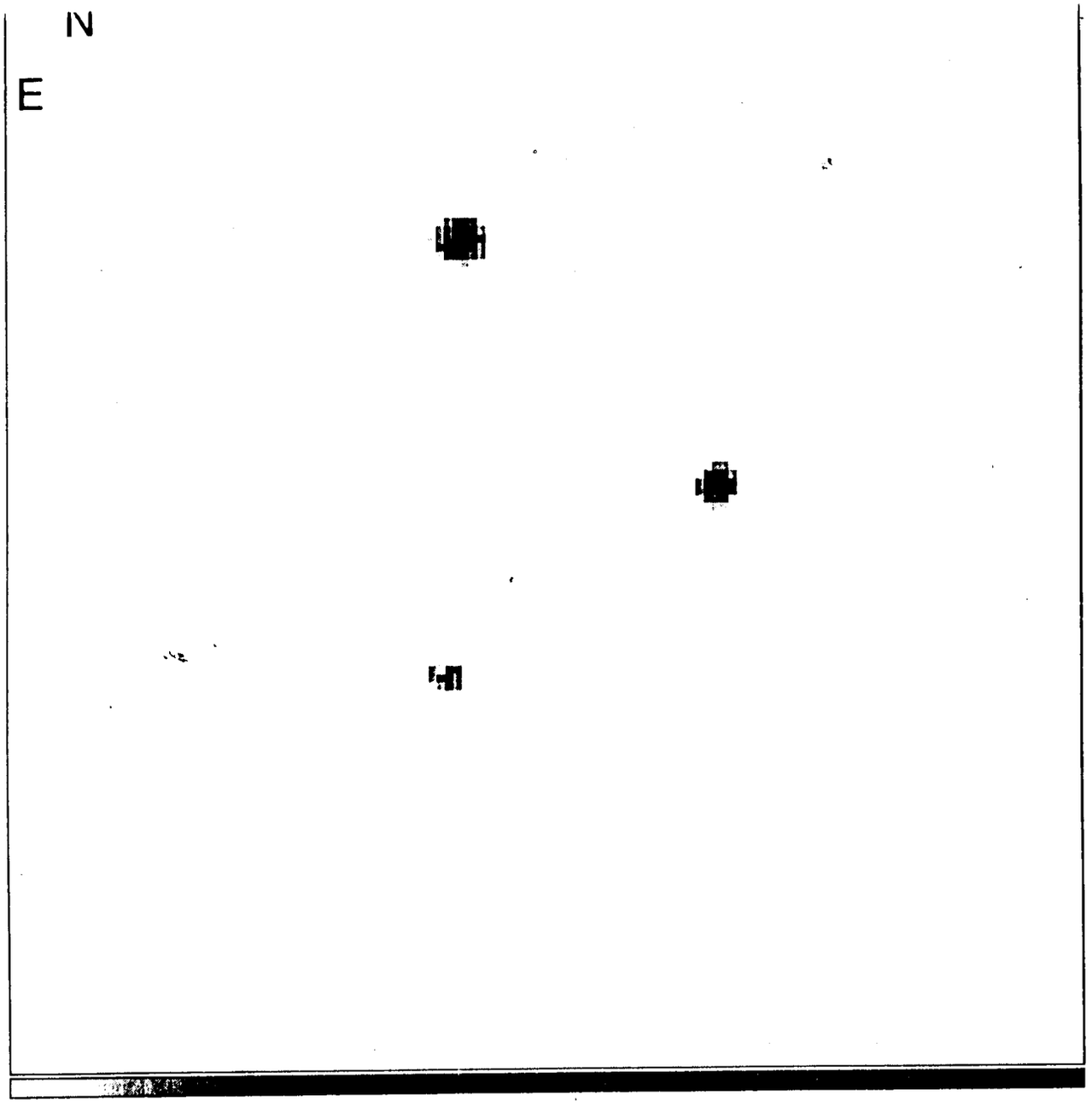
N
E

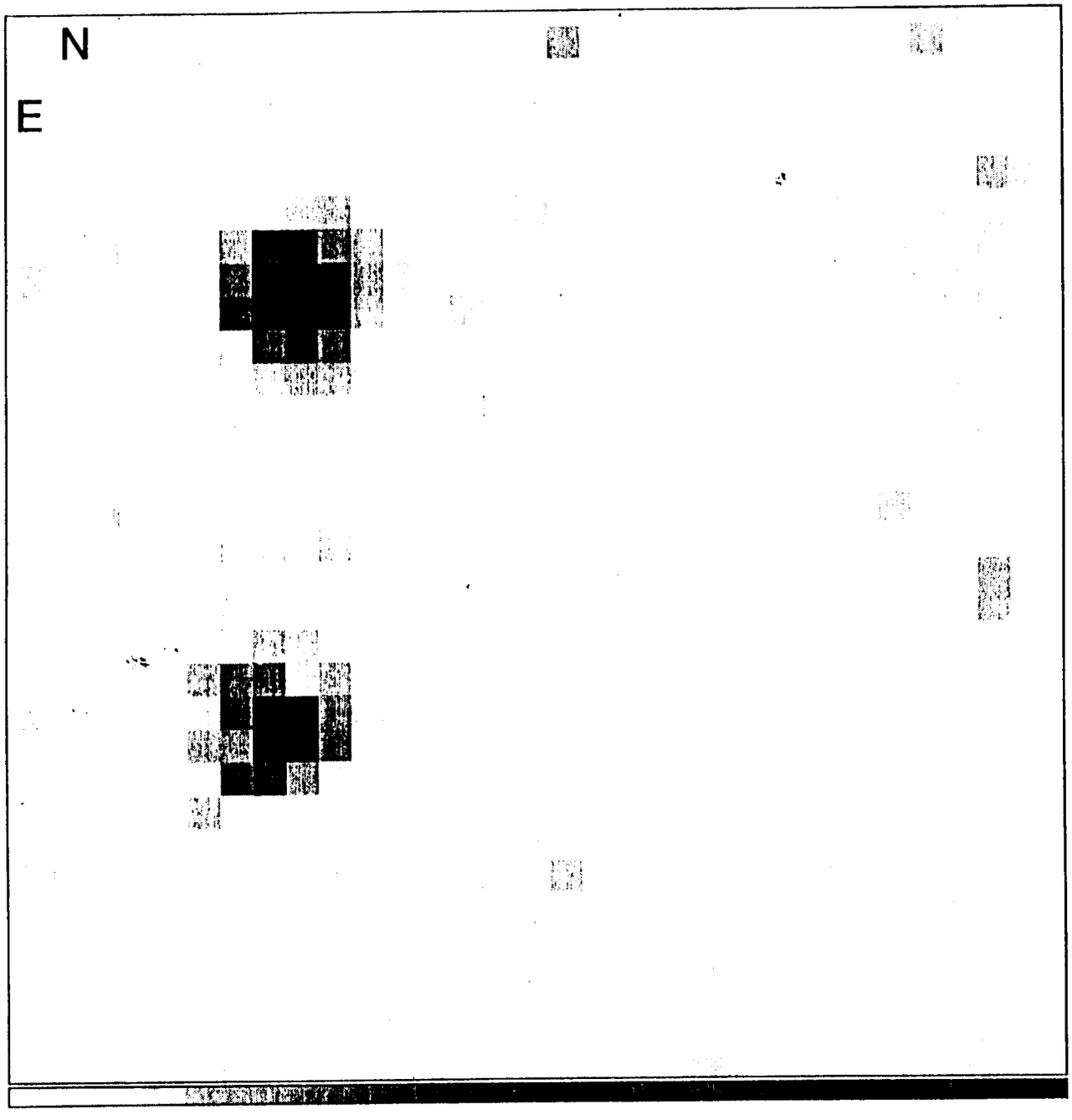
N
E

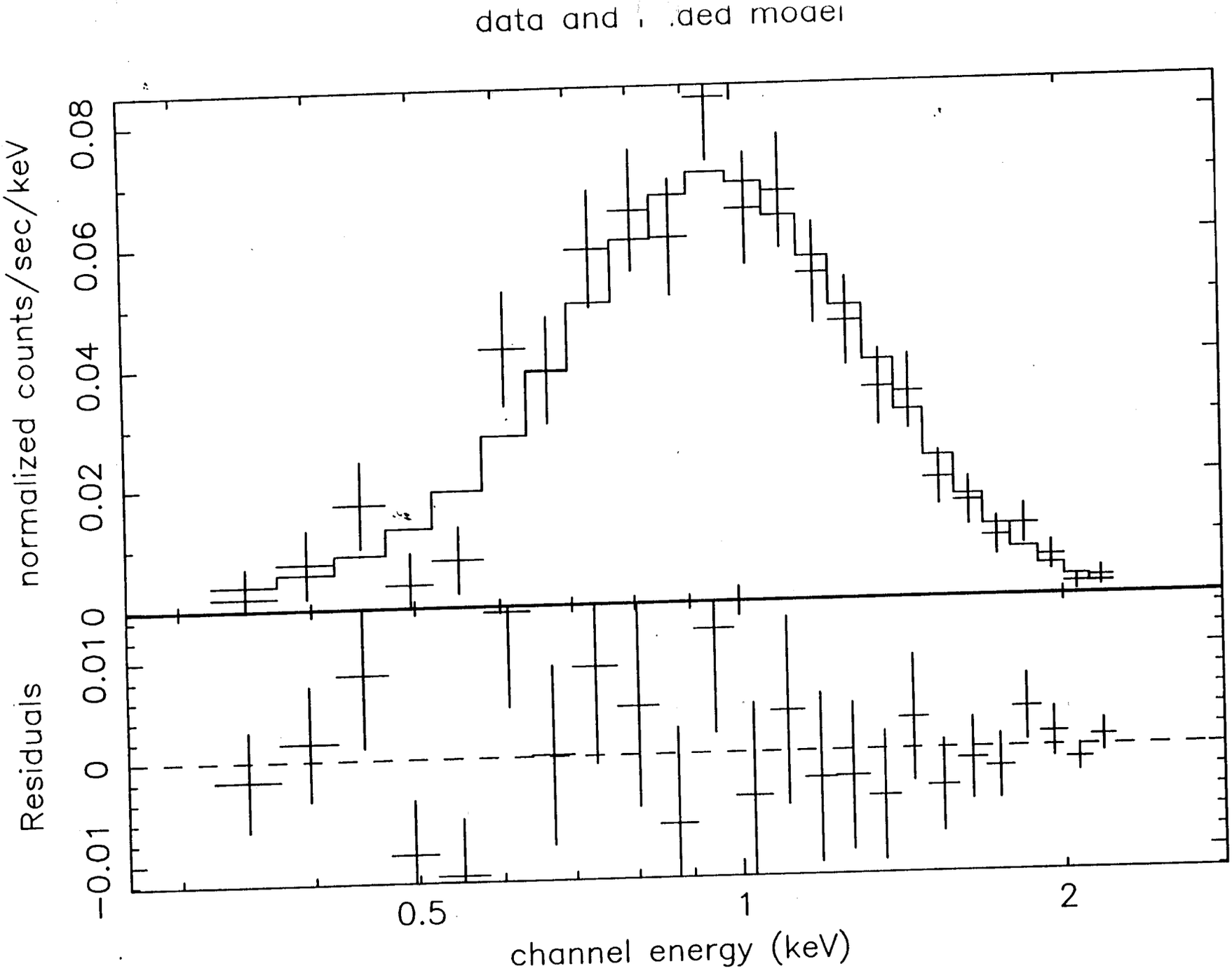
data and
ded model
normalized counts/sec/keV
0.08
0.06
0.04
0.02
Residuals
0.010
0
−0.01
0.5
1
2
channel energy (keV)

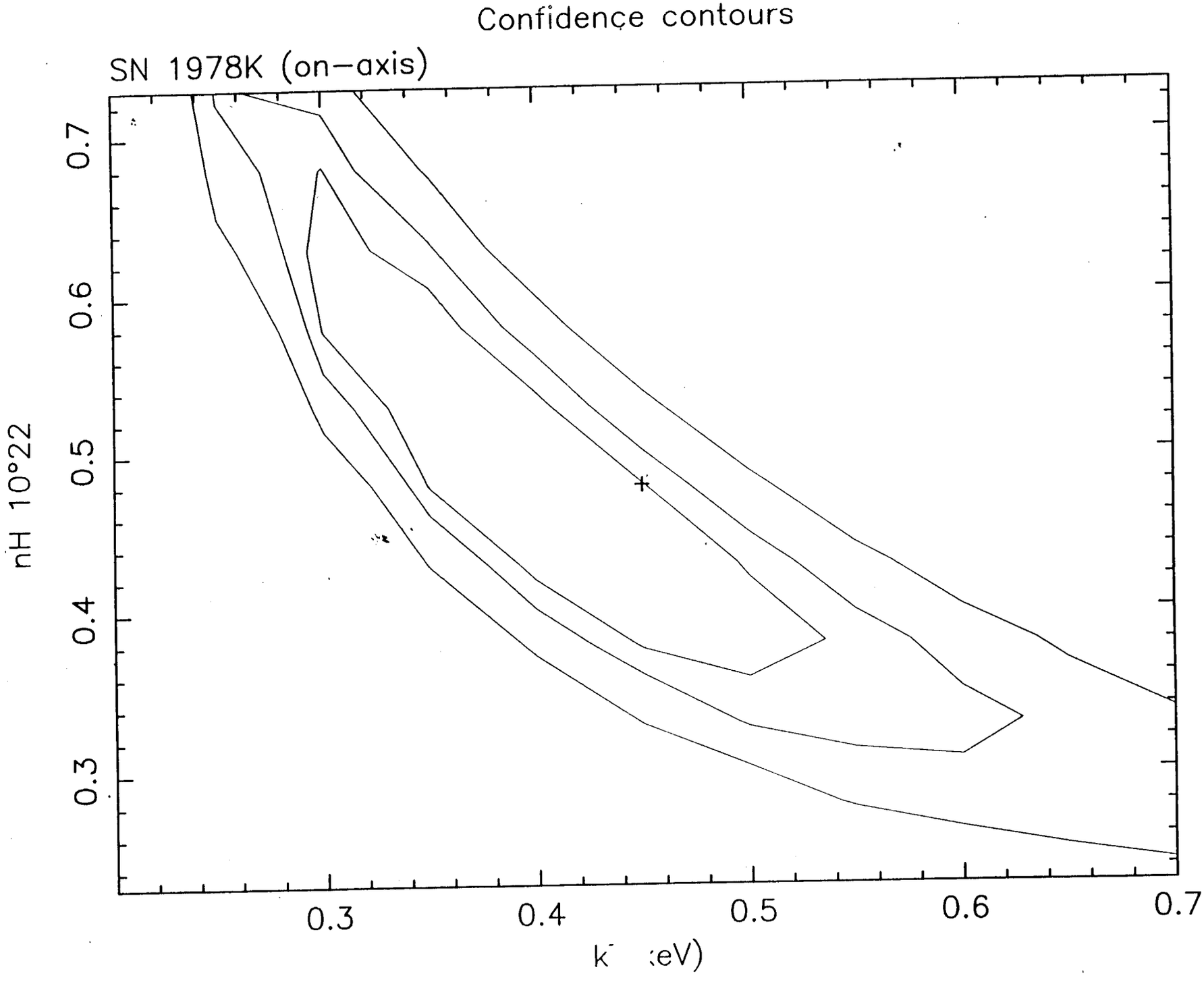
Confidence contours
SN 1978K (on-axis)
nH 10^22
0.3
0.4
0.5
0.6
0.7
0.3
0.4
0.5
0.6
0.7
k (eV)

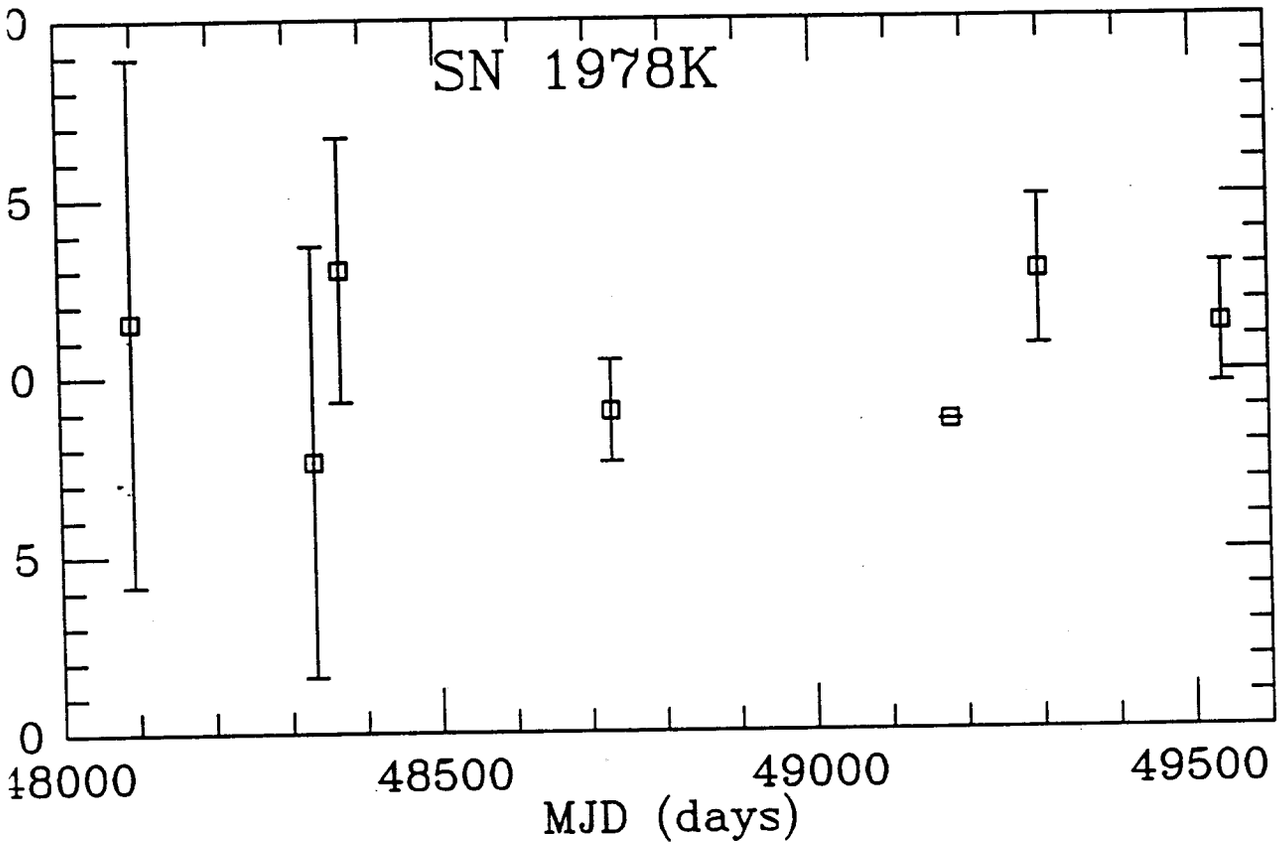
SN 1978K
0
5
0
5
0
48000
48500
49000
49500
MJD (days)

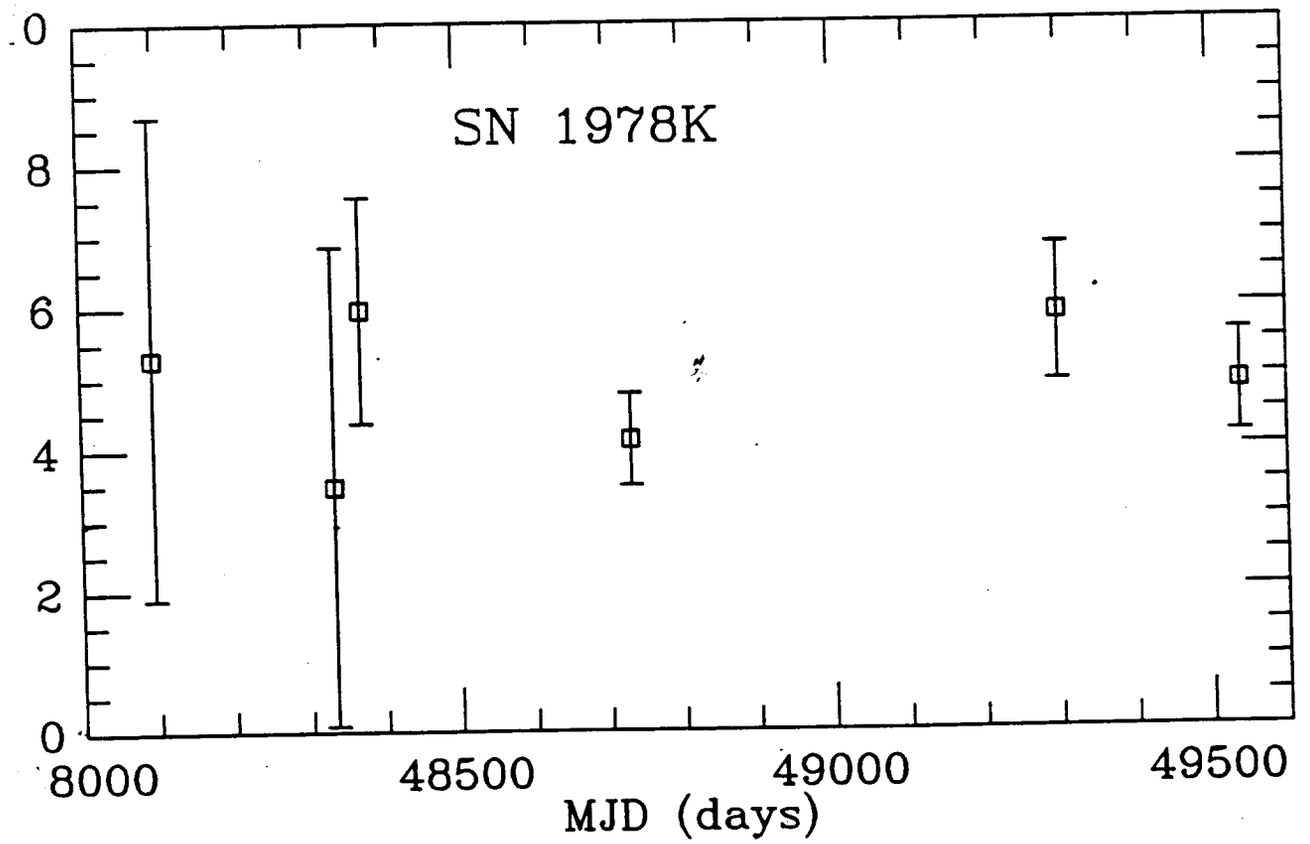
SN 1978K
.0
8
6
4
2
0
8000
48500
49000
49500
MJD (days)

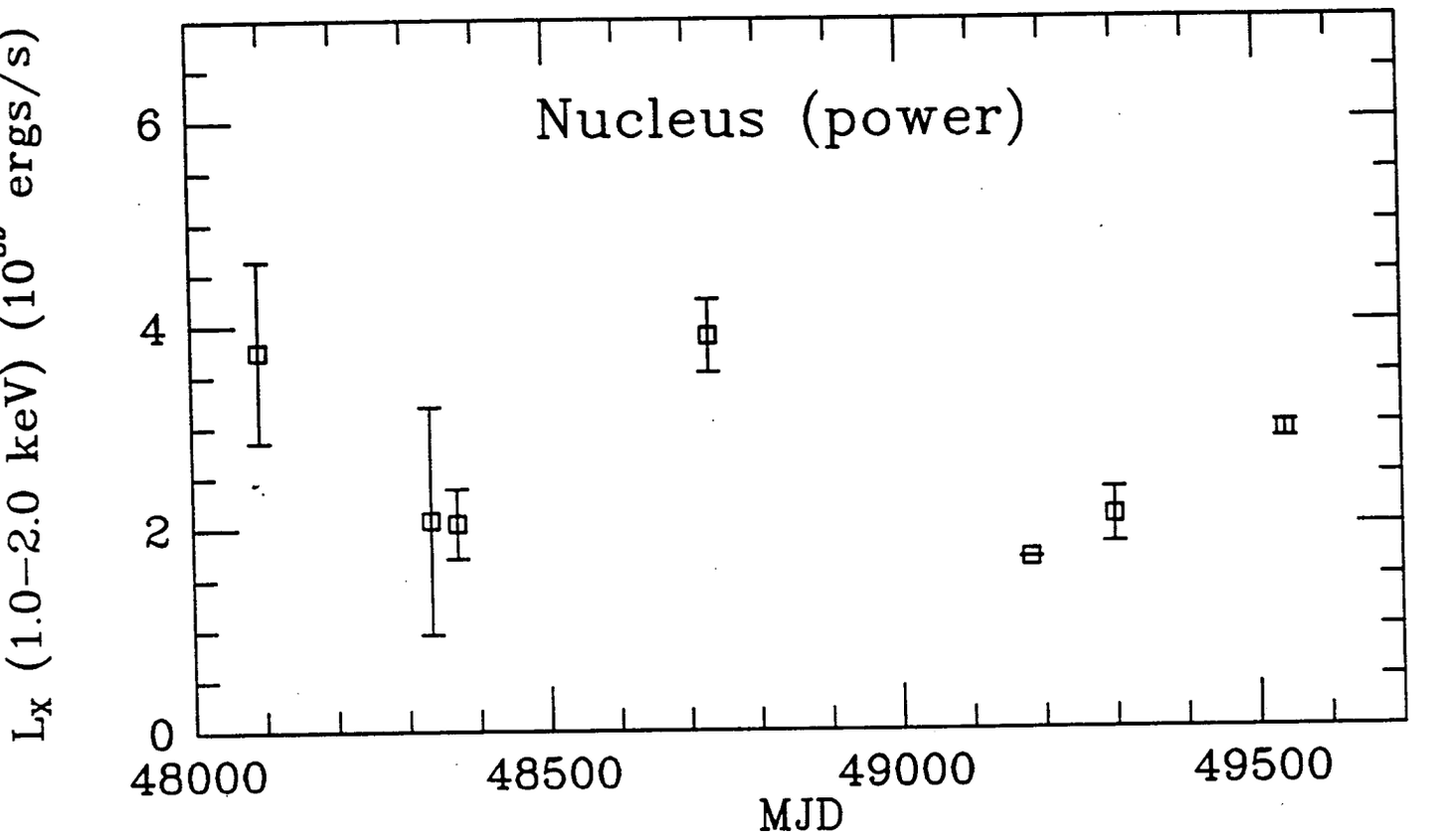
Nucleus (power)
L_X (1.0–2.0 keV) (10^{39} ergs/s)
0
2
4
6
48000
48500
49000
49500
MJD

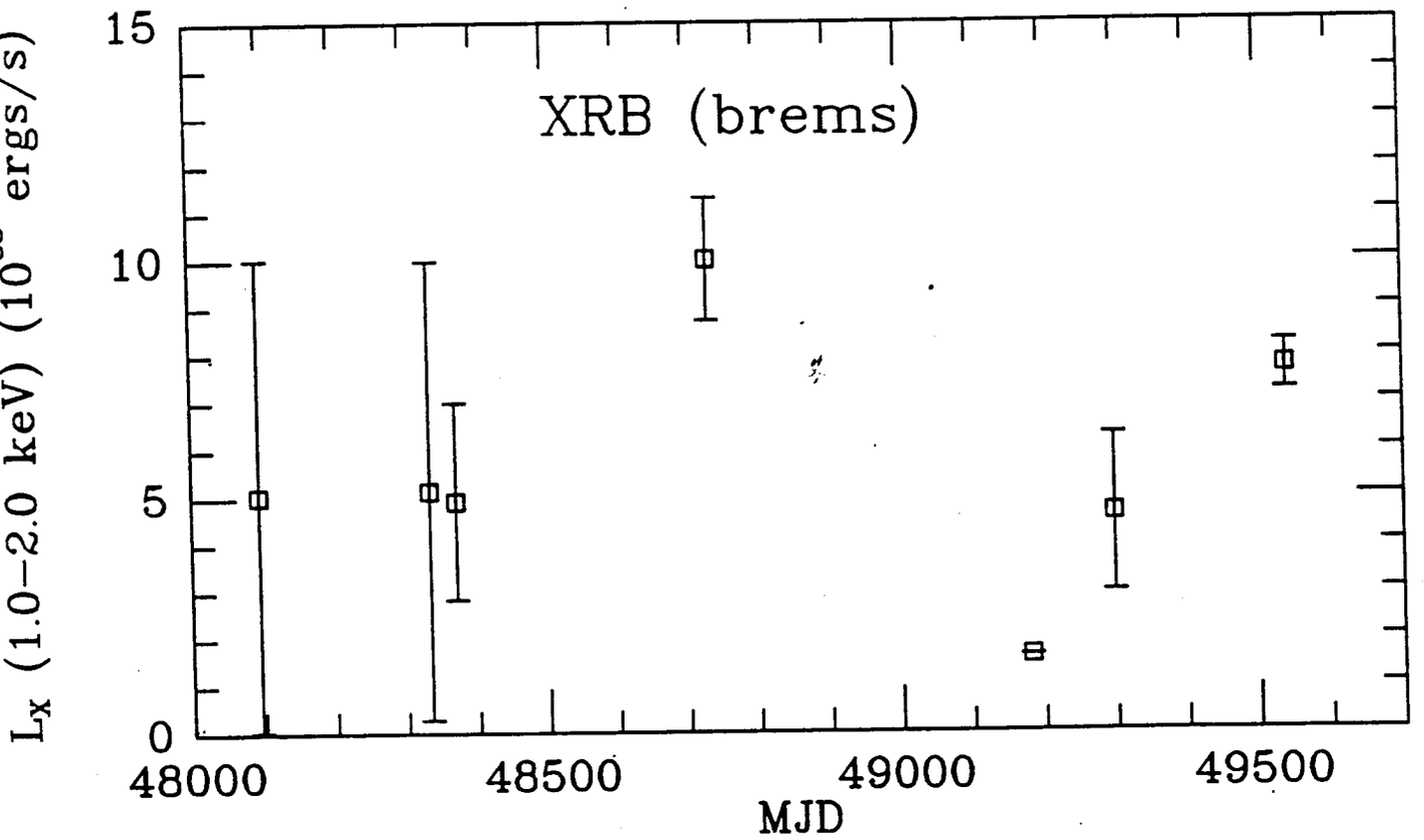
XRB (brems)
L_X (1.0–2.0 keV) (10^{38} ergs/s)
0
5
10
15
48000
48500
49000
49500
MJD

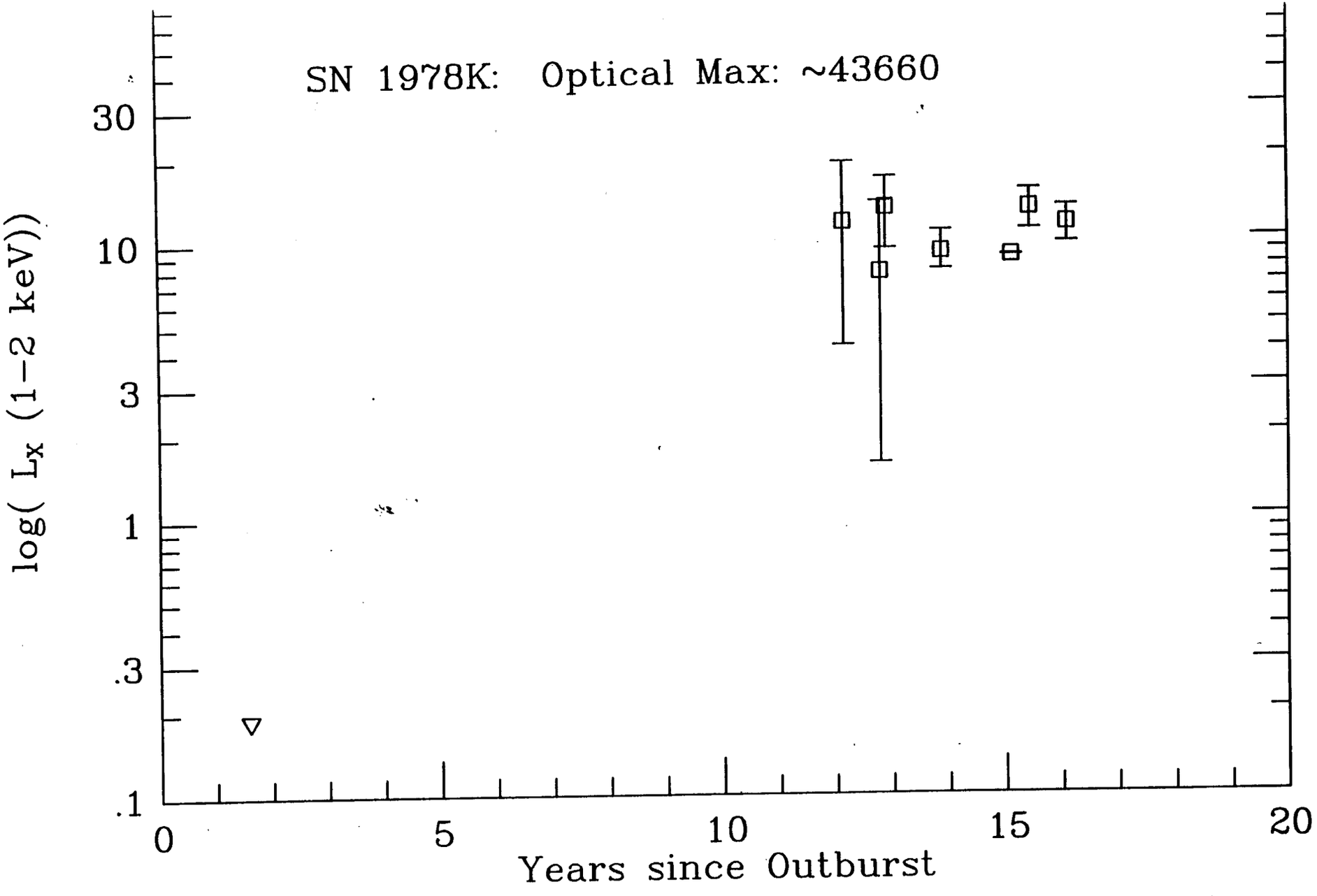
SN 1978K: Optical Max: ~43660
log(Lx (1-2 keV))
30
10
3
1
.3
.1
0
5
10
15
20
Years since Outburst

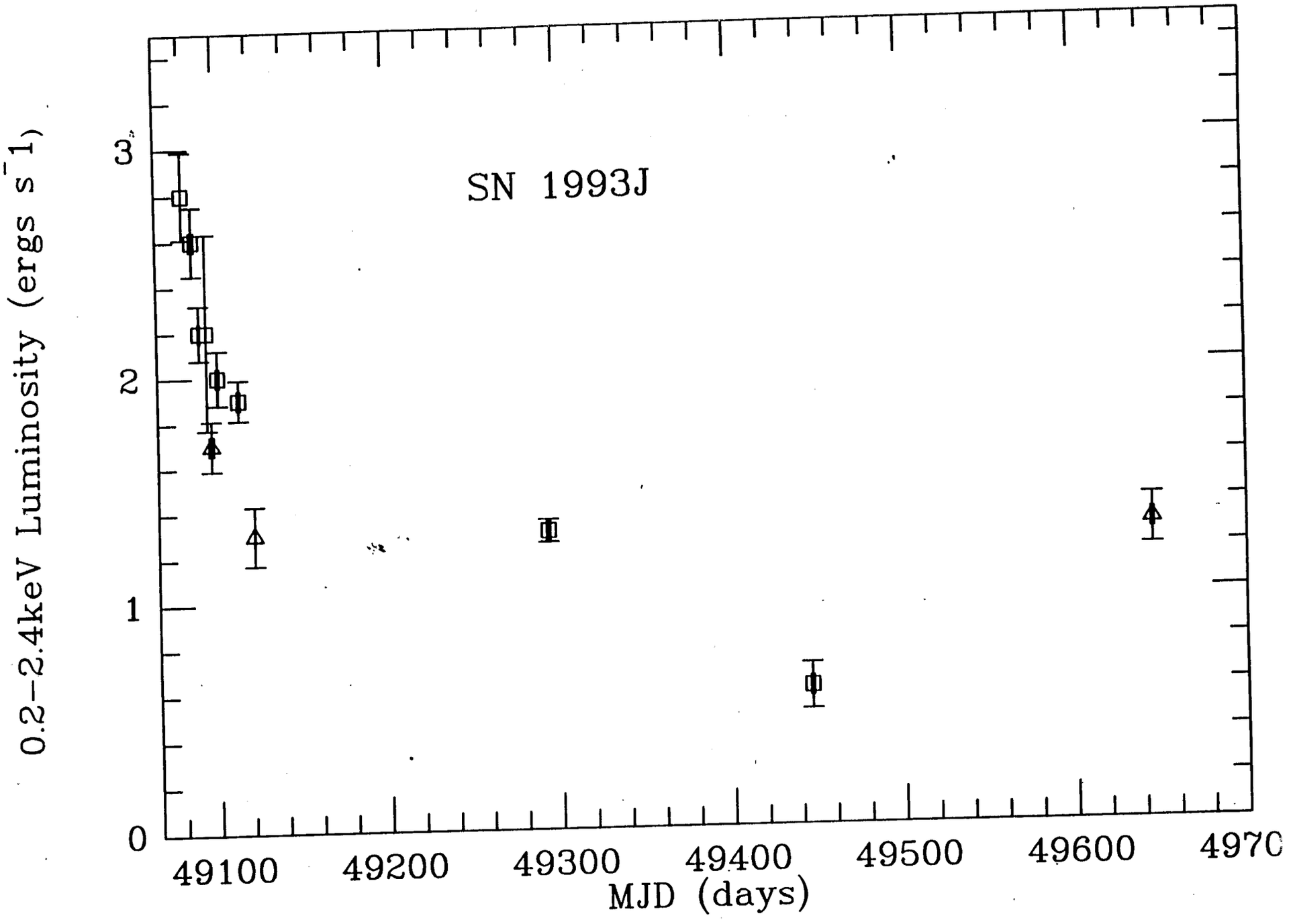
SN 1993J
0.2–2.4keV Luminosity (ergs s^{-1})
0
1
2
3
49100
49200
49300
49400
49500
49600
4970
MJD (days)

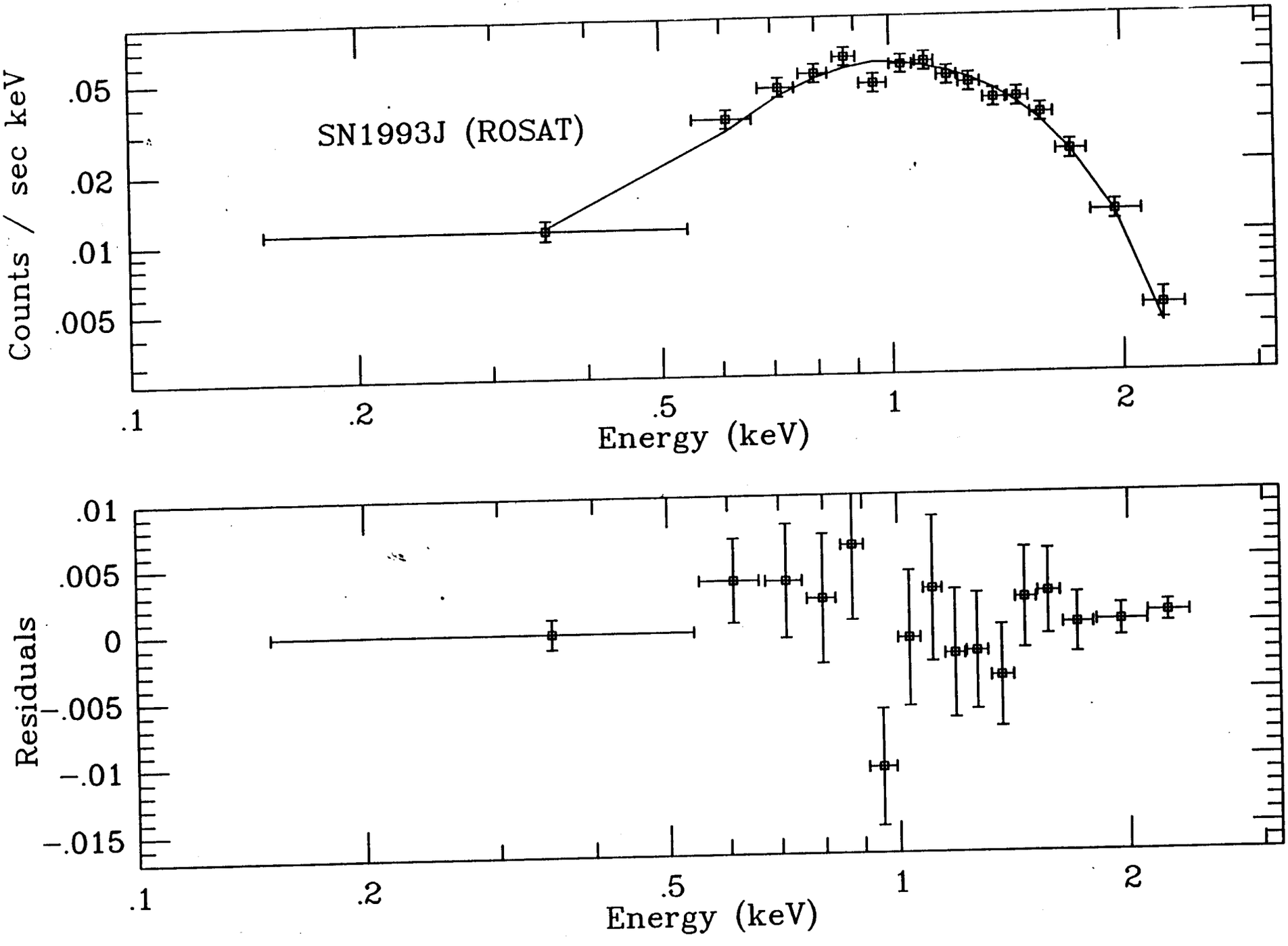
SN1993J (ROSAT)
Counts / sec keV
.05
.02
.01
.005
.1
.2
.5
1
2
Energy (keV)
Residuals
.01
.005
0
−.005
−.01
−.015
.1
.2
.5
1
2
Energy (keV)

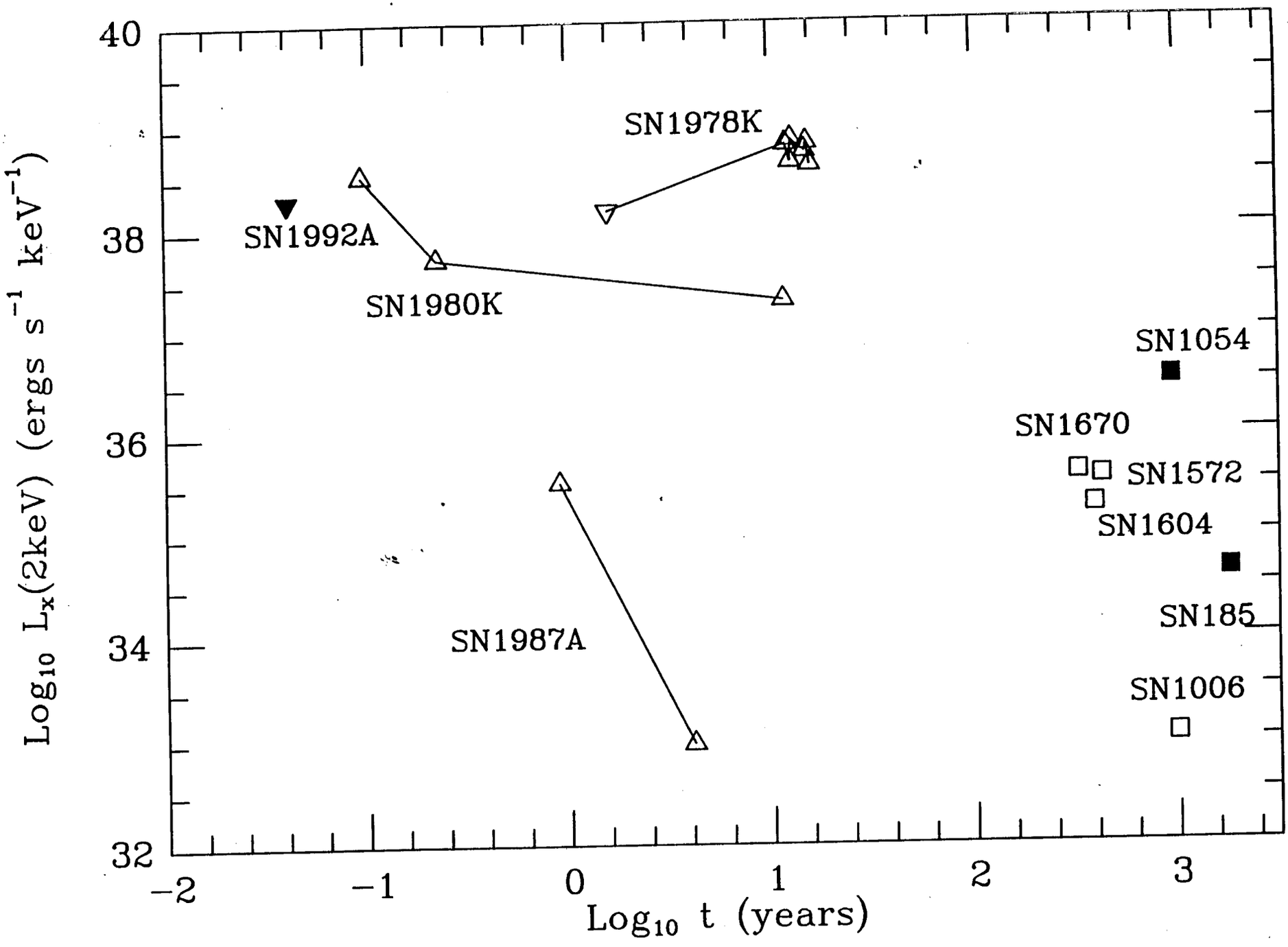
40
38
36
34
32
−2
−1
0
1
2
3
Log10 Lx(2keV) (ergs s−1 keV−1)
Log10 t (years)
SN1978K
SN1992A
SN1980K
SN1987A
SN1054
SN1670
SN1572
SN1604
SN185
SN1006